INSPECTION OF DEFECTS IN THE SEAL REGION OF FLEXIBLE FOOD PACKAGES USING THE ULTRASONIC PULSE-ECHO TECHNIQUE

BY

AYHAN OZGULER

B.Sc., Middle East Technical University, 1991
M.S., University of Illinois, 1995

THESIS

Submitted in partial fulfillment of the requirements
for the degree of Doctor of Philosophy in Food Science
in the Graduate College of the
University of Illinois at Urbana-Champaign, 1999

Urbana, Illinois

INSPECTION OF DEFECTS IN THE SEAL REGION OF FLEXIBLE FOOD PACKAGES USING THE ULTRASONIC PULSE-ECHO TECHNIQUE

Ayhan Ozguler, Ph.D.
Department of Food Science and Human Nutrition
University of Illinois at Urbana-Champaign, 1999
Scott A. Morris, Advisor

Although flexible food packages such as pouches and trays have numerous advantages over traditional packages such as metal cans and glasses, container integrity is still a major problem for flexible food packages. Current inspection techniques are not capable of detecting microscale defects in the seal region of these packages, which might compromise the safety and cause product loss. In addition, many of the techniques provide only statistical assurance, which does not guarantee the safety of the untested package. A rapid, dependable method of on-line package inspection will allow wider implementation of energy- and material-efficient retortable pouches and trays, by reducing inspection costs.

Nondestructive ultrasonic pulse-echo testing by the imaging method, Backscattered Amplitude Integral (BAI), was developed and evaluated for use in seal defect detection. Channel defects (6-15 μm in diameter) and simulated food strands (20-60 μm in diameter) perpendicular to the sealing direction were fabricated within the seal region of both all-plastic and foil-containing retortable pouches. Results showed that 17.3-MHz pulse-echo BAI-imaging detected channel defects and strand-inclusion defects in both types of package materials.

In the second phase of the study, the contrast of the defect on the BAI-mode image was evaluated for various packaging materials, defect types and sizes. For this purpose, channel (6-100μm in diameter) and inclusion defects (strands of mouse tail tendons, 20-150μm) were fabricated in the seal area of all-plastic and foil-containing packaging films. The 17.3-MHz ultrasonic pulse-

echo Backscattered Amplitude Integral (BAI) method was used to visualize and evaluate the contrast of these defects. It has been shown that there is a linear relationship between the defect size and the contrast value, denoted ΔBAI , and that different defect types and packaging materials have a significant impact on the ΔBAI value. The utility of ΔBAI for detecting defects makes it a useful and reliable sensing method for package inspection.

Although performance of the BAI-mode imaging technique to detect microscale defects was outstanding, it was poor for macroscale defects such as non-bonding, wrinkles, and bubbles when they were abundantly present in the seal region. Macroscale defects were created by varying the sealing-bar temperature. The average and the coefficient of variation of the BAI-values in the seal region were calculated. The study indicated that the combination of the average and the coefficient of variation of BAI-values would detect the macroscale defects and provide a real-time, on-line control by being able to sense whether seal has achieved a proper state of fusion or not.

In conclusion, the techniques developed in this study can provide safety assurance of flexible food packages and make these packages more financially competitive by reducing inspection costs.

DEDICATION

To my wife Irmak Ozguler, for her love, encouragement, care, and patience over the years. To my father, who was unable to see the completion of my study, my mother, sister and brother. No words can truly express my gratitude to them for having supported me in my pursuit of academic excellence.

ACKNOWLEDGEMENT

I would like to express my gratitude to Dr. Scott A. Morris for his patience, guidance, friendship, and support during my education at the University of Illinois. I am extremely grateful for his trust and inspiration. I also would like to thank to Dr. William D. O'Brien, Jr., my co-advisor, for his guidance, encouragement, and friendship. His constructive suggestions inspired me to reach new levels of academic achievement. I also thank to my committee member: Dr William Artz and Dr. James Faller for their advice, and reviewing this manuscript.

I am very grateful to all of my lab mates in both Packaging Laboratory and Bioacoustic Research Laboratory for their advice and help.

I wish to express my sincere appreciation to Mrs. Vera Walsh, the Department of Food Science and Human Nutrition Secretary, for her help.

I would like to acknowledge the professional assistance with validation of samples produced in Chapter-4 by Dr. James F. Zachary, Department of Veterinary Pathobiology.

Finally, I would like to thank the Department of Food Science and Human Nutrition, Bioacoustic Research Laboratory, and the Value-Added Research Opportunities Program, Agricultural Experiment Station, University of Illinois for providing the opportunity to continue my education.

TABLE OF CONTENTS

Page

Page

Page

LIST OF TABLES

LIST OF FIGURES

Figure **Page**

Figure **Page**

Figure **Page**

LIST OF SYMBOLS

A, amplitude of vibration

ACF, air-filled channel defect in foil-containing film

ACP, air-filled channel defect in all-plastic film

AF, Aluminum foil

A.O.A.C, Association of Official Analytical Chemists

BAI, Backscattered Amplitude Integral (V·μs)

$\overline{BAI}$, Average of BAI-values (V·μs) in BAI-value matrix

$\overline{\overline{BAI}}$, Average of $\overline{BAI}$-values (V·μs)

$BAI_{background}$, average unnormalized BAI-value of ten spatially separated random locations from regions, which do not include defect

BAI_{defect}, average unnormalized BAI-value in the defect location (V·μs)

BAI_{max}, maximum BAI value in the BAI-value matrix (V·μs)

$BAI_{mid\text{-}channel}$, average unnormalized BAI-value from the center location of the channel location (V·μs)

$BAI_{undisturbed}$, average unnormalized BAI-value from the undisturbed region adjacent to the channel defect (V·μs)

BOPP, Balanced oriented polypropylene

BW, beam width (m)

c, speed of sound (m/s)

CV, coefficient of variation (%)

$d_{lateral}$, lateral size of the defect (μm)

d_{major}, size of the defect on its major axis (μm)

d_{minor}, size of the defect on its minor axis (μm)

d_{wire}, diameter of the tungsten wire (μm)

D, diameter of the transducer (m)

D_{axial}, axial resolution calculated using $\tau_{(-20\text{-dB})}$

$D_{lateral(-6\text{-dB})}$, lateral resolution at -6-dB transmit-receive beam width

ER, Epoxy resin

ESPI, Electronic Speckle Pattern Interferometry

EVOH, Ethylene-vinyl alcohol copolymer

f, frequency (Hz)

$f^{\#}$, f-number of the focused transducer (=ROC/D)

f_c, center frequency of the focused transducer (Hz)

$f_{lateral}$, lateral size fraction of the defect

f_{defect}, eccentricity of the elliptic geometry of the defect

F, focal length (m)

F_z, the -6-dB transmit-receive depth of focus

FDA, Food and Drug Administration

GPIB, General Purpose Interface Bus

HFI, Hold For Investigation

IDF, inclusion defect in foil-containing film

IDP, inclusion defect in all-plastic film

L, longitudinal wave

LDPE, Low density polyethylene

MRE, Meals Ready to Eat

MRI, Magnetic Resonance Imaging

N, length of the near field (m)

NCFST, National Center for Food Safety and Technology

NFPA, National Food Processors Association

ON, Oriented nylon

PE, Polyethylene

PET, Polyethyleneterephthalate

PO, Polyolefin

PP, Polypropylene

PRF, pulse repetition frequency (Hz)

PRP, pulse repetition period (s)

PVDC, Polyvinylidene chloride

R^2, correlation coefficient obtained by linear regression analysis

RF, Radio frequency

ROC, radius of curvature of the focused transducer (m)

S, shear wave

SLAM, Scanning Laser Acoustic Microscopy

T, period of vibration

TIFF, tagged-image file format

TOT, time-of-transition (μs)

USDA, United States Department of Agriculture

WCF, water-filled channel defect in foil-containing film

WCP, water-filled channel defect in all-plastic film

y(t), axial distance

Z, characteristic acoustic impedance (rayl = $kg/(m^2 \cdot s)$)

Greek Letter Symbols

α, significance level in ANOVA test

ΔBAI, contrast descriptor of a defect in the BAI-mode image

λ, wavelength (m)

ρ, density (kg/m^3)

θ, Diffraction angle

τ, pulse duration (μs)

$\tau_{(-20\text{-dB})}$, the pulse duration between times when the pulse amplitude is at -20-dB of its maximum values

-1-

INTRODUCTION

Thermal processing is an effective way to meet food preservation demands, both in economy and quality, because it can effectively retard or suppress microbial growth. As long as the package remains hermetically sealed, commercial sterility of the product remains intact, and therefore, it does not need refrigeration. An important requirement for any packaging material used in packaging thermally processed foods is that integrity of the container be maintained after filling and sealing, to prevent the possible penetration of microorganisms.

Flexible food packages such as microwaveable retort pouches and trays offer consumers lightweight, durable, easy-to-open packaging. Preservation of foods in them is superior to traditional cans and glass containers. Container integrity is well understood for traditional can and glass containers, but it is still a major problem for flexible food packages, and thus, these packages can not be produced economically because of inspection costs.

Flexible packages have a fusion weld of two comparable polymeric surfaces, and the integrity of these seals is central to the utility and safety of the package and product. Any compromise of the seal area may cause contamination or leakage in the package. Since government agencies such as U.S. Department of Agriculture are pressing for zero tolerance of pathogens in foods, some of the food products packed in these packages are still refrigerated or frozen although they should not be. Unfortunately, space for refrigeration and freezers is a scarce piece of

real estate at the retail level.

The food processing industry commonly uses destructive testing such as burst testing to perform spot checks of materials and sealing equipment. However, destructive testing is slow and expensive due to the personnel costs and product loss, and gives only statistical assurance, which does not guarantee the safety of untested package.

Currently, the manual inspection of seal defects is mandated [U.S. Code of Federal Regulations, 9CFR§381.301(d)]. Producers visually inspect each container, once after the post-fill sealing and again after thermal treatment in a steam retort. Even though this inspection procedure is not destructive, its inefficiency and high personnel costs restrict economical use of these packages. Furthermore, human ocular resolution is approximately 50 μm, and anything smaller than this size may not be detected by the simple visual inspection. In order to overcome those problems a dependable non-destructive inspection method is necessary to ensure the product safety and enable rapid detection of flexible food packages.

The primary objective of this study was to develop a nondestructive sensing method for seal defects using the ultrasonic pulse-echo method. The on-line implementation of such a nondestructive inspection technique will allow wider implementation of energy- and material-efficient retortable pouches and trays, by reducing inspection costs.

-2-

BACKGROUND

2.A. RETORTABLE FLEXIBLE FOOD PACKAGES

Retortable flexible food packages have joined glass and metal containers to package thermally processed food products to provide a shelf-stable product (Long, 1962; Mermelstein, 1976). Retortable pouches and trays are containers, which withstand sterilization temperature of the product and retorting pressure. The concept of retortable pouch was pioneered by researchers at the University of Illinois (Hu et al., 1955; Nelson and Steinberg, 1956; Nelson et al., 1956). The two major areas of applications for retortable flexible plastic films are (a) cooking and pasteurizing processed meat and poultry products and (b) preservation and distribution of high acid and/or hot filled products (Badenhop and Milleville, 1980).

2.B. MATERIALS FOR FLEXIBLE PACKAGING

Flexible containers such as retort pouches and trays are constructed of polymeric laminates and coextrusions with little or no metallic content (at most, an extremely thin (<25 μm) foil layer laminated in the interior of material). The basic requirement for such packages is the heat resistance because they must be tough enough to withstand retorting temperature of approximately 250°F, yet allow convenient peel opening by the consumer prior to placing the product

in the oven. Other important requirements for retort pouches and trays depend on the characteristics of the product, the type of packaging machine to be used, and shelf-life demands (Yamaguchi, 1990; Bakker, 1986). Table-2.1 lists some examples of typical pouch and tray structures.

2.C. ADVANTAGES OF FLEXIBLE PACKAGING OVER CANS

2.C.1. Product Quality

Lampi (1977) suggested that pouched products exhibited flavor, color, textural, and nutrient quality improvements compared to canned products. Adams et al. (1983) reported that retort-pouch processing of different types of seafoods such as mackerel, red snapper, blue crab, and shrimp was an excellent alternative to conventional canning due to the greater flavor retention of pouched products. According to Good Housekeeping Institute's survey (Sloan, 1985), most consumers strongly agreed that the quality of retort pouch foods is better than that of frozen foods and far superior to canned foods. In the study of Durance and Collins (1991), the pouch-processed chum salmon was firmer, drier, and chewier and had a greater volume of free liquid within the container than the canned product. Sensory panelists reported greater acceptance of pouch-processed products. As a final example, Kluter et al. (1994) reported the quality improvement of sliced peaches in the retort pouch compared to freeze dried peaches in a military field ration.

The pouch has a thinner profile than cans and the "cold spot" in it is much closer to the heating surface than that in cans, i.e., the cook-time required for commercial sterility decreases in flexible containers. Thus, the sensory and nutritional quality of foods in retort pouches is superior to the similar products

Table - 2.1. Typical pouch structures

Package Type	Material Composition
Plastic Pouch-2 ply[1]	15 μm ON/70 μm PP
Plastic Pouch-2 ply[2]	12 μm ON or PE/70 μm PO
Aluminum Foil Pouch-3ply[1]	15 μm PE/ 7-9 μm AF/70 μm PP
Aluminum Foil Pouch-3ply[2]	12 μm PE/9-12 μm AF/70 μm PO
Aluminum Foil Pouch-4ply[2]	2 μm PE/9-12 μm AF/12 μm PE/70 μm PO
Plastic Tray[1]	Lid: 350-450 μm PP/PVDC or EVOH/PP Body: ER/50-100 μm AF/50 μm PP
Aluminum Foil Tray[1]	Lid: ER/ 50-140 μm AF/ 50 μm PP
Pouches for High Speed Packaging Machines[3]	PET/LDPE/AF/LDPE
Processed Meat Packaging Pouches[3]	PET-PVDC/LDPE
Pouches for Alcohol Wipes[3]	11 μm BOPP/PE/15 μm PET
Pouches for Medicinal Wipes[3]	11 μm BOPP/PE/AF/PE/15 μm PET

References:

1 Yamaguchi, 1990
2 Paine and Paine, 1992
3 Bakker, 1986

Abbreviations:

AF=Aluminum foil
BOPP=balanced oriented polypropylene
ER=epoxy resin
EVOH=ethylene-vinyl alcohol copolymer
LDPE=low density polyethylene
ON=oriented nylon
PE=polyethylene
PET=polyethyleneterephthalate
PO=polyolefin
PP=polypropylene
PVDC=polyvinylidene chloride;

in conventional cans.

2.C.2. Product Cost

The retort pouch was indicated as an alternative packaging system for the meat industry by virtue of the constantly rising cost of metal cans (Delaquis et al., 1986). Furthermore, pouches occupy less space in storage than cans. In the report of Badenhop and Milleville (1980), replacing canning and freezing methods by retort pouch processing technique required less brine and sugar syrup for commodity-type foods such as corn, green beans, pears, and peaches. The reduction in the brine and sugar syrup, most of which is already discarded by the consumer, results in a weight reduction with the appreciable savings in raw material, energy consumption and shipping costs. In addition, the product with the reduced liquid retains more flavor since less flavor will be lost to the syrup.

Steffe et al. (1980) indicated that the use of retort pouch provided for declines in energy consumption during container manufacture and delivery, food processing, product transportation and storage. The processing time and, therefore, the thermal energy requirements for retorting pouches are less than for the similar product in cans because of the pouch geometry which provides more advantageous heat transfer than that of cans. Equipment manufacturers have estimated as much as 70% reductions in processing time for pouches to cook an equal mass of food in a sterilizing retort (Williams et al., 1983). In addition to that, freight and energy costs for food products packaged in retort pouches are less than those in cans because the equivalent amount of product is transported by fewer shipments with a lower final energy requirement. Finally, empty pouches save up to 85% in storage space compared to empty cans (Mermelstein, 1976).

2.C.3. Convenience

In 1979, the military started to replace the canned "C-Ration" with the retort pouch because it offered several advantages (Badenhop and Milleville, 1980; Morris, 1989). The U.S. military terms this packaged-food concept as "Meals Ready to Eat" (MRE). As with canned food products, those protected in retortable pouches are also shelf-stable, i.e., no refrigeration needed. Unlike traditional metal cans which can not be put in microwave ovens, retortable pouches excepting those which contain foil are microwaveable. Since traditional metal cans are made up of rigid materials, when they are heated in boiling water, the vapor pressure can cause the package to burst. However, the flexibility of retortable plastic pouches provides the reconstruction of the food product when they are heated in boiling water. Moreover, pouches are light and easy to slip into a purse; therefore, they are more portable than traditional cans. Finally, metal cans generally require a can opener but plastic pouches can be opened easily by tearing them from a notch in the seal (Mermelstein, 1976; Morris, 1989).

In summary, advantages of using retortable pouches over traditional cans are: no refrigeration needed; microwaveability (excepting foil containing pouches); reconstruction of the product by heating the pouch in boiling water; portability; easy opening and disposing of.

2.D. FORM-FILL-SEAL PACKAGING OPERATION AND HEAT SEALING

The retort food manufacturing system is composed of food-preparing equipment, package-forming machines, filling and sealing machines, and retorting equipment. Historically, the "form/fill/seal" packaging machines evolved for packaging product in pouches. It automatically forms a pouch from plastic or laminate web and

dispenses product into this formed pouch. In the production line, the package is finally sealed (Yamaguchi, 1990; Paine and Paine, 1991).

The primary method of closing flexible packages is heat sealing. Generally, the inner component of the laminated film structure is a thermoplastic material that softens with application of heat and pressure and solidifies when the source of heat is removed. On the other hand, the outer face of the structure directly contacts the heating bar without melting and transmits heat to the sealing interface to join the two surfaces.

2.E. PACKAGE INTEGRITY

Post process contamination of aseptically and traditionally processed foods is linked to seal and package integrity issues (Put et al., 1972; Put et al., 1980; Ahvanainen, 1988; McEldowney and Fletcher, 1990). The important requirement for retort pouches and trays used in food packaging is the complete fusion of opposing seal surfaces to prevent the entrance of microorganisms. A good fusion seal protects the post-process contamination of food products (Lampi et al., 1976; Floros and Gnanasekharan, 1992; Gnanasekharan and Floros, 1994).

Non traditional shelf-stable packaging such as retort pouch and tray is a serious contender for the production volume occupied by canning because of potential energy, space and cost savings. As with all-shelf stable thermally processed foods, the hermetic integrity of the package is vital to human safety and product quality. Container integrity has been researched scientifically for traditional packages, particularly metal cans, for more than sixty years. However, understanding the factors affecting that is still in its infancy for plastic containers (Harper et al., 1995; Flexible Package Integrity Committee of the National Food Processors

Association (NFPA), 1989).

2.F. TYPES OF SEAL DEFECTS

Can experts working in the NFPA and Can Manufacture Institute (CMI) have categorized metal container defects according to their significance (Flexible Package Integrity Committee of the NFPA, 1989). Throughout this process, the increased use of flexible containers has created continuing concerns about food safety and package quality, and the industry has reminded regulatory agencies about the new plastic packages that did not have the history of safety of metal cans. When the work for metal cans was completed, the industry wanted NFPA to do the same type of defining and defect classification in flexible food packages. On January 26, 1984, fewer than 10 industry members were present at the new NFPA Flexible Package Integrity Committee. In 1989, this committee had more than 130 industry experts to develop a bulletin with three specific goals.

The first goal of this committee was to provide a pictorial dictionary of common defects for producers, developers, and processors of flexible packages. The second goal was to develop "Hold For Investigation" (HFI) guidelines for industry approval, which provide the manufacture of acceptable packages. Finally, the third goal was to provide appropriate test methods for these types of packages.

The Flexible Package Integrity Committee of the NFPA (1989) has divided seal defects in plastic containers into three main categories: critical, major, and minor defects.

Critical defects are defects that cause the hermeticity loss of the container or evidence that there is, or has been, microbial growth in the package contents.

Major defects are defects that bring about a container that does not show visible indications of having lost its hermetic seal but is defective such that it may have lost its hermetic seal.

Minor defects are defects that have no adverse affect on the hermetic seals.

Table-2.2 demonstrates seal defects, their definition, and categories, which were prepared by the recommendation of industry experts on flexible packages to the NFPA Flexible Package Integrity Committee. These experts also pictured all these defects which were incorporated into the FDA poster of "Classification of Visible Exterior Flexible Package Defects" published by Association of Official Analytical Chemists (A.O.A.C). The poster also includes some information about some techniques to eliminate those defects and the good manufacturing practice.

The NFPA committee indicated that critical defects would be considered a potential public health problem. If these defects are found in any lot during the packaging or storage, the NFPA recommends a thorough inspection to ensure that no containers that have lost their hermetic seal are distributed.

The channel defect in the seal area - a critical defect type - has gained a particular interest among researchers since the minimum defect size that permits microbial contamination is still in question. Microbiological tests have attempted to quantify the approximate minimum size of a critical defect. Maunder et al. (1968) used *Aerobacter aerogenes*, a gas-producing microorganism, to detect the minimum leak size through which the microorganism penetrated the pouch. The size they found was approximately 33 μm in diameter. Lampi (1980) determined that the critical-defect dimension of bacterial penetration for flexible pouches by biotesting was 11 μm, and Chen et al. (1991) supported Lampi's value. Gilchrist et al (1989), however, found nearly twice of that (22 μm).

Table - 2.2. Defects in the seal region of plastic containers (adapted from Flexible Package Integrity Committee of the NFPA, 1989)

Type of Defect	Defect Definition	Category[1]
Blister	A void within the bonded seal	**, ***
Channel leaker	A patch of non-bonding across the width of the seal	*
Compressed seal	A seal formed by excessive pressure and/or heat	**, ***
Contaminated seal	Foreign matter in the seal area such as, but not limited to, water, grease, or food	**, ***
Convolution (Embossing)	A slight visual impression in the seal indented on one side and raised on the other side	***
Crooked seal	A seal which is not parallel to the cut edge of the pouch	***
Delamination	A separation of the laminate materials	**, ***
Misaligned seal	Improper seal position	**, ***
Non-bonding	Failure of two sealant films to combine during the sealing process	*
Seal Creep	Partial opening of inner border of seal	**, ***
Stringy seal	Presence of plastic threads at the edge of the cutoff seal	***
Uneven seal juncture	Wavy or rough appearance of bonded polymer at the inner seal juncture	***
Wrinkle	A fold of the material in the seal area	**, ***

*: Critical defect, **: Major defect, ***: Minor defect.

1 Some defects fall into both major and minor defect categories, i.e., if the defect is pronounced it becomes a major defect, and if it is slight and does not affect hermeticity, it becomes a minor defect.

Table - 2.3. Critical defect size for bacterial penetration (adapted from Blakistone, 1994)

Critical Defect Size (μm)	Experimental Technique	Author
10	Predictive equation	Floros (1994)
0.2	Filtration of certain water borne bacteria	Howard and Duberstein (1980)
11	Immersion test on pouches	Lampi (1980)
~10	Aerosol test	Keller et al. (1995)
<10	Immersion test	Blakistone et al. (1996)
80	Electrolytic test on aseptic packages	Axelson et al. (1990)
22	Immersion test on pouches	Gilchrist et al. (1989)
10	Immersion test on vials	Chen et al. (1991)
5	Spray on vials	
<10	Biocell test	Harper (1995)
< 7	Microperfusion test	Rose (1994)

Blakistone (1994) presented a compilation of minimum defect sizes (Table-2.3) that has resulted from the work of various researchers. This table demonstrates the variation of the "critical" leak size between 0.2 and 80 μm in diameter, giving no clear-cut lower limit. Harper et al. (1995) attributed this broad variation to different experimental procedures. Recent work indicated that critical-leak dimensions were 10 μm in diameter and 10 mm in length (Blakistone et al., 1996). Although Harper (1995) found virtually the same results, it was also implied in the study that this was not necessarily a practical guideline for on-line seal-defect detection systems because the method was not a definitive procedure that determines the minimum penetration size.

2.G. TESTING SEAL PERFORMANCE

As with all shelf-stable thermally processed foods, seal integrity is vital to human safety and product quality. Since seal defects and loss of seal-strength cause product loss and compromise the safety, and since government agencies such as U.S. Department of Agriculture are pressing for zero tolerance of pathogens in foods (Blakistone et al., 1996), it is imperative that packaging be checked for the presence of such defects before the package is stored. Package integrity testing can be divided into two main categories: destructive and nondestructive testing.

2.G.1. Destructive Tests

Destructive tests are invasive tests, which result in loss of package and product. To conduct these tests, a statistically significant number of samples are taken from a production line at designated time intervals. According to the NFPA Flexible Package Integrity Committee (1989), all packages in a production line should be checked for acceptable seals at the time of start-up and a minimum of once every 30 minutes thereafter.

Table-2.4 summarizes destructive seal integrity tests used by researchers and the food industry. In this table, burst, compression, drop, tensile, and vibration tests are used for measuring the structural integrity of a package whereas the other techniques are for detecting the leak in the seal region.

During filling of packages and sealing, random splattering of food fibers into the seal area may cause the formation of channel microleaks that are not clearly visible. The food industry conventionally relies upon destructive testing such as burst and tensile testing to determine a loss of seal strength in flexible

Table - 2.4. Destructive techniques for seal integrity testing

Technique	Applications/Comments
Biotest - Aerosol technique[10]	The package with its product is located in a chamber through which both aerosol- a liquid-gas phase- and a microorganism culture are injected by two separate vanes. After exposing the package in the chamber, and incubating it for certain period of time, the microbial growth in the package is tested.
Biotest - Immersion technique[2, 6, 9, 12, 15]	The package with the product is dipped into a cell culture for a discrete time period to assess the microbial integrity of the seal. Microbial growth is detected by visual observation of swelling after a period of incubation.
Biotest - Spray cabinet technique[4, 12, 19]	Packages are evaluated by directly spraying the diluted cell culture onto the surface of packages. The package integrity is evaluated by visual and/or compositional changes in packaged products caused by microbial penetration.
Bubble testing[5,7,16,18]	The package is immersed in a liquid (typically water) container, and the vacuum in the container is drawn. By virtue of a pressure differential across the package and the liquid, air or gas flow creates bubbles outside the package. This test is simple, cost efficient, and relatively rapid for large leaks; however, its sensitivity is very low, and if the food material is viscous, the leak has the tendency to get clogged.
Burst testing[5,7,11,13,14,20]	A pouch containing the product is punctured with a needle. Next, the air is added at a controlled rate until a specified pressure is attained, and this pressure is maintained for a predetermined length of time. If the container bursts before the critical pressure or during the preset time interval at the critical pressure, it fails. Since the pressure inside the package uniformly stresses in all direction, it determines the location of the leak.

Table - 2.4. (...continued)

Technique	Applications/Comments
Compression test[5,7,8]	This test measures the strength of the container against stacking in warehouses. The leak or occluded product in the seal region decreases the strength of the container. The test is conducted by compressing the container using two hydraulically driven plates until a predetermined pressure is attained. The package fails if it bursts before the critical pressure (failing load).
Drop/Impact tests[5,7,8]	They measure the performance of packages, which could be abused during the distribution cycle. The fact that the correlation of these tests with the actual distribution experience is low makes them unfavorable for the performance testing.
Dye penetration test[5,6,7,16]	This test is generally applied as a confirmatory test after the electrolysis test has detected the leak. The container is cut open and the product is drained. The chemical penetrant or dye is placed and the container is rotated slightly to allow it to wet the entire inside sealed circumference. If there is a leak, the penetrant seeps into leak indicating the failure. The major advantage of the test is that it does not require pasteurization because of the capillary action of penetrant, which makes this test to be recognized by regulatory agencies such as FDA and USDA for integrity testing of aseptic packages.
Electrolytic test[1,3,5,7]	The package is cut in half, partially filled with an electrolyte solution such as NaCl, and located in a vessel containing the same solution. The method is based on the fact that the defected package allows the electron transfer through the leak, which causes an immediate voltage difference in an electrolytic cell. The technique would not be successful if the product clogs the leak since the electron transfer is cut off.

Table - 2.4. (...continued)

Technique	Applications/Comments
Tear/Tensile testing[5,7,14]	This test is used to assess the inherent sealing qualities of flexible packaging films. Each end of a seal is mechanically pulled apart at a controlled rate until separation occurs. The total force required to cause the separation is recorded. If this force is below a previously designated critical range, the seal strength of the package becomes suspicious. The major problem of this test is the detection of any channels or stress points, and occluded particles or other weak areas within the seal that might be obscured by the adjacent high-strength areas. Therefore, the test is generally used as the surveillance of material sealability and for spot-checking.
Vibration test[5,7]	This measures the performance of packages, which could be abused during the distribution cycle. Modern vibration testers can be adjusted to simulate the sequence of vibrations of varying frequency that might happen during the distribution cycle.

References:

1 Axelson et al., 1990
2 Blakistone al., 1996
3 Charbonneau and Arndt, 1995
4 Chen et al., 1991
5 Floros and Gnanasekharan, 1992
6 Gilchrist et al., 1989
7 Gnanasekharan and Floros, 1994
8 Griffin et al., 1985
9 Harper, 1995
10 Keller et al., 1995
11 Lampi et al., 1976
12 Lampi, 1980
13 Lin et al., 1984
14 Matty et al., 1991
15 Maunder et al., 1968
16 McMaster, 1982
17 Morton, 1987
18 Morton et al., 1989
19 Pestka and Henyon, 1991
20 Yam, 1995

plastic pouches and to perform spot checks of materials and sealing equipment. The National Center for Food Safety and Technology (NCFST) (Argo-Summit, IL) has recently conducted the burst and tensile tests to correlate the channel size in the seal region with the break-point load (Harper et al., 1995). They found that burst and tensile tests were not capable of detecting channel leaks smaller than 200 μm in diameter. Destructive methods are excellent indicators to determine the seal strength of the package if statistically significant amount of packages are tested; however, they can not reliably indicate a loss in seal integrity because they are not successful detecting channel microleaks.

The most common problem with techniques compiled in Table-2.4 (except for biotests) is their inability to detect a leak which is plugged with food, which may provide a path for microorganisms to "grow through" the seal because product inclusion in the seal region prevents gas flow. Lampi et al. (1976) indicated that occluded particles in the seal region resulted in the decrease in the overall bursting strength of retort pouch seals after six months of storage. Inspection of such defects by the destructive techniques may give a "false positive" result if immediately tested after the production, which might jeopardize the seal strength of the package during the distribution. Thus, occluded particles as well as microleaks require detection by more advanced techniques.

Warrick (1990) conducted a survey in Europe and demonstrated that nearly 50% of 120 aseptic systems had at least one non-sterile package per 10,000 packages and that less than 20% of these systems accomplished the required sterility in their packages. Warrick (1990) also indicated that more than 2% of total production volume in packaging operations is lost, and that about 7% of the total operating time is wasted due to destructive testing.

These findings demonstrate that destructive inspection techniques are costly and inadequate for indicating channel microleaks and obscured particles in the seal region. Furthermore, these tests rely upon a statistical assurance of integrity that does not guarantee complete indication of randomly occurring defects, since they can not test all packages. Therefore, there is a need for a reliable, fast, and inexpensive nondestructive technique to evaluate the seal integrity of shelf-stable flexible plastic packages if they are to economically replace traditional, less material- and energy-efficient rigid cans and jars.

2.G.2. Nondestructive Tests

Nondestructive testing is the examination of the sample under investigation by such a procedure that the test does not impair its usefulness for future applications. The rapid automation of industrial processes and commitment to total product quality of the industry require highly effective and inexpensive nondestructive techniques to inspect any deviations from the predetermined product specification.

Nondestructive inspection can also ensure the product safety and may enable rapid detection of defects in the seal region of flexible food packages. Table-2.5 summarizes nondestructive techniques for the seal defect inspection, which have been evaluated by several researchers.

Human visual inspection is currently mandated for quality control by the U.S. Code of Federal Regulations in 9CFR§381.301(d) and by 21CFR§113. However, several researchers (Nughes, 1974; Tsutsumi, 1974; and Lampi et al., 1976) have already proved its disadvantage due to subjectivity and human error. The lowest failure level by visual on-line 100% inspection was about 0.01% for seal defects in pouches, i.e., one defected package in every 10,000 package would pass the

Table - 2.5. Nondestructive techniques for seal integrity testing

Technique	Applications/Comments
Acoustic - Scanning Laser Acoustic Microscopy (SLAM)[7,15]	It is an acoustic transmission microscope, which uses transmitted sound waves instead of light. It can determine point-by-point measurements of the bulk wave ultrasonic propagation properties of a thin specimen. Even though it has recently detected channel microleaks as small as 10 μm in diameter, its on-line implementation is impractical since the equipment is cumbersome and expensive. Speed: real time (30 per sec)
Acoustic - Ultrasonic tap test[6,10]	This test characterizes materials based on their acoustic resonance. If a composite material is well formed, i.e., good bonding, an ultrasonic pulse can excite it, and it resonates with specific frequency. If there is a delamination in the same material, its resonant frequency will be altered. The test has been conducted to measure metal delaminations and no information is avalible for testing the delamination in plastic retortable pouches.
Acoustic - Ultrasonic transmission technique[9]	This technique has recently been described for testing the seal integrity of a package having a lid bonded to the container rim by a U.S patent. An average transmitted ultrasonic signal is obtained from the undisturbed region of the seal, and the signal is compared with the reference signal. Its sensitivity to channel microleaks is in question since experiments have been conducted only for product contamination type defects, and their size was relatively large (one mm^2 of meat fiber). Speed: not available
Backscatter/absorption gas imaging[6,13]	It is a 3-D vapor visualization technique. Tracer gas, which should absorb the laser light for this technique to work, is pumped into the vessel containing the package. If there is a leak, the gas penetrates into the package. Back-scattered laser light is then illuminated to produce the 3-D video image of the gas escaping from the package through the leak. Even though it provides a real-time information on leak location, it would not work for clogged leaks. Speed: not available
Caliper test[4,5,11]	Calipers are used to measure any irregularities in seal thickness. Occluded particles and fold-type seal wrinkles could be detected, but their size has to be larger than that detectable by infrared scanner. Even though it is inexpensive, its sensitivity against microscale defects is poor. Speed: not available

Table - 2.5. (...continued)

Technique	Applications/Comments
Capacitance test[2,7]	The package is passed between conducting plates, and the capacitance, which is a proportionality constant expressing the potential difference between the plates, is measured in Farads. Although it requires less processing time than machine vision imaging does, it detects defects larger than 120 μm in diameter. Speed: Real time (30 per sec).
Eddy current probe test[2,3,7,8,14]	The package is exposed to metal to transmit the electrical current. Whereas it can not detect the defects in clear plastics, it works for foil laminate pouches. It detects macro defects (>200 μm). Speed: Real time (30 per sec).
Electronic Speckle Pattern Interferometry (ESPI)[1]	ESPI is also known as shearography that provides both quantitative and qualitative information about materials and structure. It produces an image of the strain field of the sample under inspection using the laser illumination. In this test, the sample is illuminated with laser light, and a reference image is captured. After the pressure is applied to the sample, a second image is captured and subtracted from the reference, which reveals the fringe pattern of a change in strain. This method has been applied to rigid plastic containers. Seal integrity of flexible packages has not been evaluated by this technique so far. Speed: not available.
Fiber optic array[7]	A beam of light at visible spectrum through a transparent object is measured. It does not work for opaque materials, and its sensitivity for transparent materials is limited to macroscale defects (>200μm). Speed: Real time (30 per sec).
Infrared thermography[4,7,11,12,16]	This method measures thermal fields that are characteristics of a material. Thermal fields are generated either by stress (cyclic loading) or heat source. If the heat flow impedes the defect in the material, the normally uniform isotherms created are distorted in that location and this temperature alteration can be detected by infrared microscope. The technique can deal with opaque packages but extremely sensitive to environmental conditions. Thus, it requires a precise temperature control. Its sensitivity is currently limited to macroscale defects (>1000μm). Speed: not available.

Table - 2.5. (...continued)

Technique	Applications/Comments
Infrared laser[7]	It measures the transmittance of a beam of infrared light through a transparent object. Its sensitivity is limited to macroscale defects (>125 μm for solids; >200 μm for gas). Speed: Real time (30 per sec).
Magnetic Resonance Imaging (MRI)[7,14]	MRI uses magnetic fields and radio waves to produce two- and three-dimensional images. The principle is that after an exterior radio signal is applied to a sample, protons (hydrogen nuclei) in the sample absorb energy and emit radio signals, which are used for image formation. Signals emitted by protons in the defective region are different from those in the non-defective region. The MRI does not detect voids while it detects channel leaks with water in the seal area as small as 30 μm because the MRI signals are extracted from protons in water. If the defect does not contain water, the MRI does not produce useful signals to construct the image. Speed: In the order of seconds.
Machine vision imaging[7]	A video camera in combination with image processing techniques is used. The method is only limited to clear materials. The technique will detect only surface artifacts of defects and inclusion in the heat seal, and not the defect or inclusion itself. For example, star burst defects, which occur when foreign materials are trapped in the seal region of foil packages, can be visualized by an appropriate image processing technique. The method works for macroscale defects (>269 μm). Speed: In the order of seconds.
Pressure difference method - External pressure technique [4,6,17,18]	The package is located in a vessel where the pressure is increased to create a pressure difference between the package and vessel. If there is a leak, the external pressure as a driving force causes the test gas in the vessel to flow through the package. The gas flow through the package causes the deflection, which can be measured by a proximity sensor. This technique detects 50-μm-diameter channel leaks. If the leak is occluded by a product, there will be no flow, i.e. the test will result in a false positive. Speed: not available

Table - 2.5. (...continued)

Technique	Applications/Comments
Pressure difference method - vacuum technique[4,6,17,18]	The technique is very similar to the External pressure technique. The difference is that the vessel is vacuumed, and the flow occurs from the container to the vessel if a leak exists. A proximity sensor measures the structural change. If the package contains CO_2 or N_2 in its headspace, sensitive gas sensors can also measure this. The method gets insensitive when measuring microleaks since the product in the package tends to clog the leak due to outward flow. It can be used for detecting macroleaks (>100μm). Speed: not available
Pressure difference method - Trace gas "sniffer" technique[4,6]	The method consists of applying an over pressure of tracer gas to the outside of the package. Next, the package is located in a vessel where the vacuum is drawn to create a pressure differential across the package wall. If a leak exists, the tracer will be forced to flow through it. O_2, CO_2, N_2, He, and water vapor are commonly used tracers. Trace gas detection involves analytical determination of the presence of the gas in the package. For measurements, infrared detectors, gas chromatography, and mass spectrometers are used. Even though the technique is the most sensitive method (>17 μm in diameter) currently available, it will not be successful if the leak is clogged with a product, or if any moisture inside the package plug up leaks. Speed: not available
X-ray[3,7,8]	This technique is highly sensitive to defects such as water droplet and sees through opaque packages. However, the technique has a significant disadvantage against the microscale air voids because the microleak in the seal should contain only materials with significantly higher electron density than the hydrocarbons of the package such as water and carbohydrates of the food in the package. Speed: Real time (30 per sec).

References:
1 Allemeier, 1995
2 Bray and Stanley, 1997
3 Boving, 1989
4 Floros and Gnanasekharan, 1992
5 Foxboro, 1966
6 Gnanasekharan and Floros, 1994
7 Harper et al., 1995
8 Hull and John, 1988
9 Jarman et al., 1994
10 Jones and Berger, 1989
11 Lampi et al., 1973
12 Lampi et al., 1976
13 McRae, 1989
14 Mix, 1987
15 Safvi et al., 1997
16 Scott and Scala, 1982
17 Staufer, 1988
18 Yam, 1995

visual inspection and directly go to the consumer. Furthermore, visual inspection has high personnel costs; estimated at $10,000/million packages (Harper et. al, 1995) and has low sensitivity to detect surface artifacts smaller than approximately 50 μm. It also offers no capability of seeing through opaque material such as the MRE (meal ready to eat) foil containing pouches already used by the U.S. army.

Harper et al. (1995) evaluated some of the nondestructive techniques in Table-2.5 for seal integrity testing based on start-up cost, speed, and the resolution of sensors. These techniques were machine vision imaging, infrared imaging, infrared laser/fiber optic array, capacitance, spectrophotometer, X-ray, eddy current probes, magnetic resonance imaging (MRI) and Scanning Laser Acoustic Microscope (SLAM). Harper et al. (1995) indicated that they had some application possibilities; however, only X-ray, MRI, and ultrasound have the resolution to detect microchannels within the seal. X-ray systems have so far not been able to demonstrate the ability to find an air filled microleak although it has an excellent resolution for water filled microchannels. MRI has an extremely long computation time by production line standards and does not detect air filled defects. On the other hand, Safvi et al. (1997) indicated that SLAM - an ultrasonic transmission technique- can nondestructively image microchannels (as low as 10 μm in diameter) in the seals irrespective of the type of the inclusion in the leak as well as optical properties of the material. In short, ultrasound has offered the best combination of accuracy, speed and safety among all nondestructive techniques evaluated so far.

2.H. ULTRASOUND

2.H.1. Terms and Classification of The Acoustic Spectrum

Acoustics is the science of sound and involves its production, transmission, and reception. The entire frequency range of sound is termed the acoustic spectrum. The frequency, Hz, is equal to one vibration per second, or one cycle per second. The acoustic frequency ranges are classified into three ranges: *infrasound, audible sound,* and *ultrasound. Infrasound*, which is the lowest classification in the acoustic spectrum, has a frequency range below 20 Hz, and human ear does not sense the vibration at this frequency. *Audible sound* is what humans hear and has an approximate frequency range of 20 Hz to 20 kHz. *Ultrasound* means a region of acoustics above the upper limit of sound frequencies which the human ear responds to (>20 kHz). The term *ultrasonics* refers to the science and technology that deal with the generation, propagation, detection, and use of ultrasound. (Leonard and Gardner, 1973; Kinsler et al., 1982; Szilard, 1987).

2.H.2. The Nature of Sound

Sound is the rapid motion of molecules and is produced when a body vibrates. These molecular vibrations are not random, as in the case of thermal vibrations, but are orderly, oscillatory vibrations generated by an external energy source. The vibrations transport energy through both fluid and solid media. They are transmitted from one mass to another by direct and intimate contact between the masses. In that regard, they differ from light and other forms of electromagnetic radiation, which travel freely through the vacuum whereas acoustic vibrations do not exist in a vacuum (Blitz, 1960; Kinsler et al., 1982).

2.H.3. Acoustic Waves

A wave is a disturbance whose position in space changes with time. Sound propagates in waves. Acoustic waves mean that this disturbance is of an elastic nature; that is if a particle (or small volume element) of the material is displaced from its equilibrium position by any applied stress, internal forces tend to restore the system to its original equilibrium. During the propagation of a sound wave, molecules get closer together (compression), and then they separate (rarefaction). Due to the rapid back and forth motion, the sound is called either a mechanical wave, or an elastic wave, or a mechanically propagated wave. Particles making up the medium are not traveling in a direction away from the source but are only vibrating about their mean positions. It is the energy that is moving progressively from molecule to molecule. The actual displacement of particles in ultrasonic wave is very minute (Blitz and Hogarth, 1960; Kinsler et al., 1982).

There are a number of different types of acoustic wave motions that can be propagated, mostly in solids.

(a) Longitudinal waves: In a medium where the boundaries are so far away from the site of original motion, that they have no effect on the waves, particle vibrations occur in the same direction as the motion of the sound (Figure-2.1). Since particles in the medium move back and forth, the density and pressure of the medium will fluctuate. For this reason, these waves are also called compressional or pressure waves (Szilard, 1987; Bray and Stanley, 1997)

(b) Transverse or shear waves: The displaced particles vibrate in a direction perpendicular to that of wave propagation (Figure-2.2).

(c) Rayleigh waves: They are very similar to shear waves, but they travel

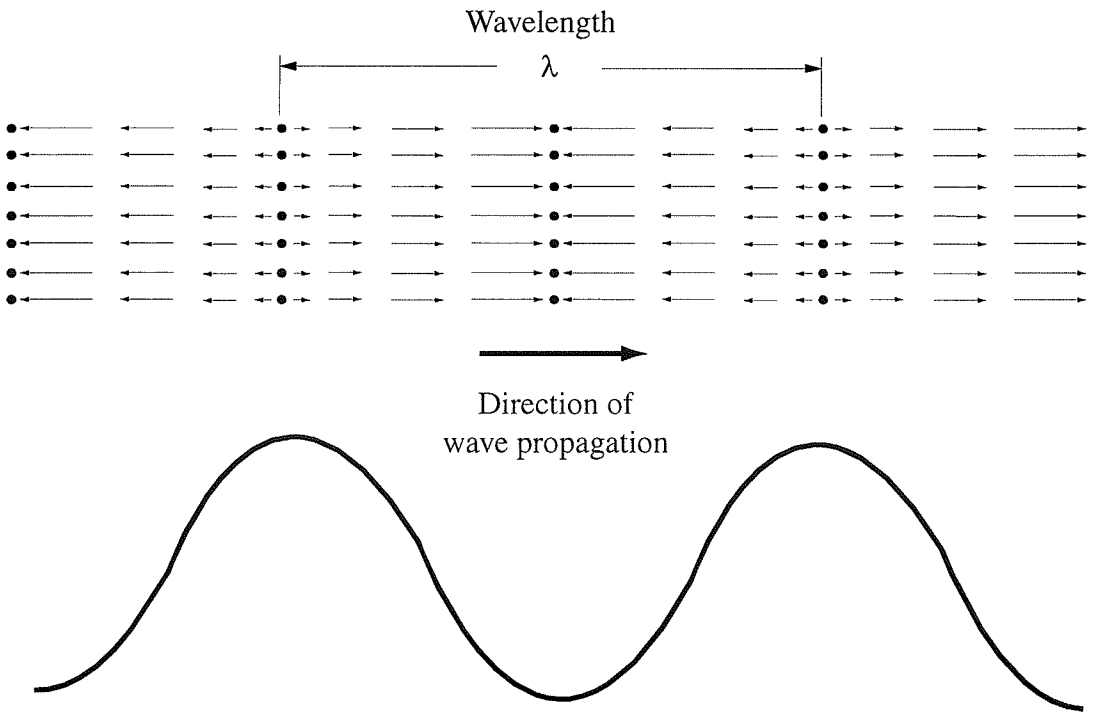

Figure - 2.1. Particle motion for a longitudinal wave

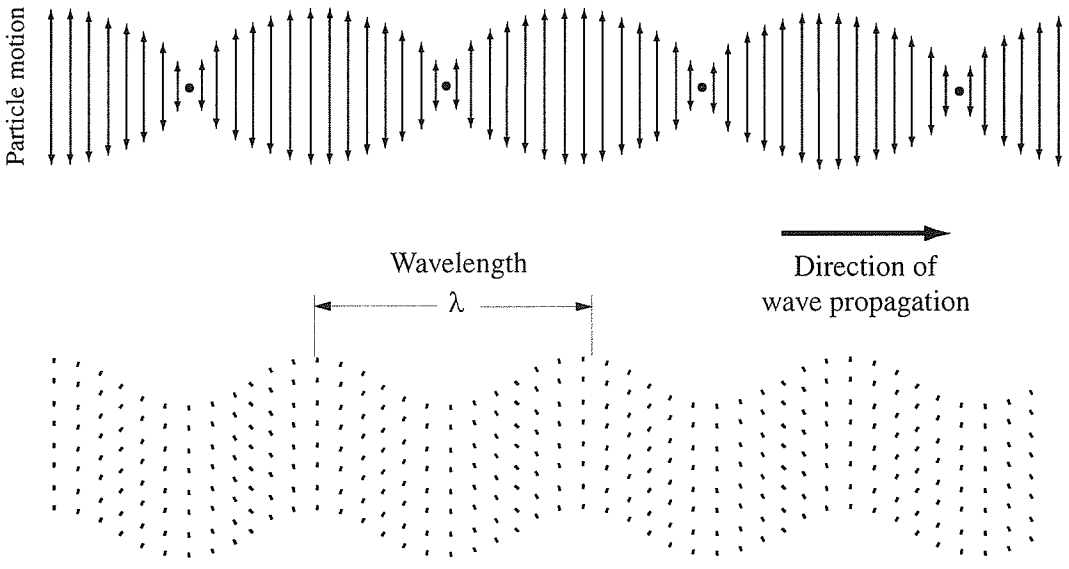

Figure - 2.2. Particle motion for a shear wave

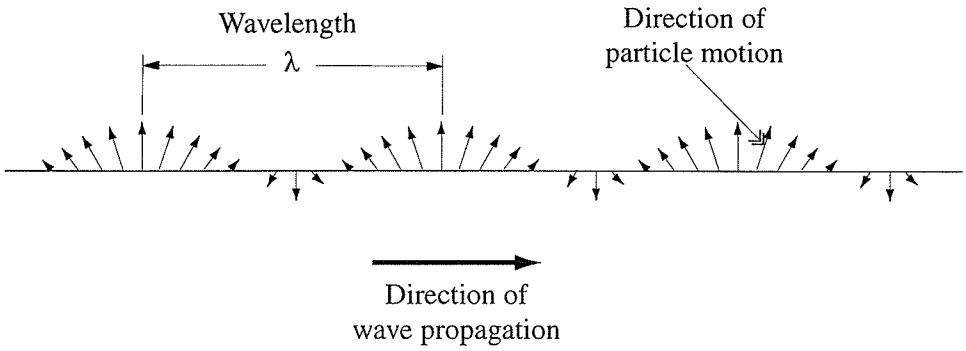

Figure - 2.3. Particle motion for a Rayleigh wave

across the surface of a solid medium similar to the ripples on water surfaces (Figure-2.3). Thus, they are also called surface waves. The unique feature of these waves is that the energy concentrated on the surface makes them useful for detecting surface defects.

(d) Torsion waves: They are also called rod waves or flexural waves since they occur in rods or wire when the driving source performs an oscillatory, twisting action about the rod axis.

(e) Lamb waves: The propagation of wave occurs in thin specimen or plates, resulting in flexural vibrations of plate. Delaminations near the surface of composite materials can be detected using these waves.

Although longitudinal waves can propagate in any elastic/compressible medium (solid, liquid, or gas), shear waves can barely propagate in gases and liquids.

2.H.4. Speed of Sound

Physical properties of the medium such as elastic constants and density

determine the speed of sound, which is given by (Szilard, 1987):

$$c = \sqrt{\frac{\text{Elastic Modulus}}{\text{Density}}} \qquad 2.1.$$

where elastic modulus is a material constant describing its elasticity by relating stress to deformation, i.e.,

$$\text{Elastic Modulus} = \frac{\text{Stress}}{\text{Strain}} \qquad 2.2.$$

where stress is the deforming force applied to the unit area and has the unit of Newton per meter square (N/m^2), or Pascal:

$$\text{Stress} = \frac{\text{Force}}{\text{Area}} \qquad 2.3.$$

In addition, strain is the dimensionless deformation constant represented in terms of a relative change in dimensions when subjected to a stress:

$$\text{Strain} = \frac{\text{Change in Dimension}}{\text{Original Dimension}} \qquad 2.4.$$

Each particle in the medium vibrates in a simple harmonic motion. Figure-2.4 demonstrates the sinusoidal displacement of particles in the medium as a function of time (a) and of distance from the source (b). The high crests and low troughs depict the amplitude values of the wave and correspond to peak compressional and peak rarefractional values, respectively. The time that it takes for one cycle to occur is called the period (T in Figure-2.4a), and its reciprocal is frequency ($f = 1/T$). The distance from one crest to the next in Figure-2.4b is called the wavelength (λ). Thus, the propagation speed of sound, c, is equal to

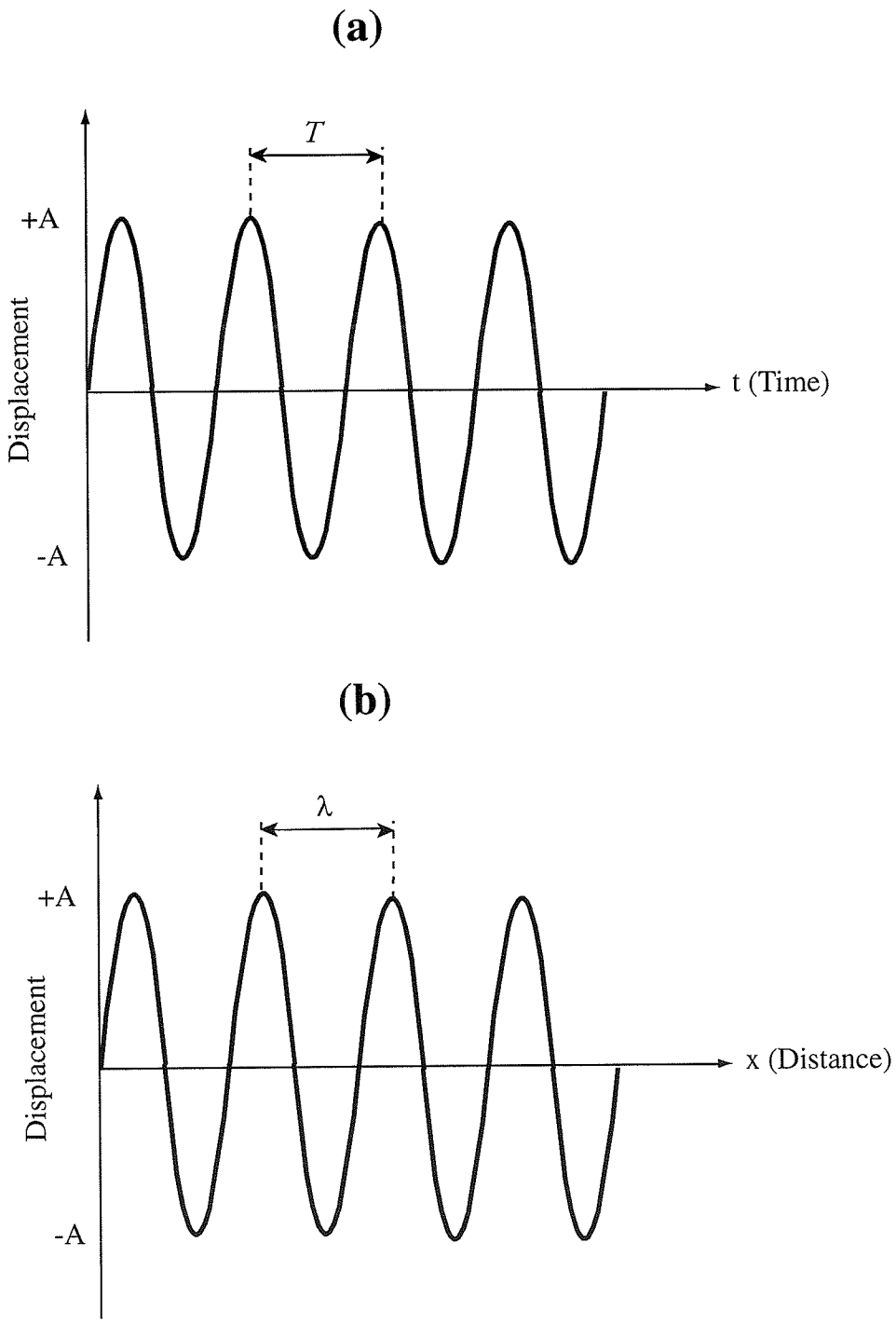

Figure - 2.4: (a) Vibratory particle displacement at a fixed point; (b) the spatial variation of the displacement at a fixed time in a material for the sound wave (A = amplitude of vibration; T = period of vibration; λ = wavelength)

$$c = \frac{\lambda}{T} = \lambda \cdot f \qquad 2.5.$$

2.H.5. Sound Waves at Interfaces

There are limits for sound propagation at an interface between two media of differing elastic properties. When an ultrasonic wave propagating in a medium faces a boundary with another medium, reflection, refraction, and mode conversion may occur. Refraction and mode conversion occur when the ultrasonic wave approaches the boundary at an oblique incidence whether the incident wave is longitudinal or transverse. Mode conversion is partial conversion of the acoustic energy from a longitudinal wave to a shear wave or vice versa.

Figure-2.5 shows the sound propagation from medium (A) to (B) at normal incidence. As the sound travels across a boundary from a medium (A) to another

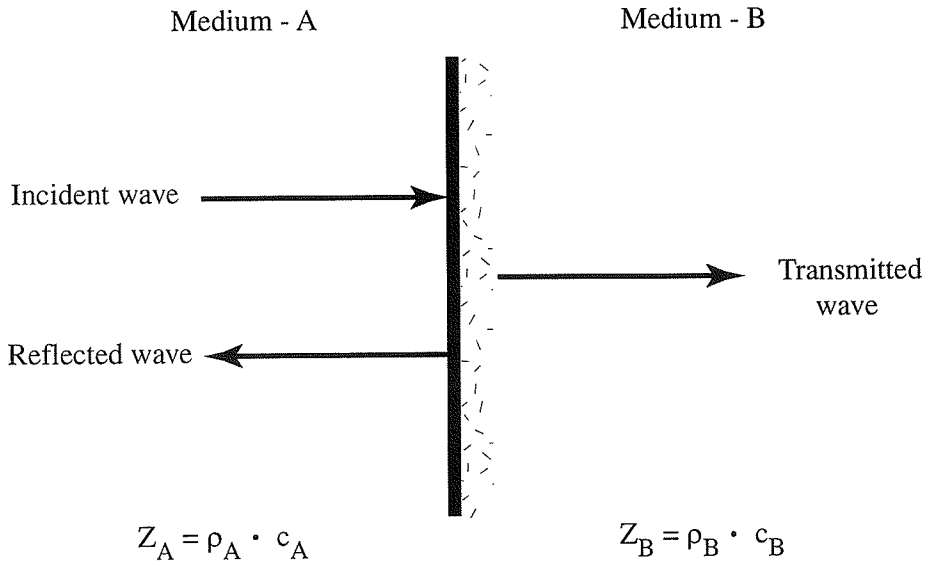

Figure - 2.5. Reflection and transmission of sound waves normally incident on a boundary

medium (B), part of the energy is transmitted across the boundary to the medium (B), and part is reflected back into medium (A) (Kinsler et al., 1982).

The multiplication of two physical quantities (sound speed (c) and density (ρ)) of a material produces an important parameter; it is called the characteristic acoustic impedance, $Z=\rho \cdot c$ whose unit is $kg/m^2 \cdot s$ or rayl (Kinsler et al., 1982). The ratio ($m = Z_A/Z_B$) determines the amount of energy reflected or transmitted. When m is unity, no reflection occurs, i.e., all of the energy is transmitted through from medium A to B; when it is much greater or less than unity, most of the energy will be reflected.

Table-2.6 demonstrates typical density, propagation and characteristic acoustic impedance values for isotropic media - the media whose physical properties do not influence the direction of the ultrasonic wave, i.e., the sound energy is equally transported in all directions. The characteristic acoustic impedance of solids is exceedingly larger than that of both liquids and gases, and that of liquids is

Table-2.6. Characteristic density, propagation, and acoustic impedance values for isotropic materials (adapted from Selfridge, 1985)

	Characteristic Density (kg/m^3)	**Characteristic Sound Speed (m/s)**	**Characteristic Acoustic Impedance (Rayl=$kg/(m^2 \cdot s)$)**
GAS	10^{-1} - 1	100 - 1000	100 - 500
LIQUID	800 - 1200	900 - 2000	$0.8 - 1.8 \cdot 10^6$
SOLID	1200-10000	1800 - 8000 (L) 1500 - 5000 (S)	$3 - 60 \cdot 10^6$ (L) NA (S)

(L) Longitudinal wave
(S) Shear wave
NA Not available

much larger than that of gases. When ultrasonic wave is attempted to propagate from a gas medium with a low characteristic acoustic impedance to a solid medium with a high characteristic acoustic impedance or vice versa, the incident energy propagated in the first medium will be barely transmitted through the second medium. For example, reflection of sound at an air/steel interface is practically 100% and, therefore, sound can not be transmitted easily into a metal across an air gap. To overcome that problem, a coupling agent, such as water, oil, gel or cream is generally used to transmit the acoustic energy to the interior body of the other medium through an ultrasonic transmitter. For instance, approximately 6% of the incident sound energy will be transmitted across the water/steel interface.

2.H.6. Sound Attenuation in The Material

Attenuation is the loss of the sound energy from a sound beam as it travels through the material. Attenuation has three main components that dominate the process (Kinsler et al., 1982; Bray and Stanley, 1997).

1 - *Absorption*: In a homogeneous medium such as a gas, a liquid, an amorphous solid, or a single crystal, part of the acoustic energy is degraded into thermal energy due to internal friction (viscous losses), heat conduction losses, losses associated with molecular exchanges of energy, and relaxation.

2 - *Scattering*: In a polycrystalline solid or a basically homogeneous material containing particles of different characteristic impedance, part of the acoustic energy is lost in the form of scatter, which is the reradiation of the small amount of acoustic energy in different directions.

3 - *Beam divergence*: It is basically a geometric function where the intensity (W/m^2) is reduced as the beam area increases at greater distances from the transmitter.

The intensity decreases with the square of the distance traveled if the radius of the souce (a) is small compared to a wavelength (λ) so that $ka<<1$, where k ($=2\cdot\pi/\lambda$) is the wave number.

2.H.7. Generation of Ultrasound

The most common method of producing ultrasonic waves for nondestructive testing is to utilize the piezoelectric or ferroelectric effect in a crystal which mechanically deforms when an electric field is applied to it (Hull and John, 1988). Conversely, if a piezoelectric material is deformed by the application of external mechanical stress, it becomes electrically polarized and produces a voltage difference that is proportional to the amount of the strain. A piezoelectric crystal has the ability to perform the opposite function in converting mechanical pulse into an electrical signal and, therefore, it can be used as both a generator and a receiver. Some of the piezoelectric materials are quartz, lithium sulfate, zinc oxide, cadmium sulfide, and ceramic materials such as lead zirconate titanate and barium titanate (Leonard and Gardner, 1973; Szilard, 1987). Any device that converts one type of energy into another type is known as a "transducer". The term transducer will be used here to describe devices which convert mechanical energy to electrical energy, and vice versa.

2.H.8. Characteristics of Ultrasonic Beam

In ultrasonic nondestructive evaluation, there are multiple transducer shapes. The circular shaped, unfocused, plane piezoelectric transducer produces ultrasonic waves, which, for most practical purposes, behave like waves diffracted through a circular aperture. These waves will emerge initially as a parallel-sided beam that later diverges (Figure-2.6). The ultrasonic field demonstrated in the figure is the spatial distribution of the transducer's radiated energy. The field is divided

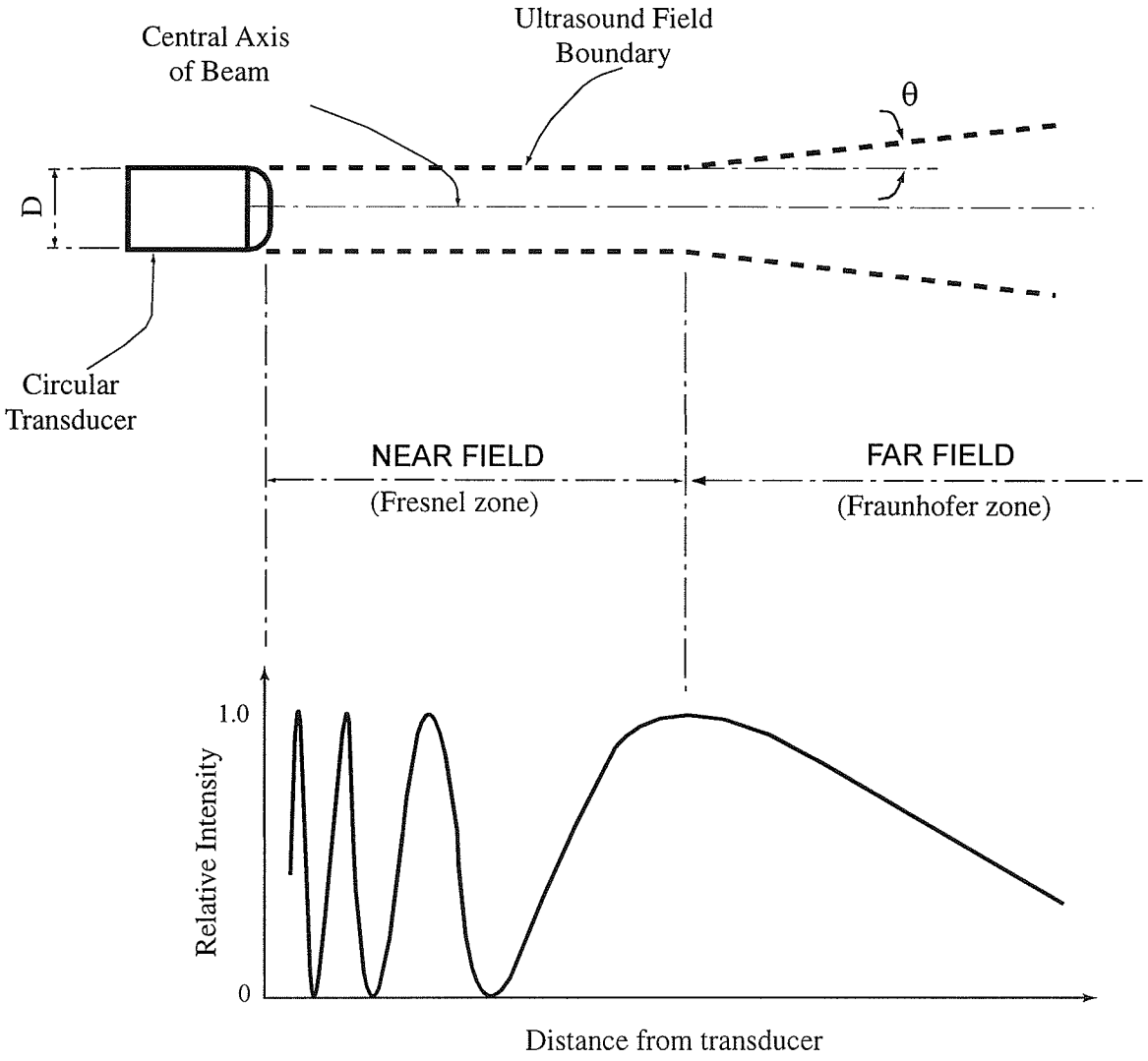

Figure - 2.6. The axial intensity distribution of an ideal circular transducer

into two regions - the near field or Fresnel zone and the far field or Fraunhofer zone (Kinsler et al., 1982; Mix, 1987).

Near field or Fresnel zone: In this zone, there exists axial variations in beam intensity with maxima and minima as shown in Figure-2.6. The length of the near field can be expressed as:

$$N = \frac{D^2 - \lambda^2}{4 \cdot \lambda} \quad (\text{if } D >> \lambda) \qquad 2.6.$$

where λ is the wavelength of the ultrasound beam and D is the diameter of the transducer. Due to the strong fluctuation of beam intensity, the detection sensitivity is not constant throughout this zone. Knowing the length of zone is important so that it may be avoided for some measurements.

Far field or Fraunhofer zone: This is the region beyond the near zone where the beam begins to spread outwards, and the far field starts beyond the last area of the maximum beam intensity. A slow divergence of the beam occurs in the beam intensity, which is typically a smooth falling-off of beam intensity (Figure-2.6). The beam diverges at an angle, θ, which is given by

$$\sin \theta = 1.22 \cdot \lambda \cdot D \qquad 2.7.$$

In the near field the beam width is equal to the diameter of unfocused transducer whereas it is dependent upon the diffraction angle (θ) in the far field. From the formula for near and far fields, it is evident that both λ (or frequency) and D affect the form of beam field and width (BW). Figure-2.7a demonstrates the beam width of two, unfocused circular transducers operating at the same frequency (or same wavelength, λ) of different diameters ($D_1 < D_2$). The first transducer has smaller near field and larger diffraction angle in the far field

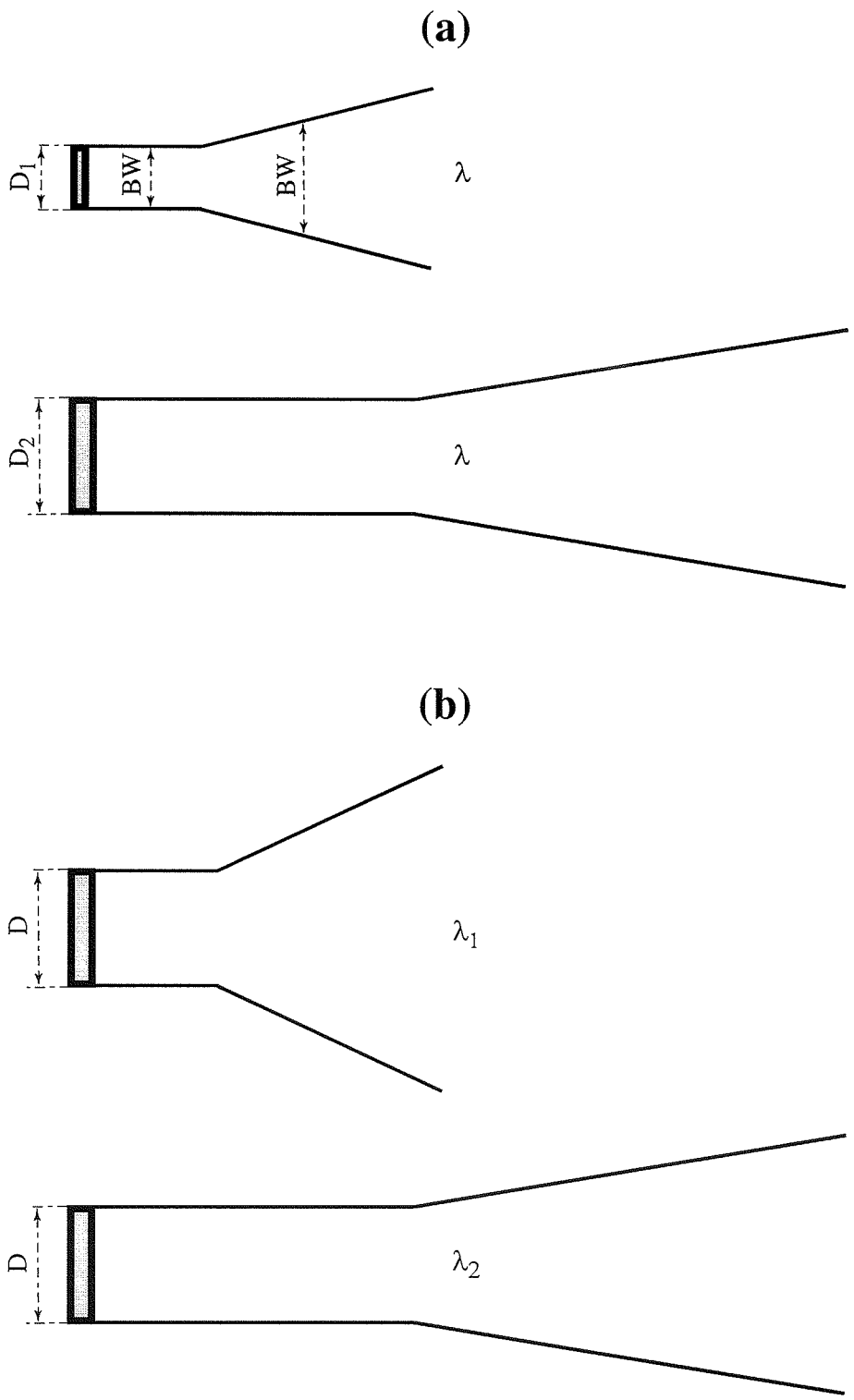

Figure - 2.7. Beam forms and beam width (BW) (a) at the same wavelength (λ) with different transducer diameters ($D_2 > D_1$); (b) at different wavelength ($\lambda_1 > \lambda_2$) with the same transducer diameter (D).

than the second transducer has. Thus, increasing D actually causes a decrease in the overall beam width in the far field. In Figure-2.7b, two transducers have the same diameter, but this time they operate at different wavelengths ($\lambda_1 > \lambda_2$ or $f_1 < f_2$). It is evident from formulas the shorter the wavelength, the longer the Fresnel zone and the smaller the angle of divergence θ. Consequently, it is easier to produce narrow beams at high frequencies.

The lateral resolution, which is the ability to resolve the discrete structures perpendicular to the beam axis, is determined by the beam width. The engineering trade-off of ultrasonic imaging is between the penetration distance and the resolution. The reason is that although increasing the frequency gives a better resolution of defects due to the narrower beam width, the beam will have a lower penetrating distance by virtue of the decrease in the beam intensity. Thus, an optimum value for the transducer diameter should be calculated to give an acceptable beam shape and width at each frequency.

2.H.9. Beam Formation by Focused Transducers

In some cases, a much narrow beam compared to the one generated by a flat, disc-shaped transducer is required for high lateral resolution. A focused beam can concentrate the ultrasonic energy at localized regions using either an ordinary transducer and an acoustic lens or a focused transducer (Szilard, 1982; Cartz, 1996). When the transducer is focused, the focal range exists in the near field of the transducer, and beyond that the ultrasonic beam again diverges; thus, focused beams are most sensitive to flaws at the focal region.

Figure-2.8 diagrammatically demonstrates the beam width from the focused transducer operating at the same frequency but for two different focal lengths. The focal length - the distance along the beam axis from the transducer to the

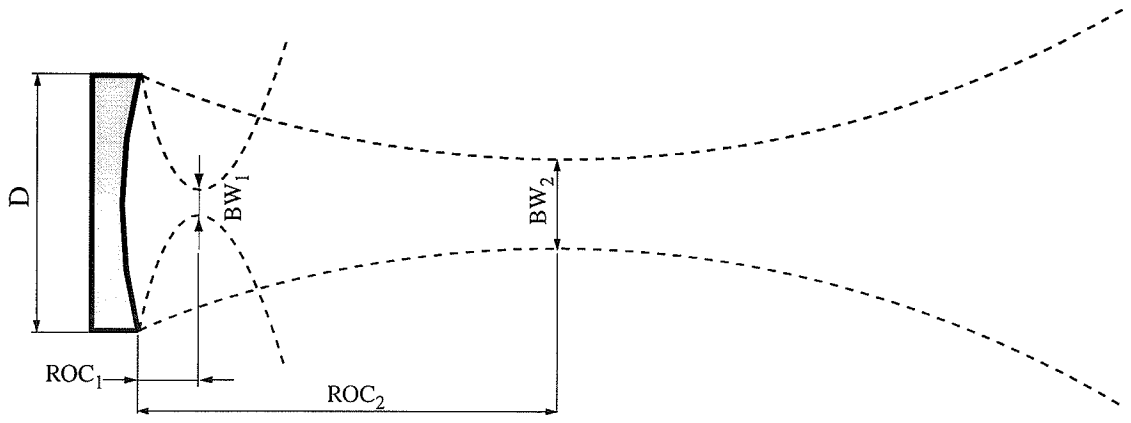

Figure - 2.8. A focused transducer with two separate ROCs

focus- is equivalent to the radius of curvature (ROC) of the transducer. Increasing the ROC results in the beam width (BW) to enlarge, and that is approximated by

$$BW = 1.028 \cdot \lambda \cdot \frac{ROC}{D} = 1.028 \cdot \lambda \cdot f^{\#} \qquad 2.8$$

where the term "f number" or $f^{\#}$ is often used in ultrasonic imaging to quantitate the focusing at the same frequency. The lower the BW or the $f^{\#}$, the better the focusing and, therefore, the better lateral resolution. As with the unfocused, flat, disc-shaped transducer, the increase in frequency generates a narrower beam in the far field.

The major drawback of focused transducers in nondestructive evaluation is their fixed focal length. As long as the region to be inspected falls into the focal range, these transducers would be the best choice for inspecting flaws in materials.

2.I. ULTRASONIC TESTING OF DEFECTS

Ultrasonic techniques are divided into two main categories; low-power and high-power applications. Low-power ultrasonic applications do not result in any permanent change in the medium under evaluation. Thus, their nondestructive nature is used to detect defects (particularly in steel, other metals and plastics), obstacles, anatomical structure, material properties, and flow. High-power applications intentionally produce waves with high energy that result in some changes in the medium of propagation exerting specific, desirable effects. These applications include medical therapy, cleaning, machining hard materials, and welding dissimilar materials (McGonnagle, 1966; Szilard, 1987; Gross, 1997). In this thesis, low-power ultrasound has been applied to evaluate package seals, so the high-power applications will not be discussed in detail.

There are two common ultrasonic techniques used for flaw detection; through-transmission and reflection techniques.

2.I.1. Through-Transmission Technique

In the through-transmission technique, separate transmitting and receiving transducers are positioned on the opposing sides of the specimen as shown in Figure-2.9 (McGonaggle, 1966; Szilard, 1987). A pulse of ultrasonic energy is propagated through the specimen at a constant repetition rate, and the receiving transducer detects the transmitted energy. Because material discontinuities in the path of the ultrasonic waves results in an obstacle, through which they can penetrate only partially, the amplitude of the transmitted beam decreases. Any defect getting into the path of the ultrasound beam will bring about an "acoustic shadow" on the receiver, resulting in a drop in, or a complete lack of received signal. Even the shape of the defect and the angle at which it is lying can be

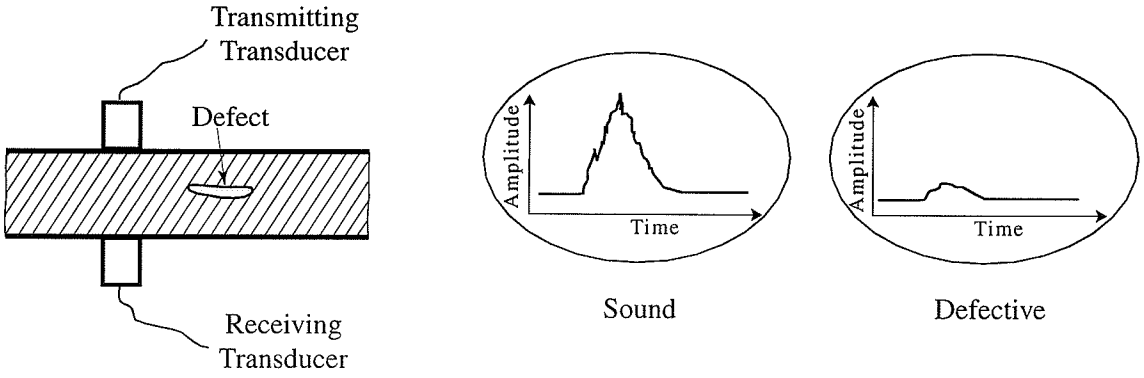

Figure - 2.9. Arrangement of transducers for detecting flaws in through-transmission technique

determined by a proper arrangement of two transducers. In some cases, coupling of transducers may be required to transmit the ultrasonic energy through the specimen. Coupling may be obtained by either immersing the sample and transducer in water or spraying on water or applying a coupling agent. This technique is commonly applied in the detection of lamination, cracks and other forms of discontinuities in sheet metals.

Scanning Laser Acoustic Microscope (SLAM) is a through-transmission device, which has been used for sample validation in this study. SLAM is an analog of the optical microscope. It can determine bulk wave ultrasonic properties of a thin specimen (Briggs, 1985; Smith, 1986; Briggs, 1992). The ultrasound reaching the surface opposite the source is detected by a rapidly scanning laser beam in synchronization with a television monitor, thus producing image of ultrasonic field at that surface as shown in Figure-2.10. The transmitter is usually angled with respect to the sample surface (typically 45^{o}). The transmitted sound penetrates the sample and strikes on a semi-reflective cover slip lying on the top of the

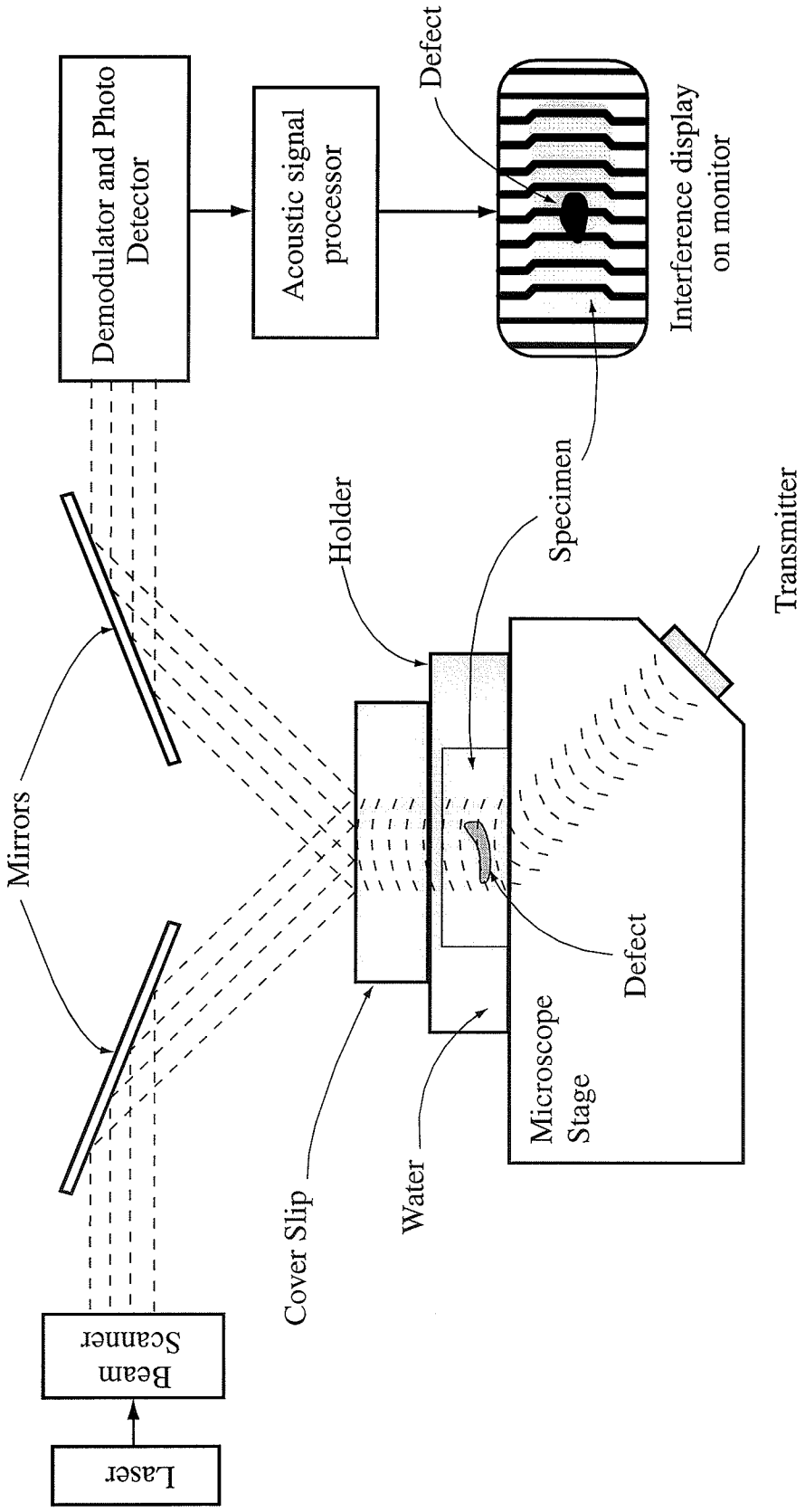

Figure - 2.10. Typical components of scanning laser acoustic microscope and the interference pattern (interferogram) for a specimen

sample. A focused scanning laser beam hits on the reflective surface of the cover slip. Next, the reflected laser beam is detected by a demodulator and photo detector and processed to produce the acoustic image, from which the attenuation coefficient of the sample can be measured (Goss and O'Brien, 1979; Pohlhammer et al., 1981; Tervola et al., 1985). In addition to that, SLAM can be used to produce interference pattern (interferogram) of the sample on the monitor, from which the sound speed of the specimen can be measured. The interferogram is made by several vertical interference lines, which are shifted to the right or left with respect to portions of sample with higher or lower speed (O'Brien, 1981; Embree et al., 1984;). If the discontinuity in the specimen includes air or any other material with much higher or lower impedance than specimen, interference lines at this location will either shift highly or vanish, which provides significant contrast in the image.

2.I.2. Reflection Technique

When an ultrasonic wave packet is propagated through the couplant into the sample, part of its energy will be reflected from the top and bottom surfaces of the specimen, and from any discontinuities. These reflections are detected either by a separate receiver or by the same transducer as shown in Figure-2.11a (Blitz, 1960; Szilard, 1982; Mix, 1987; Hull and John, 1988; Ensminger, 1988; Bray and Stanley, 1997). If the propagated sound strikes inhomogeneities and flaws, the detected defect signal appears between the signals received from the top and bottom surfaces of the specimen (Figure-2.11b).

Pulse-echo method - a reflection technique- is the most versatile of the ultrasonic diagnostic systems used both in nondestructive testing and in medicine (Ensminger, 1988). This method is generally used to detect flaws such as cracks,

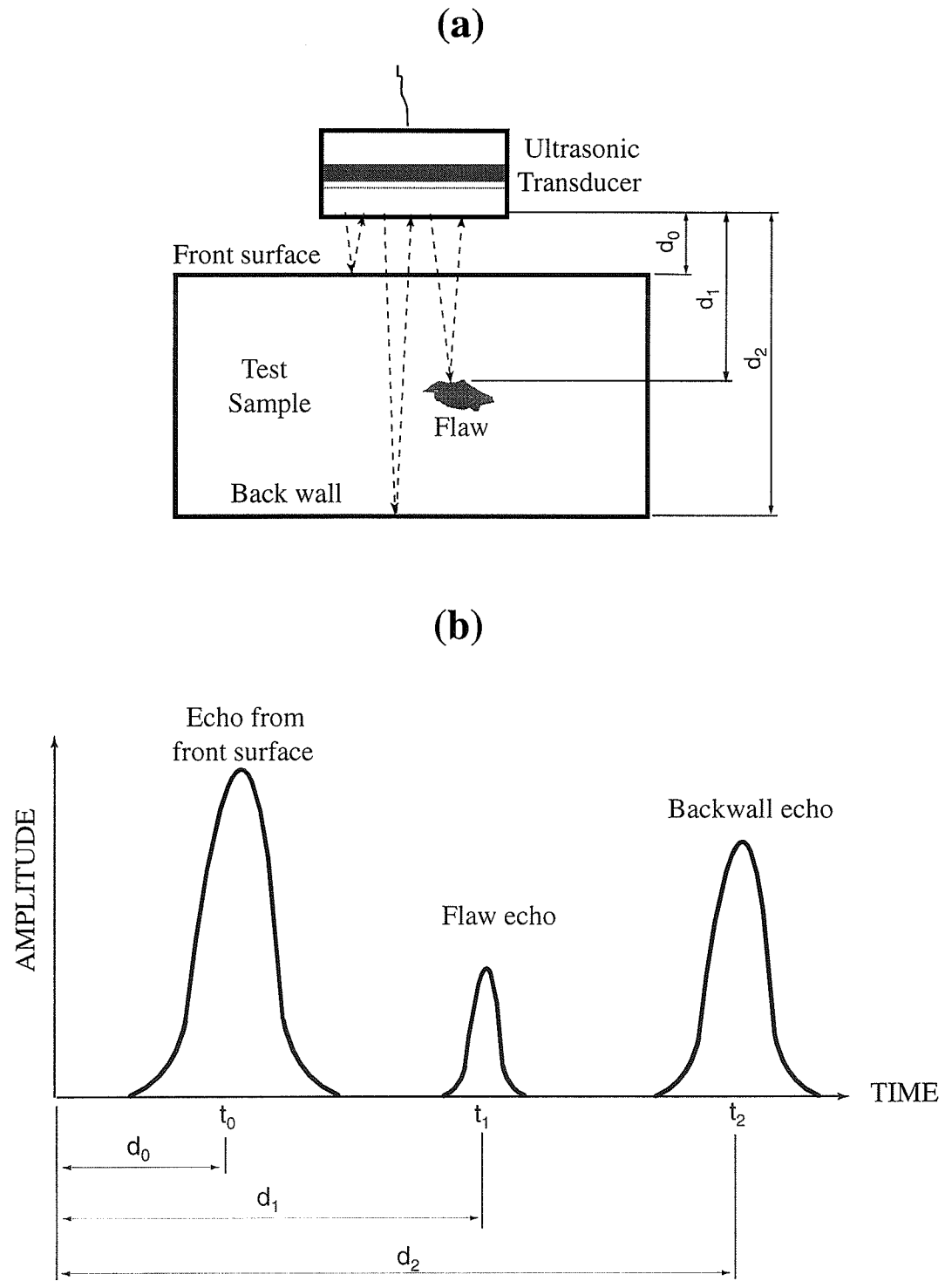

Figure - 2.11. (a) Typical pulse-echo system; (b) ideal appearance of signals on an oscilloscope

folds, inclusions, laminations, partial welds, voids, segregations, shrinks, porosity, and flaking (McGonnagle, 1966; Szilard, 1982; Mix, 1987; Szilard, 1987; Boving, 1989). Although it has been used mostly for steel and other metals, it can also be applied to many other materials.

The pulse-echo technique has an advantage over the transmission technique since the transmission technique requires access to both sides of the test piece; however, the pulse-echo technique can detect defects by accessing only one side of the test piece, and the transmitting transducer may serve as the receiving transducer as shown in Figure-2.11a (Hull and John, 1988; Gros, 1997), reducing the complexity of the test apparatus.

Pulse-echo systems depend upon the transmission of a burst of energy and the reception of returning echoes (Blitz, 1960; Halmshaw, 1991). The pulse generator is the starter for the system, firing the high voltage spike that sets the transducer into the oscillation at the transducer's own natural frequency. An ultrasonic wave is shaped when it is transmitted from the transducer. After the transducer produces a wave train, it becomes inactive for a period of time and then may act as a receiver. Echoes returning to the transducer are converted to electrical signals, and time intervals that elapse between the initial pulse and arrival of echoes are measured and often displayed with an oscilloscope.

There are four quantities required to quantify a repeated pulse; amplitude of pulse, frequency of ultrasonic signal in the pulse, pulse duration, and pulse repetition frequency. Figure-2.12 demonstrates a waveform of repeated pulses excited by a transducer. Pulse duration (τ) is the period during which the pulse is on. The pulse repetition frequency (PRF) or pulse repetition rate is the number of pulses generated in one second, and its reciprocal is called pulse repetition

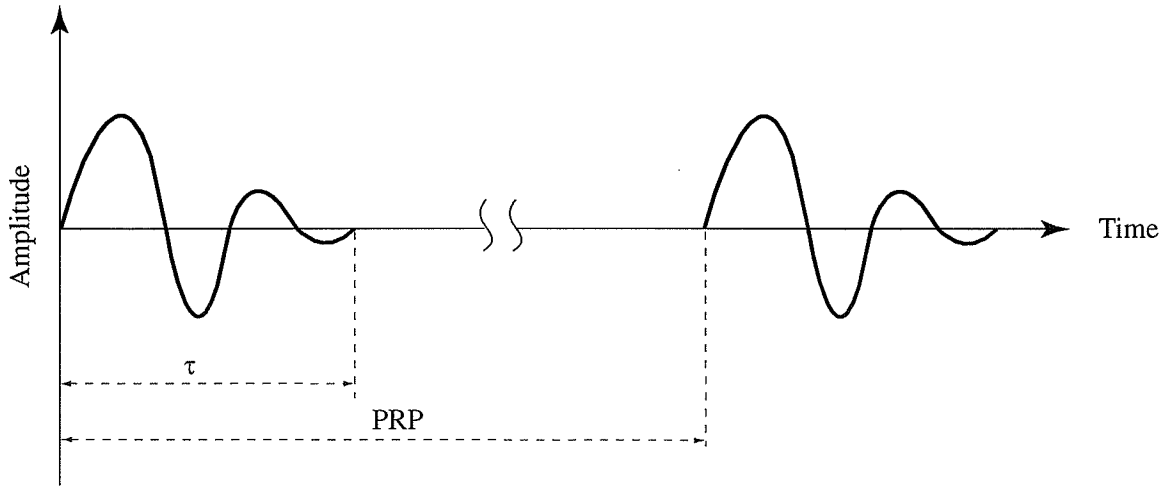

Figure - 2.12. A waveform of repeated pulses (τ= pulse duration, PRP = pulse repetition period)

period (PRP).

2.J. TYPES OF SCANNING AND DISPLAY

The data collected during an ultrasonic test can be displayed in several ways. Three types of data presentation, however, are most commonly used in reflection testing: the A-scan, the B-scan, and the C-scan (Szilard, 1982; Hull and John, 1988; Halmshaw, 1991; Cartz, 1996; Gros, 1997).

The *A-scan* or amplitude mode is a one-dimensional presentation of the specimen (Figure-11.b). The x-axis represents the time of flight of pulses, which can be converted into distance (penetration depth) if the sound velocity of the specimen is known. The y-axis indicates amplitudes of echoes. The A-scan shows the existence of flaws, their position, and gives an estimate of their size.

The *B-scan* or brightness mode is a single line scan made up of a series

of parallel A-scans collected along the line (Figure-2.13.a). It shows a cross-sectional view of the specimen along that line, indicating reflections from the top and bottom of the specimen and from flaws. The advantage of this type of display is that both the length of the flaw and its depth below the surface are revealed.

The *C-scan* or contrast mode is a rectangular scan and consists of series of parallel A-scans, which are carried over the surface (Figure-2.13.b). The display is a plane projection of the internal details of specimen if echoes are restricted to a particular time, which corresponds to a constant depth in the specimen. To produce a C-scan display, the probe must be scanned automatically over the surface in a regular raster pattern as shown in Figure-2.13.b.

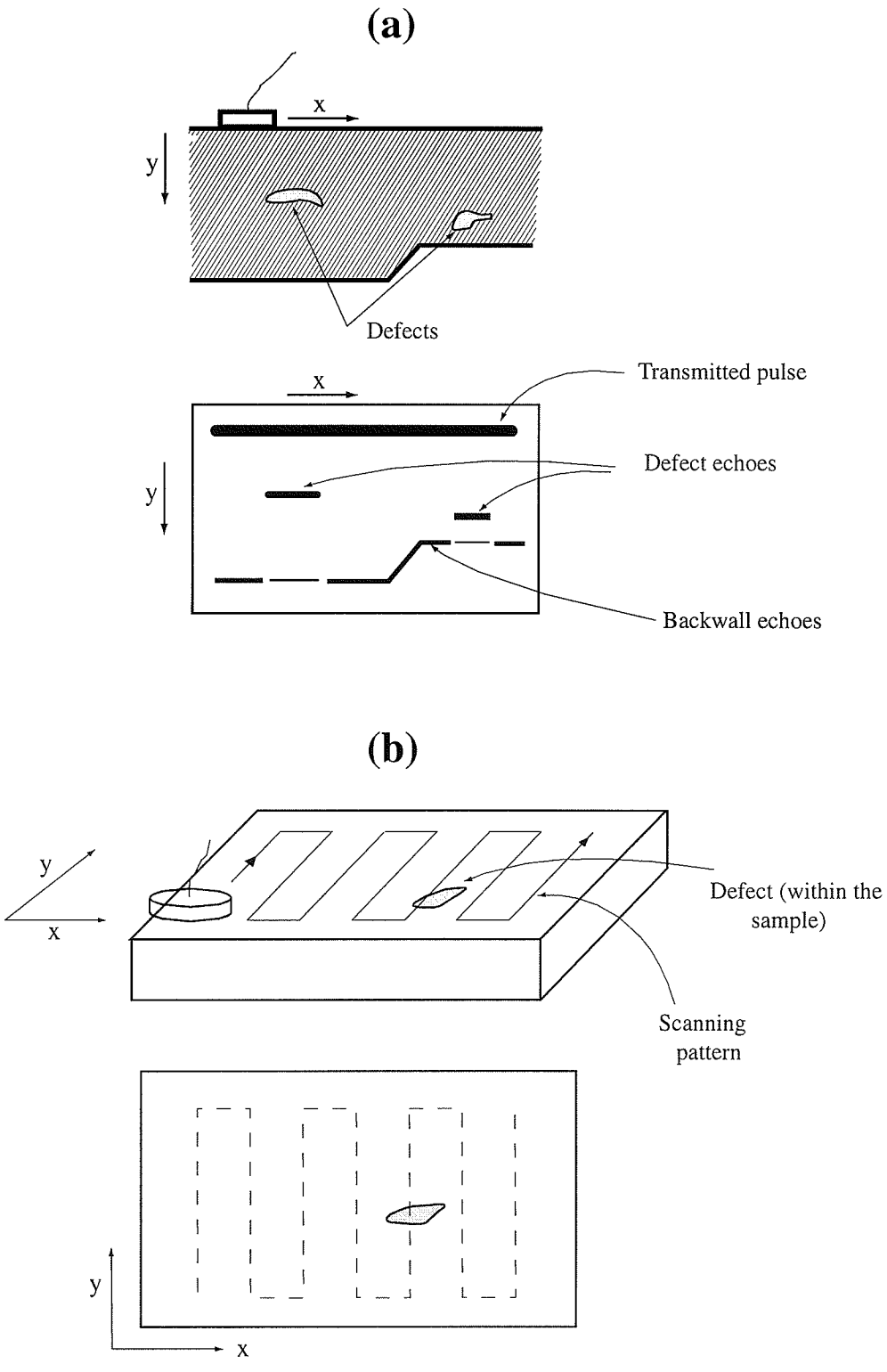

Figure - 2.13. (a) B-scan display; (b) C-scan display

-3-

BACKSCATTERED AMPLITUDE INTEGRAL (BAI) MODE IMAGING

3.A. INTRODUCTION

A U.S. patent (Jarman et al., 1994) describes an ultrasonic transmission technique for testing the seal integrity of a package having a lid bonded to the container rim. In that patent, an average reference signal (A-scan) was recorded from the undisturbed region of the seal, and the peak of signals obtained from the seal was evaluated relative to the reference signal. A decrease in the magnitude of the peak showed that the bond was not complete, and hence faulty. The device detected contaminating type defects such as silicon grease, Teflon® inclusions, and meat fibers in the seal region of the package. However, in this patent no information was available about the detection of microscopic channel leaks, which might cause microbial penetration (Floros and Gnanasekharan, 1992; Harper, 1995; Yam, 1995; Blakistone et al., 1996). Furthermore, tests were run with approximately one mm^2 of meat fiber mix positioned in the seal region. Although there is no official minimum size specification of any inclusion defect for package recontamination, the detected meat fiber in this study is much larger than that necessary to cause recontamination as previously discussed in section 2.F.

In a recent study, Safvi et al. (1997) showed that the Scanning Laser Acoustic Microscope (SLAM), a transmission technique, detected 10 μm channel defects

within the seal region of both polyethylene films and retortable plastic pouches at an ultrasonic frequency of 100 MHz. Even though this study demonstrated the ability of ultrasound to be an effective and precise way to image defects in certain food packaging materials, the on-line implementation of a SLAM-based method might be impractical since the equipment requires sensors for two sides of the specimen, i.e., through-transmission tehnique. Thus, a more practical approach to the problem is required to detect defects in the seal region of flexible packages.

A pulse-echo techniques, which may test the specimen by accessing only one side and being a more practical package inspection technique than through-transmission, has not been used for package inspection before. In addition to that, Jarman et al. (1994) assumed that the pulse-echo technique probably would not be sufficiently sensitive to detect very fine flaws (such as 1.0 mm^2 meat fiber) in the seal area of thin flexible packaging materials (total seam thickness was 185 μm). However, recent studies (Raum et al., 1998; Ozguler et al., 1998; Frazier et al., 1998) have shown that a pulse-echo technique combined with a new imaging technique (Backscattered Amplitude Integral (BAI) mode imaging) could detect channel defects (as small as 10 μm) within the seal region of retortable plastic pouches (total material thickness was 220 μm).

3.B. OBJECTIVES

Objectives of the study in this chapter are:

- to demonstrate the BAI-mode imaging technique;
- to evaluate the technique with two flexible packaging materials (transparent all-plastic and opaque foil-containing retort pouches) and with two types of defects (channel and inclusion defects) of different sizes;

- to determine its detection limits.

3.C. MATERIALS & METHODS

3.C.1. Sample Preparation

Two retortable pouch materials, an all-plastic and a foil-containing composite film were used as samples. The material composition of the all-plastic sample was Nylon/ Polyvinylidene chloride/ Polypropylene (Fuji Tokushu Shigyo Co. Ltd., Seto Aichi, Japan) with a film thickness of 110 μm. It was optically transparent. The other material was opaque, and its composition was Polyester/Aluminum foil/Polypropylene (American National Can Company, Chicago, IL) with a total thickness of 120 μm. Table-3.1 shows physical properties of layers in these packaging films. Polypropylene was the heat-sealing layer of both pouches. PVDC and aluminum foil, middle layers of each pouch, provide a barrier to chemical substances (Bakker, 1986). Polyester and nylon, the outer layers, give strength, resistance to shear, chemical resistance, barrier to gases, oils and fats, and scuff resistance to the printed surface (Paine, F.A. and Paine, H.Y., 1983).

Three types of defects (air-filled channels, water-filled channels and solid inclusions) in the seal region of both all-plastic and foil-containing packages were created. To fabricate different sized channel defects (air-filled and water-filled), tungsten wires (6, 10 and 15 μm in diameter: California Fine Wire Company, Grover City, CA) were used. These wires were positioned transverse to the sealing direction, sandwiched between two facing layers of pouch materials, and then sealed using an automatic band sealer (Doboy HS-C42051, Doboy Co., New Richmond, WI). The inner layer of these films, which is the heat sealant layer, was in direct contact with wires. In band sealing (Figure-3.1), endless stainless steel bands

Table - 3.1. Physical properties of packaging materials used in the experiment

Packaging Material	All-plastic film			Foil-containing film		
Layers	Inner	Middle	Outer	Inner	Middle	Outer
Layer material	PP[a]	PVDC[a]	ON[a]	PP[a]	AF[a]	PE[a]
Thickness, μm	80	15	15	NA[a]	NA[a]	NA[a]
	110			120		
Density, kg/m^3	900[b]	1600-1700[b]	1140[b]	900[b]	2700[c]	1400[b]
Sound speed, m/s	2660[c]	2380[c]	2600[c]	2660[c]	6420[c]	2340[c]
	2380[d]			2460[d]		

a AF = Aluminum Foil; ON = Oriented Nylon, 6/6; NA = Not available; PE = Polyester; PP = Polypropylene; PVDC = Polyvinylidene chloride

b Jenkins and Harrington, 1991

c Selfridge, 1985

d Measured in the laboratory

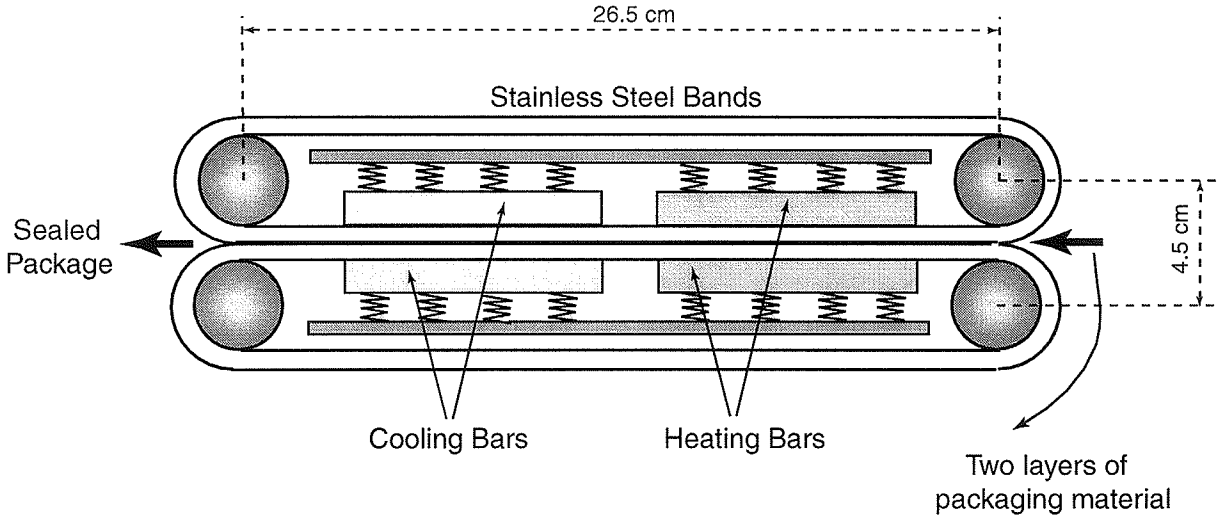

Figure - 3.1. Band type heat sealer (top view)

(with non-stick Teflon® coating) guided and pressed the two layers of package material between the heated sealing bars. The heat passed through the bands and into the pouch material, melting it to form a seal. The pouch material then traveled between a pair of air-cooled bars, where the sealed area was cooled rapidly. The speed of the machine was 0.083 m/s, and the temperature for sealing was 132°C and 152°C for all-plastic and foil-containing pouches, respectively. The sample seals were cooled in air for approximately 5 minutes before removing the wire. In order to create the air-filled channel defects; the tungsten wire was axially removed with the specimen in air. For water-filled channel defect creation, samples were immersed in the water bath, and the wire was then axially removed, drawing water into the channel. After wire removal, channel ends were sealed with the band sealer to keep the filling medium (water) inside the channel defect. Figure-3.2 illustrates schematic demonstration of defect orientation and layers in a sample. Figure-3.3 demonstrates the side and top views of the defect in a sample. The longitudinal axis of the defect was transverse to the sealing direction (named the seal's major axis in Figure-3.3).

To prepare solid inclusion defects; strands of mouse tail tendon (biomaterial to simulate meat fiber and other food fibers that might be captured in the seal region of the package) were used. These strands were longitudinally extracted from the tail of mouse (provided by Beckman Institute's Animal Care Facility, Urbana, IL) under the microscope. Each tendon was placed transverse to the sealing direction, sandwiched between two identical packaging films (as illustrated in Figure-3.2 and Figure-3.3) and heat-sealed. Tendons were left in place, and both ends of the defect region were sealed to protect from any interaction of inclusion material with water during the experiment.

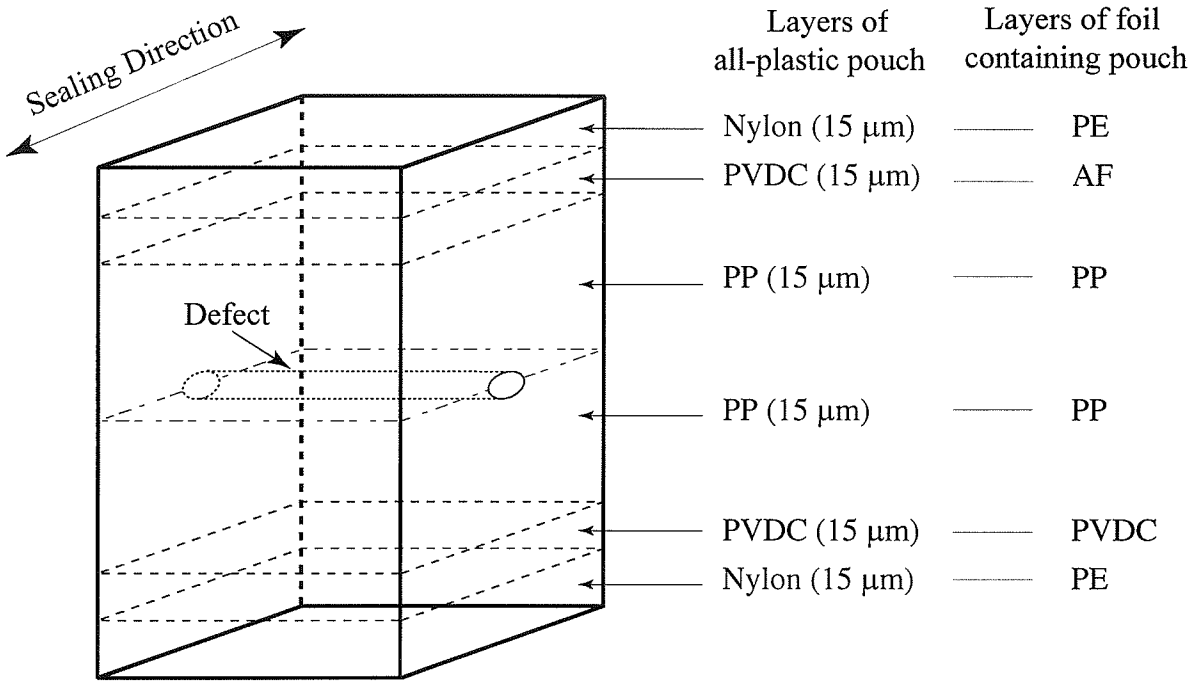

Figure - 3.2. Three dimensional, cut-away representation of two layers of the all-plastic pouch and foil-containing pouch materials with a defect shown schematically between the two layers. Individual layer thicknesses of foil-containing pouch material are not available. AF: Aluminum foil, PE: polyethylene, PP:polypropylene, PVDC: polyvinylidenechloride

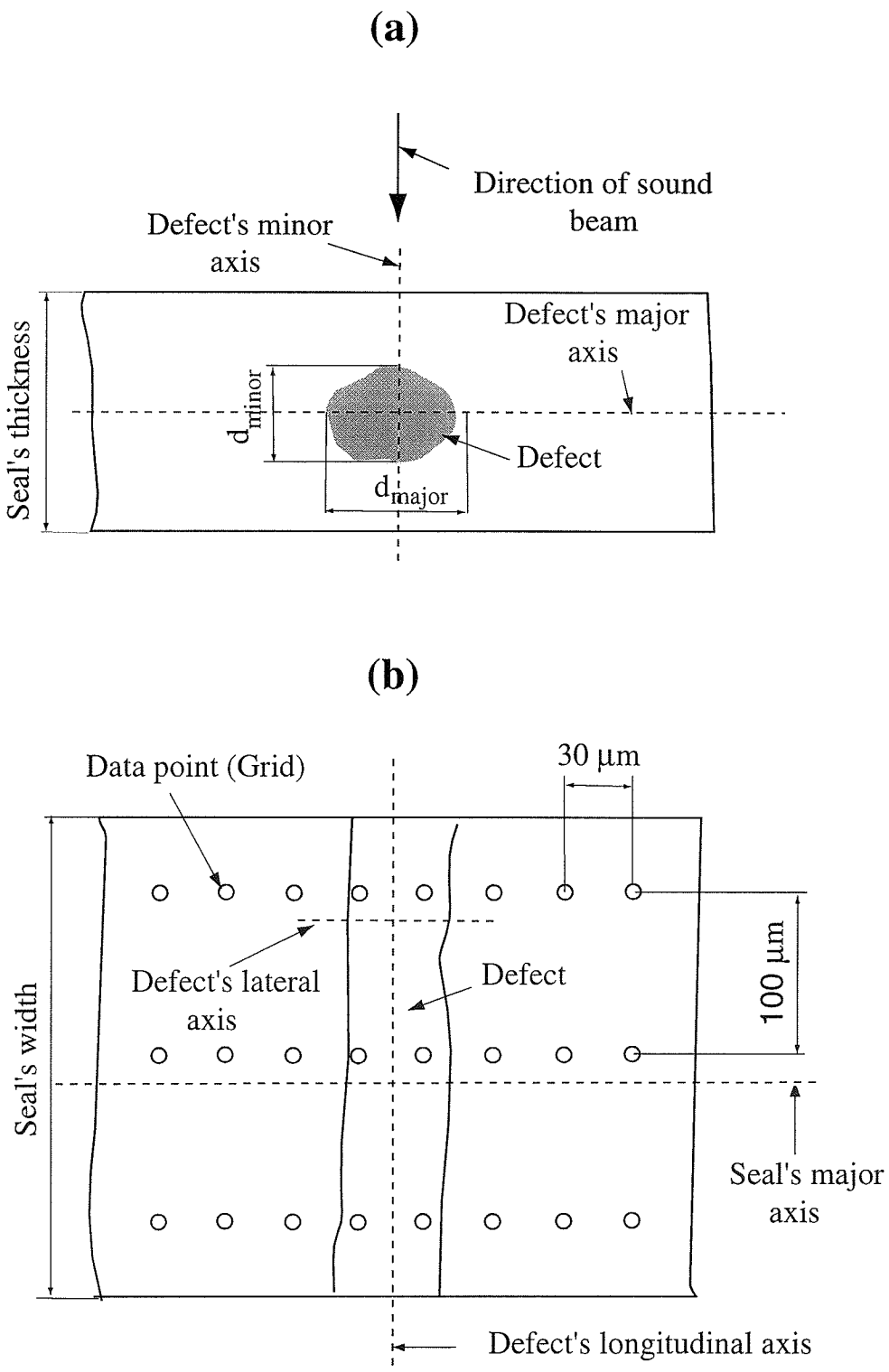

Figure - 3.3 . Diagram of a defect sample within the seal region of the package; (a) cross-sectional view; (b) top view

3.C.2. Sample Validation

The size of the channels and tendons within the seal area of both packages was determined by light transmission microscope images with a calibration grid (Reicher Jung: 2 mm divisions into subdivision of 10 μm). A Nikon Optiphot-2 light microscope, Sony CCD color video camera, RasterOps frame-grabber board, Macintosh IIci computer, and Adobe Photoshop software were used to capture images into a high quality digital format.

The lateral size of the defects was measured using the top-view microscope image. Before measuring the size from the cross-sectional view, samples were cut in the direction that is parallel to seal's major axis and transverse to the defect's longitudinal axis. To avoid distortion of samples during cutting, samples were frozen to -70°C (Forma Scientific, Model no. 80478-006, OH) for about thirty minutes, and then, they were cut from their midpoint using a cyrostat (Lipshaw Manufacturing Company, Model no. 1500, Detroit, MI).

3.C.3. System Description

A block diagram of the data acquisition system is shown in Figure-3.4. In this system, GPIB (General Purpose Interface Bus), which was controlled by a program written in C programming language (This program is in the Appendixes, A.1), communicated with a host PC (ZEOS 66 MHz 486), motor controllers, and a pulser-receiver. The mechanical movement of the transducer for scanning was achieved by a five-axis (three linear and two rotational axes) precision positioning system (Daedal Inc., Harrison City, PA) that is connected to motor controllers. The linear and rotational positional accuracy of the system were 2 μm and 0.01°, respectively. The defect sample was taped to a plastic holder and submersed in a degassed water tank (~20°C) so that its surface was approximately normal to

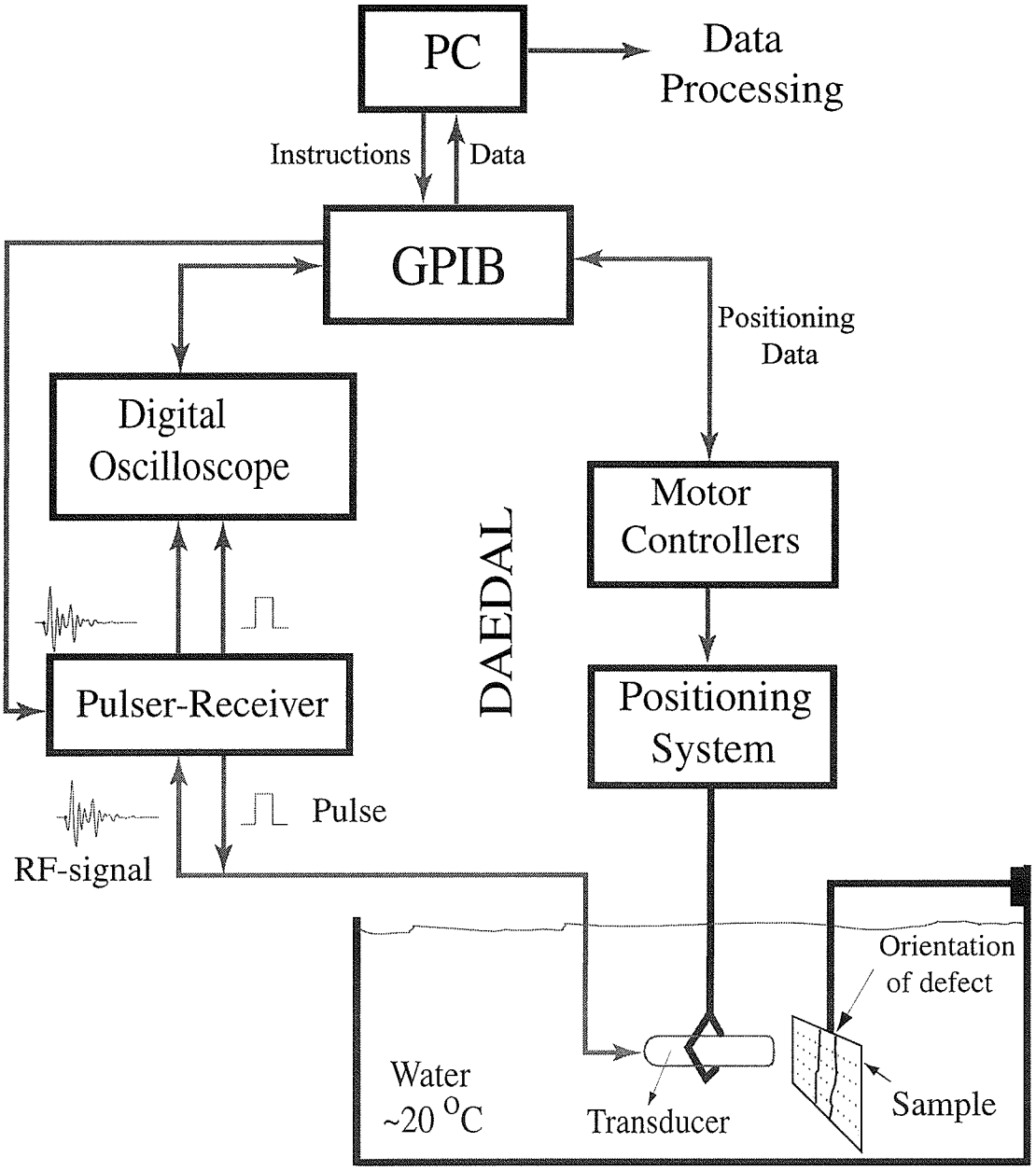

Figure - 3.4. Diagram of data acquisition system

the direction of the propagated sound beam. A pulser-receiver (Model 5800, Panametrics, Waltham, MA) operating in pulse/echo mode controlled by the PC was used to produce the 300 V monocycle pulse which excited a spherically focused ultrasonic transducer with nominal center frequency of 20 MHz (Panametrics V317, Waltham, MA). The received echo signal was amplified (20 dB), bandpass filtered (1-35 MHz) by the pulser-receiver, and then displayed (500Ms/s) on a digitizing oscilloscope (LeCroy 9374L, Chestnut Ridge, NY). The PC via IEEE-488 retrieved the digitized echo waveforms from the oscilloscope, and the stored waveforms were transferred to a SUN Sparc 20 workstation for off-line processing.

3.C.4. Spatial and Temporal Characteristic of Transducer

Raum and O'Brien (1997) measured acoustic properties and resolution limits of the transducer used in this study (Table-3.2). Some of the beam quantities were experimentally obtained using a 25-μm tungsten wire target. Other quantities were calculated using the formulas discussed below (see section 2.H.8, 2.H.9 and related figures in Chapter-2 to follow these calculations).

The transducer diameter (D) and focal length (F) were provided by manufacturer. The focal length at the geometrical focus was assumed to be equal to radius of curvature (ROC, see Figure-2.6). The $f^{\#}$ or f-number (=ROC/D) is equal to 2.0. The -6-dB transmit-receive beam width of the focus (also defined as the lateral resolution of the transducer) is approximated by

$$D_{lateral} = 1.028 \cdot \lambda \cdot f^{\#} \qquad 3.1.$$

where λ is the acoustic wavelength (= c/f_c , c= sound speed, f_c=center frequency).

Using the formula defined for acoustic pressure distribution of a spherical focusing source, the -6-dB transmit-receive depth of focus (F_z) is calculated by

Table - 3.2. Measured and calculated acoustic field properties and resolution limits of a 20-MHz manufacture-quoted spherical transducer (adapted from Raum and O'Brien, 1997; Raum et al. 1998)

Transducer or field quantity	**Panametrics V317 20-MHz Transducer**
¥ Transducer diameter, D	6.35 mm
¥ Focal length, F	12.70 mm
¥ f-number, $f^{\#}$	2.0
Measured center frequency (water, 20°C), f_c	17.3 MHz
Measured pulse duration (water, 20°C), $\tau_{(-20\text{-dB})}$	155 ns
Calculated wavelength (water, 20°C), λ_{water}	86 μm
Calculated wavelength (all-plastic), $\lambda_{plastic}$	138 μm
Calculated wavelength (foil), λ_{foil}	142 μm
D_{axial} (in water, 20°C)	115 μm
D_{axial} (in all-plastic)	184 μm
D_{axial} (in foil-containing sample)	191 μm
Measured $D_{lateral}$ (-6-dB) (in water, 20°C)	173 μm
Calculated $D_{lateral}$ (-6-dB) (in water, 20°C)	177 μm
Measured F_z (water, 20°C)	2150 μm
Calculated F_z (water, 20°C)	2436 μm

¥ denotes manufacture specification

D_{axial} is axial resolution calculated using $\tau_{(-20dB)}$

$D_{lateral\ (-6\ dB)}$ is lateral resolution at -6-dB transmit-receive beam width

F_z is the the -6-dB transmit-receive depth of focus

$$F_z = 7.08 \cdot \lambda \cdot (f^{\#})^2 \qquad 3.2.$$

$\tau_{(-20\text{-dB})}$ given in Table 3.2 is the pulse duration between the times when the pulse amplitude is at -20-dB of its maximum values. Using $\tau_{(-20\text{-dB})}$, the spatial extent of the pulse duration (also called axial resolution of the transducer) is calculated by

$$D_{axial} = \frac{c \cdot \tau_{(-20\text{-dB})}}{2} \qquad 3.3.$$

Raum and O'Brien (1997) did not work on the foil-containing material used in this study so the related parameters for this material were calculated using these equations. They concluded that the measured transmit-receive spatial characteristics of the transducer were in general agreements with the manufacturer's specification. However, the measured center frequency of the transducer (17.3 MHz) was different from the manufacturer's quoted center frequency (20-MHz). The reason was attributed to that the pulser/receiver (Model 5800, Panametrics, Waltham, MA) used in the study appeared to attenuate the higher frequency components, which brought about the estimated center frequency of the transducer in the focal plane to be lower than the manufacturer-quoted frequency.

3.C.5. Data Acquisition

The transducer was connected to the computer-controlled micro-precision positioning system (Daedal Inc., Harrison City, PA) and the angle of incidence of the ultrasound beam was approximately normal to the sample surface. The time-of-transition (TOT) for the sound beam in the water was calculated:

$$TOT = \frac{2 \cdot x(t)}{c_w} \qquad 3.4.$$

where x(t) is the axial distance, and c_w is the speed of sound in the water (1483 m/s at 20°C, Wilson, 1959). When the sample was properly positioned, the TOT was 17.16μs at the focal length of x(t)=12.7 mm. Radio frequency (RF) waveforms for each scan point were, therefore, acquired and stored between TOT=16.8 and 17.8μs to include the sample thickness as illustrated in Figure-3.6a. Each RF waveform obtained in this TOT range contained 512 data points. In order to make the sample surface approximately normal to the transducer, four edges of the rectangular sample surface were scanned. As long as all RF waveforms on these edges were within the specified TOT range, the sample was considered to be properly positioned. Otherwise, the sample was manually corrected until the signals on edges were within this TOT range.

The sample was scanned in a rectangular grid pattern by moving the transducer to the fixed-position sample (Figure-3.4). The horizontal and vertical grid spacings on the rectangular surface of the sample were 30 μm and 100 μm, respectively (Figure-3.3b). The horizontal direction on the rectangle was parallel to the seal's major axis, and the vertical direction was parallel to the defect's longitudinal axis. Field-of-view varied from 1.0 mm (vertical direction) × 2.0 mm (horizontal direction) to 1.5 mm × 3.0 mm. If it is, for example, 1.0 mm × 1.5 mm, the number of waveforms (Radio frequency (RF) echo signals) is 50 (1.5mm/30μm) in the horizontal direction and 10 (1.0mm/100μm) in the vertical direction for the total number of 500 (50 × 10) waveforms. Since each waveform included 512 data points, the three dimensional data set for this specific example contains 500 512-point RF data acquisitions. Figure-3.5 demonstrates the schematic representation of the three-dimensional data set, the defect orientation within the sample, and the direction of ultrasonic beam.

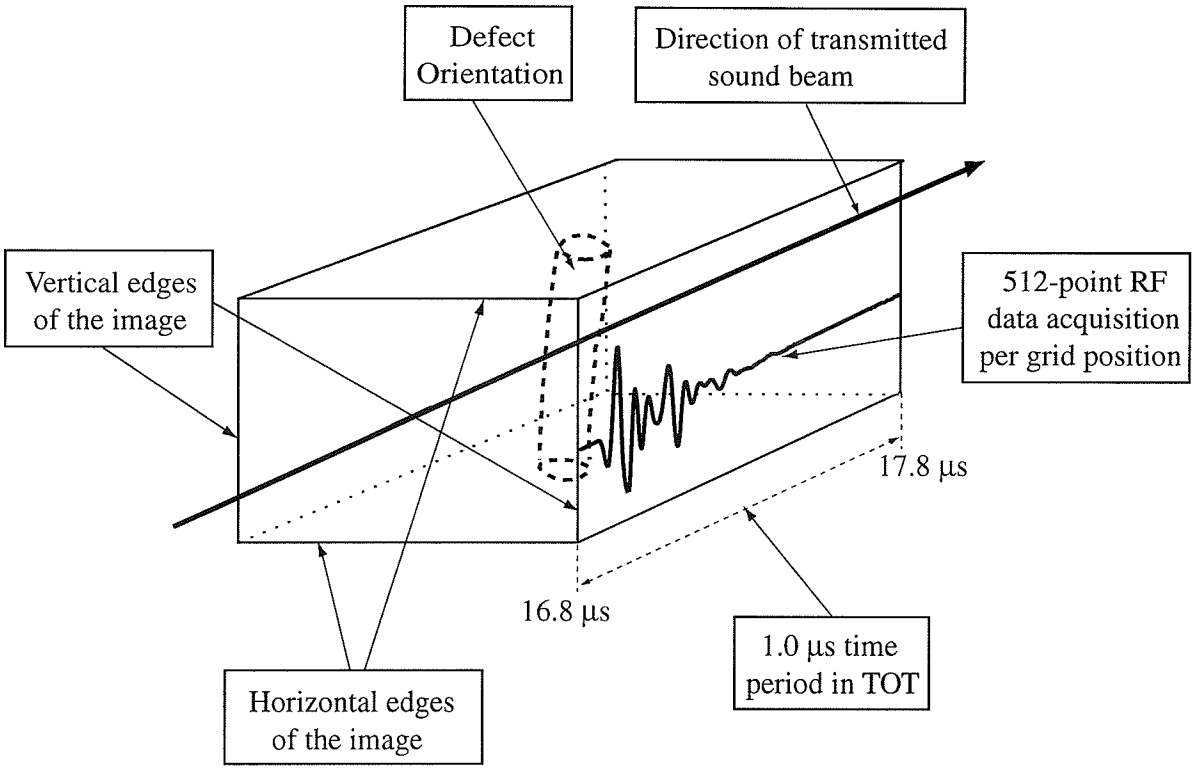

Figure-3.5. Three dimensional data set for image processing. The front surface shows the field-of-view. Each scan point comprises a 512-point RF echo signal between TOT = 16.8 and 17.8 μs. Direction of sound beam is perpendicular to the image surface.

3.C.6. Data Processing for Image Production

The three-dimensional data set has been previously examined (Raum et al, 1998) with a conventional B-mode imaging technique (see section 2.J. in Chapter-2), in which the plane of the imaged section of the object is perpendicular to the test surface. B-mode images were generated by processing the RF data acquisition for each grid point. The RF signal was first filtered using 400th order Remez-bandpass filter (3 to 27 MHz cutoff frequencies). The filtered signal was then processed by Hilbert-transformation. This transformation rectifies the

RF waveform, and the magnitude of resulting amplitudes yields an envelope (Oppenheim and Schafer, 1975; Leisk and Saigal, 1996). The resulting final envelope signal is called "A-scan". For each grid point, a corresponding A-scan was generated and it was used for the B-mode image processing. However, Raum et al. (1998) indicated that the B-mode imaging could not detect channel defects smaller than 95 μm, and concluded that it was inadequate for subwavelength imaging of typical channel defects found in flexible food packages. Based on results obtained by conventional B-mode image features, a new goal of this study was established to develop an imaging technique that would exhibit subwavelength-imaging capabilities. Some of the features in the B-mode images suggested that any discontinuity in the plastic layer could affect the received RF echo signal and possibly, the total reflected echo energy.

In the development of the new technique, the same three-dimensional data set and some processing techniques used in producing the B-mode images were utilized. The RF echo signal as seen in Figure-3.6a was Hilbert-transformed to produce the envelope signal (A-scan); without filtering it as shown in Figure-3.6b. The envelope signal was quantified by integrating it between 16.8 and 17.8 μs, i.e.,

$$\mathrm{BAI} = \int_{16.8}^{17.8} |envelope(RF(t))|\, dt \qquad 3.5.$$

where BAI represents the Backscattered Amplitude Integral. This calculation produced a single BAI-value for each corresponding RF signal. The area under the A-scan in Figure-3.6b shows the BAI-value. This calculation reduced the 3-D data set to a two-dimensional BAI-value matrix. The matrix was normalized by dividing each BAI value by the maximum BAI value obtained in that matrix

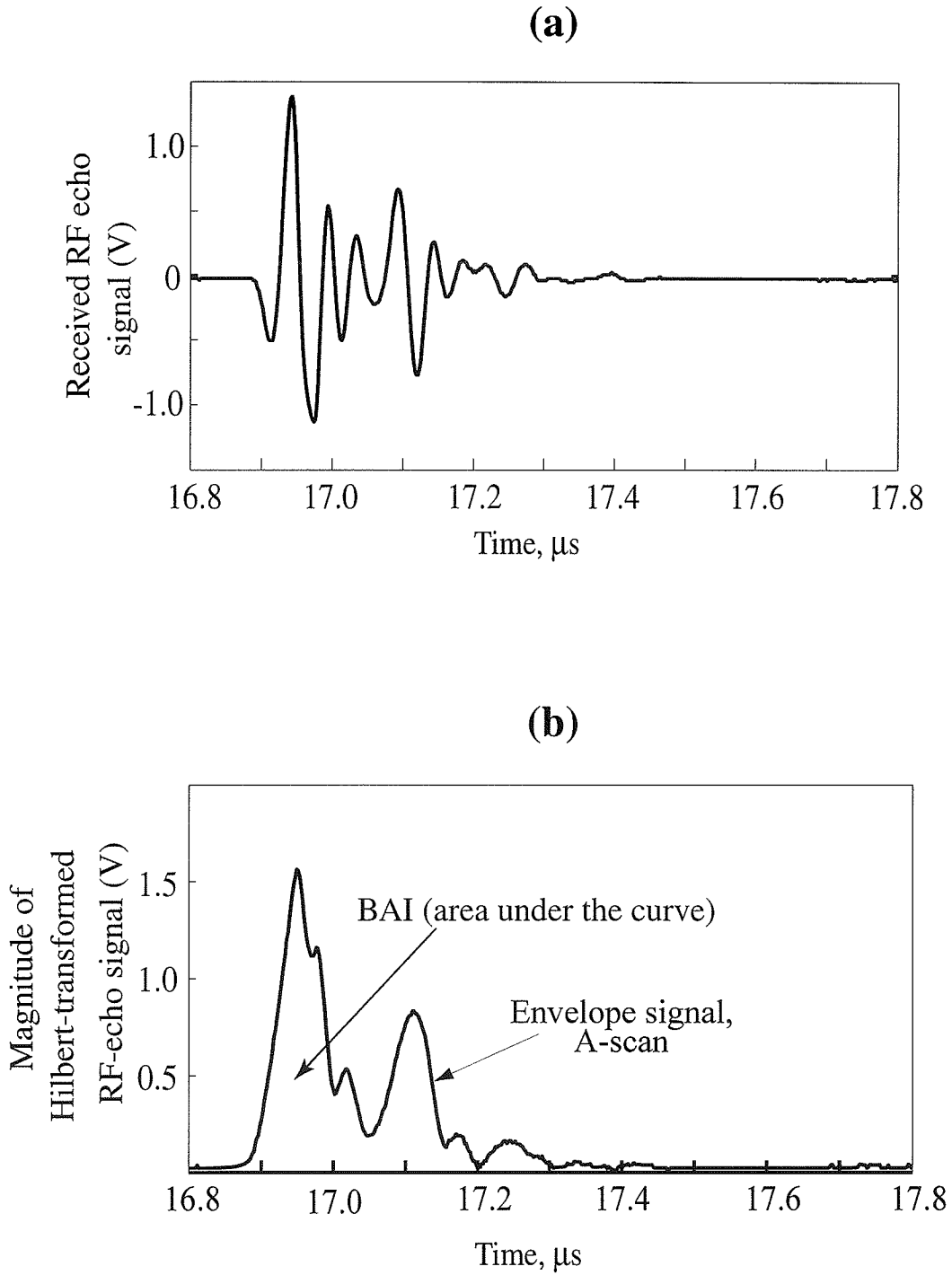

Figure - 3.6. (a) RF echo signal obtained for each grid in the image matrix; (b) Magnitude of Hilbert transformation of (a) produces the envelope signal, A-scan. The area under the curve in (b) results in the BAI value.

to provide the gray scale image. It was observed that the pixel size (100 μm × 30 μm) of the image was so large that the image was not smooth, which made the detection of the defect difficult. Therefore, this matrix was interpolated to decrease the pixel size and to make it approximately square. The matrix was interpolated by a factor of two in the direction horizontal to the image rectangle (30 μm/2) and by a factor of seven in the direction vertical to the image rectangle (100 μm/7). After linear interpolation, the corresponding pixel sizes became 14.3 μm × 15.0 μm with the number of rows and columns in the BAI matrix of 70 (10 by 7) and 100 (50 by 2), respectively. The final normalized image matrix was used to yield the gray scale image. Image processing was performed using MATLAB® (The Math Works, Inc., Natick, Mass.). The program code for image processing and the list of data files are illustrated in Appendixes, A.2, and A.5, respectively.

3.C.7. Statistical Analysis

The maximum BAI value (BAI_{max}), which was used to normalize the BAI-value matrix before producing the gray scale image, was determined from all-plastic and foil-containing retortable pouches. The average of BAI_{max} values was calculated for each pouch material. The ability of the BAI technique to distinguish two packaging materials was evaluated by comparing their average BAI_{max} value using the Analysis of Variance (ANOVA at a significance level of $\alpha = 0.05$) test. All statistical calculations were performed using Microsoft Excel 97®.

3.D. RESULTS & DISCUSSION

Six water-filled and six air-filled channel defect samples (~6 - 15 μm),

and three tendon defects (~20 - 60 μm) were fabricated for each packaging material, to give a total of thirty samples.

3.D.1. Lateral Size Measurement of Defects

Although the lateral view of defects in the transparent all-plastic retort pouch was detected by the light microscope, that in the foil-containing pouch could not be detected due to the material opacity. Figure-3.7a shows the light transmission microscope image of an air-filled channel defect within the seal area of the all-plastic pouch. The size of the defect on the image was 14.5 μm whereas the diameter of the tungsten wire used to create this defect was 15.0 μm. Lateral size of other channel defects in the all-plastic seal area was, at most, 5% smaller than the wire diameter. The lateral size of tendon defects in the transparent, all-plastic pouches varied along the tendon due to its natural structure, and thus the smallest lateral size was recorded. Figure-3.7b shows a tendon defect with the lateral size ~20 μm within the seal region of the all-plastic pouch. The dashed line shows the location where the size was measured.

3.D.2. Size Measurements from The Side View

The light transmission microscope could not detect eight of twenty-four channel defect samples (both all-plastic and foil-containing) from the side view, so the size from the cross section could not be validated for those samples. That was assumed to be due to the shear deformation of the packaging material on the cut surface, which made identification of small defects impossible. Other identified channel defect samples, however, showed an elliptic geometry in the cross sectional view. Figure 3.8 shows the light microscope image of two seal defects from their side view. The size of the defect on the major axis of the ellipse was estimated to be ~10-15% larger than that on the minor axis. All

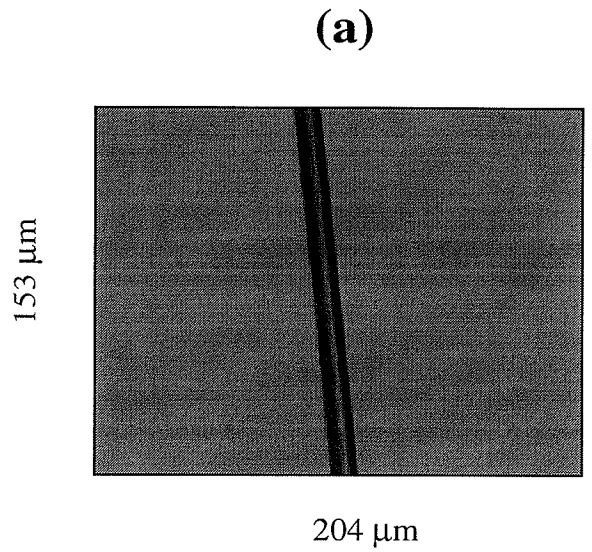

Figure-3.7. Light transmission microscope image of 14.5-μm air-filled channel defect at 40X magnification (a); and tendon defect (20 μm) at 10X magnification (b) within the seal area of the all-plastic pouch. Dashed lines show the location for the measurement.

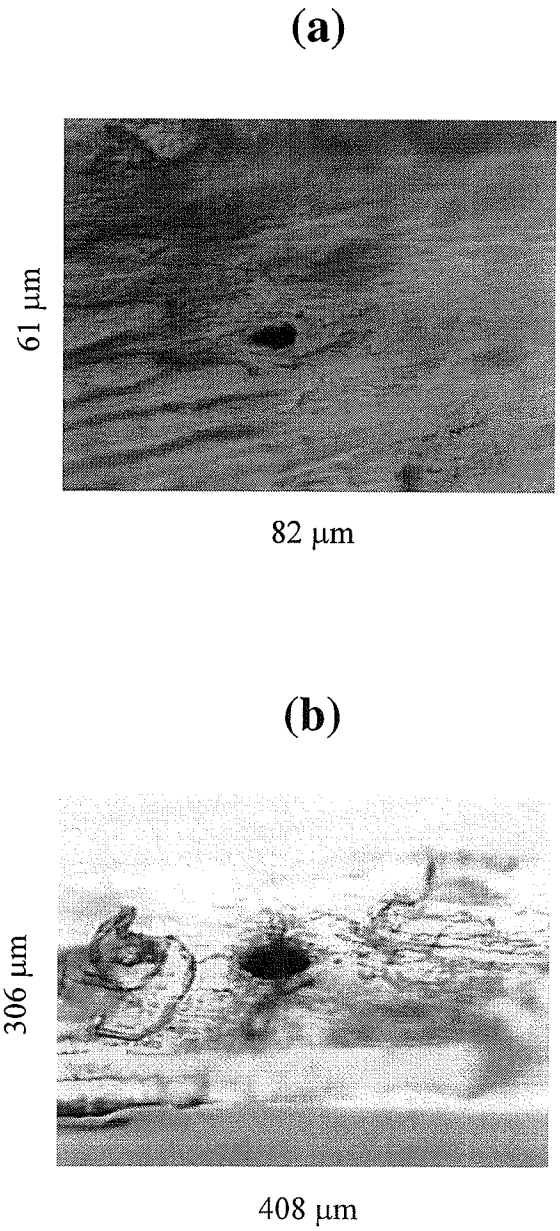

Figure - 3.8. Light transmission microscope image of seal defects from the side view. (a) 6-μm air-filled channel defect in the seal area of foil-containing pouch at 100X magnification; and (b) 55 μm tendon defect in the seal area of all-plastic pouch at 20X magnification

inclusion defects were identified from the cross-sectional view. Shapes of these defects were also elliptic, and the size on the major axis, was up to three times larger than that on the minor axis.

3.D.3. BAI-mode Images

Figure-3.9a and 3.9b demonstrate 17.3-MHz BAI-mode images of 14.5-μm air-filled and 6.0-μm water-filled channel defects within the seal region of all-plastic retortable pouches, respectively. Of twelve channel defects within the all-plastic seals, two 6-μm air-filled channel defects and one 6-μm water-filled channel defect were not detected in the BAI-mode image. Figure-3.10a and 3.10b illustrate the 9.6-μm air-filled and 6.0-μm water-filled channel defects within the seal area of the foil-containing pouch, respectively. Of twelve channel defects, only one 6-μm water-filled channel was not detected in the BAI-mode image. In summary, the 17.3-MHz BAI-mode imaging technique detected all channel defects from 9.5 to 15.0 μm in diameter regardless of medium (air-filled or water-filled) whereas it did not always detect the 6-μm defects.

Figure-3.11a and 3.11b illustrate the 17.3-MHz BAI-mode image of tendons within the all-plastic seal areas. The smallest lateral size measured was about 20.0 μm and 48.0 μm in Figure-3.11a and 3.11b, respectively. Figure-3.12a and 3.12b demonstrate the BAI-mode image of tendons within the foil-containing seal areas. Since the foil-containing pouch is opaque, the optical size measurement of tendons after sealing was not possible from the top view. Instead, their size on the major axis of elliptical geometry was measured from the side view, and this is illustrated in figures by the dashed line. The size was about 22.6 and 42.4 μm in Figure-3.12a and 3.12b, respectively. From the three samples fabricated for BAI-mode imaging, the minimum size (from ellipse's major axis) of these

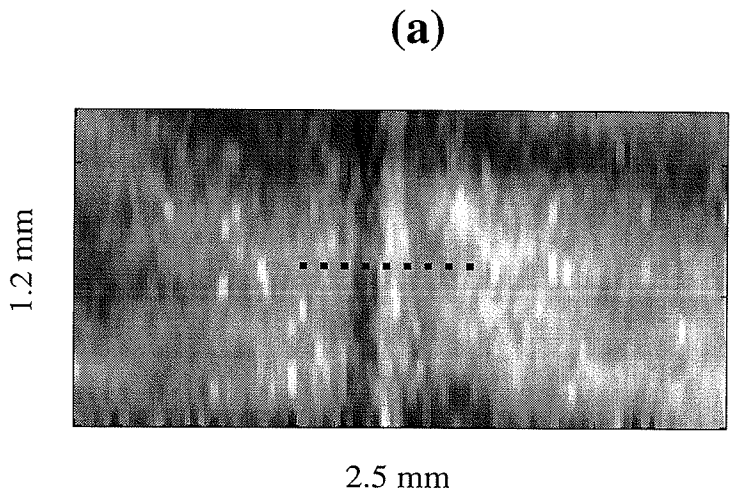

Figure - 3.9. BAI-mode image of (a) 14.5-μm air-filled channel and (b) 6-μm water-filled channel defect within the all-plastic seal. Dashed lines show the location for the measurement.

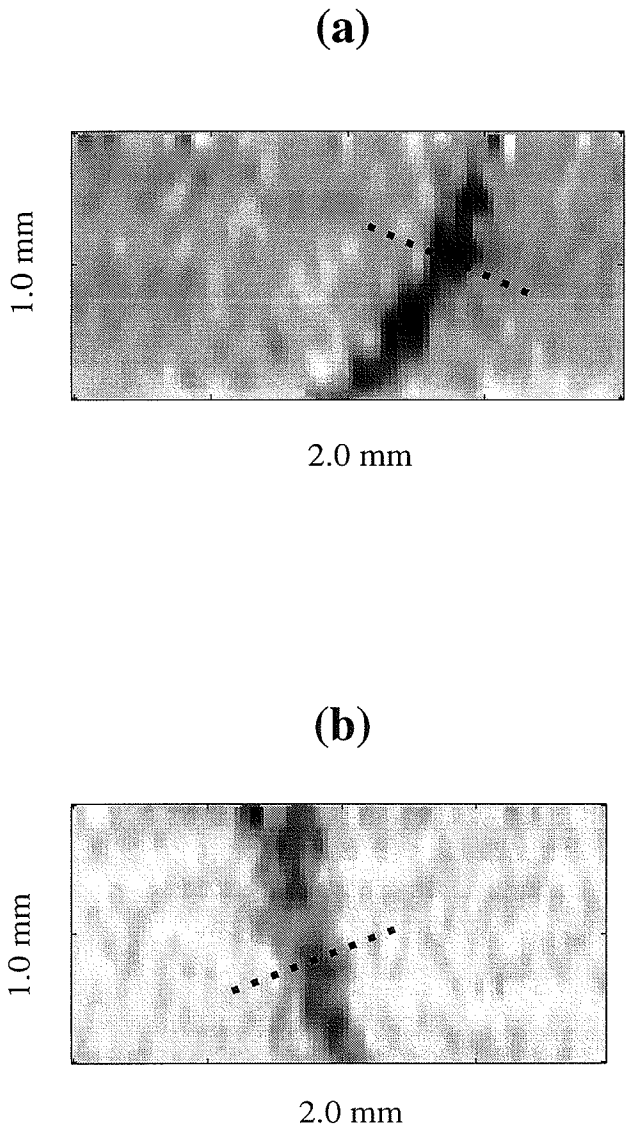

Figure - 3.10. BAI-mode image of (a) 9.6-μm air-filled channel defect and (b) 6-μm water-filled channel within the foil-containing seal. Dashed lines show the location for the measurement.

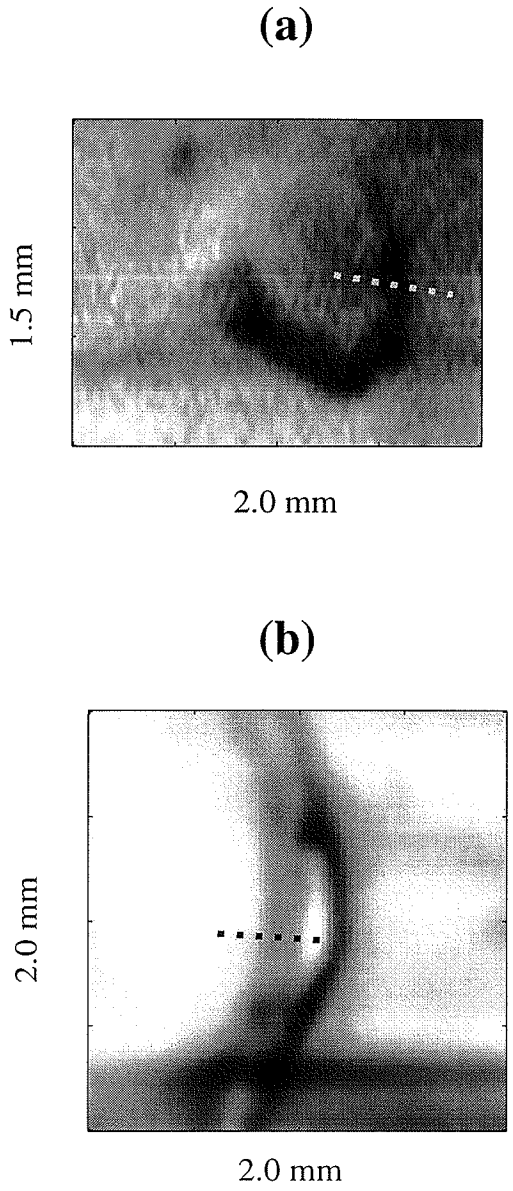

Figure - 3.11. BAI-mode images of the animal tendon within the all-plastic seal. The light transmission microscope image of (a) is in Figure-3.7b. Dashed lines show the location for the measurement.

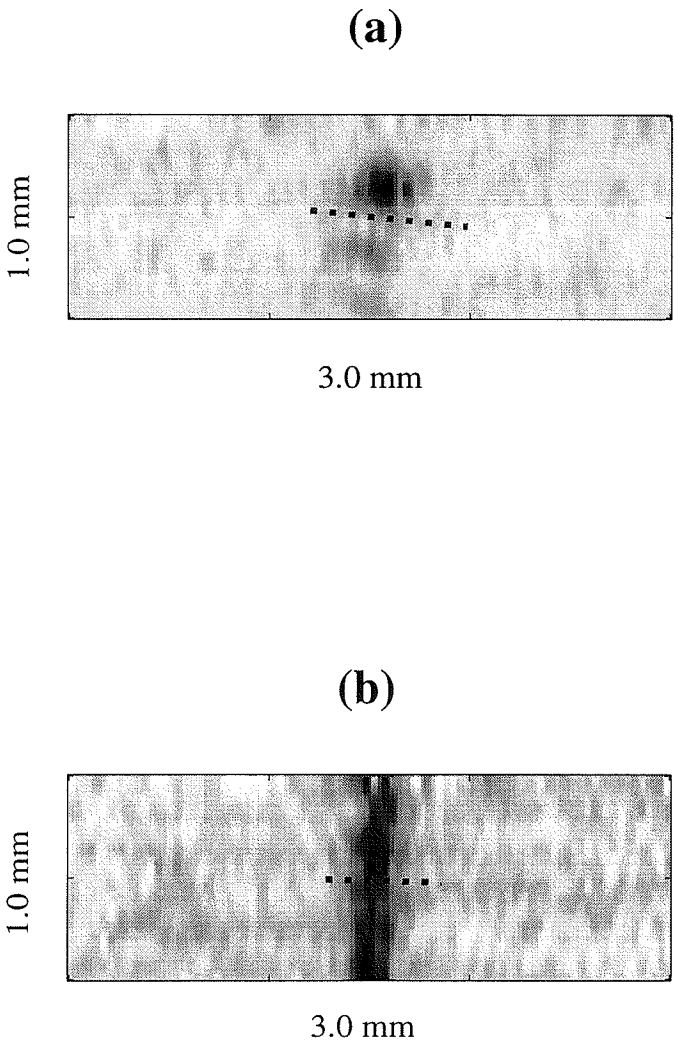

Figure - 3.12. BAI-mode images of the animal tendon within the foil-containing seal. Dashed lines show the location for the measurement.

inclusion defects within the foil-containing seals was 22.6 μm. Thus, the BAI-mode imaging technique detected tendon defects in both packaging materials from 20 to 60 μm.

The BAI values obtained at the normal incidence to the sound propagation direction were smaller in the channel leak and the tendon inclusion than in the undisturbed regions of both all-plastic and foil-containing pouches. Therefore, the defect region on the gray scale BAI-mode image can be shown as darker than the undisturbed region.

Since the BAI values in the undisturbed region were much higher than those in the defect region at the normal incidence of sound propagation, the maximum BAI (BAI_{max}) value on each image corresponds to the value obtained from the undisturbed region. The BAI_{max} value of fifteen all-plastic and fifteen foil-containing retort pouches with defects was extracted from the corresponding BAI-value matrix. The calculated average and standard deviation of these BAI_{max} values were 171.42±36.66 V·μs and 207.49±9.02 V·μs for all-plastic and foil-containing retortable pouches, respectively. These average values showed that the backscattered energy from the seal region of plastic pouches with thickness of 220 μm was significantly less than that of aluminum pouches with thickness of 240 μm (ANOVA analysis, $p < 0.001$).

The coefficient of variation, which indicates the data's magnitude of variation relative to average size (standard deviation/average), of the BAI_{max} values is 21.38% for all-plastic retortable pouches whereas it is 4.35% for foil-containing retortable pouches. This correlates with the visual observations of the seal region, i.e., the seal region of the foil-containing retortable pouches was generally much smoother than that of all-plastic retortable pouches.

Sizes of all channel defects on the 17.3-MHz BAI-mode image were approximately 150-200 μm in Figure-3.9 and 3.10; however, their actual size was approximately ten times less than that. This result was consistent with all other channel defects. It was concluded that the BAI imaging technique was limited for characterizing the defect in terms of its size. It was indicated in Table-3.2 that the lateral resolution of the transducer (the -6-dB transmit-receive beam width or $D_{lateral}$) was about 173 μm for 17.3-MHz center frequency transducer. Sizes of channel defects obtained by the BAI-mode imaging (150-200 μm) in this study are consistent with the lateral resolution. This is advantageous because the image of small defects will be magnified, and can easily be inspected even though the technique is not able to determine the size of the defect.

Figure-3.13 demonstrates the significance of the transducer position during scanning. In Figure-3.13a, a defect channel "i" (50-μm air inclusion in the all-plastic seal region), the edge of seal region "ii", and separation zone of the material "iii" are shown. Figure-3.13b and -3.13c indicate the variation of the BAI values in the direction transverse to the channel defect (I) and in the direction transverse to the edge of the heat seal and separation region (II), respectively. Even though the channel size in Figure-3.13a is very large (50 μm), identification is difficult due to the fact that the BAI values in the defect region were between those in the seal edge and separation region [$BAI_{iii} > BAI_i > BAI_{ii}$]. As long as the BAI values on the defect approach the minimum BAI value in the image matrix, the defect will have high contrast on the image. If only the seal region (under line III) were scanned, i.e., if the region above line III was removed from the image matrix, then the end result [$BAI_{iii} > BAI_i$] would bring about a high contrast and easily distinguishable channel defect on the new image matrix. Figure-3.13d shows only the section under the line in Figure-13a. These findings

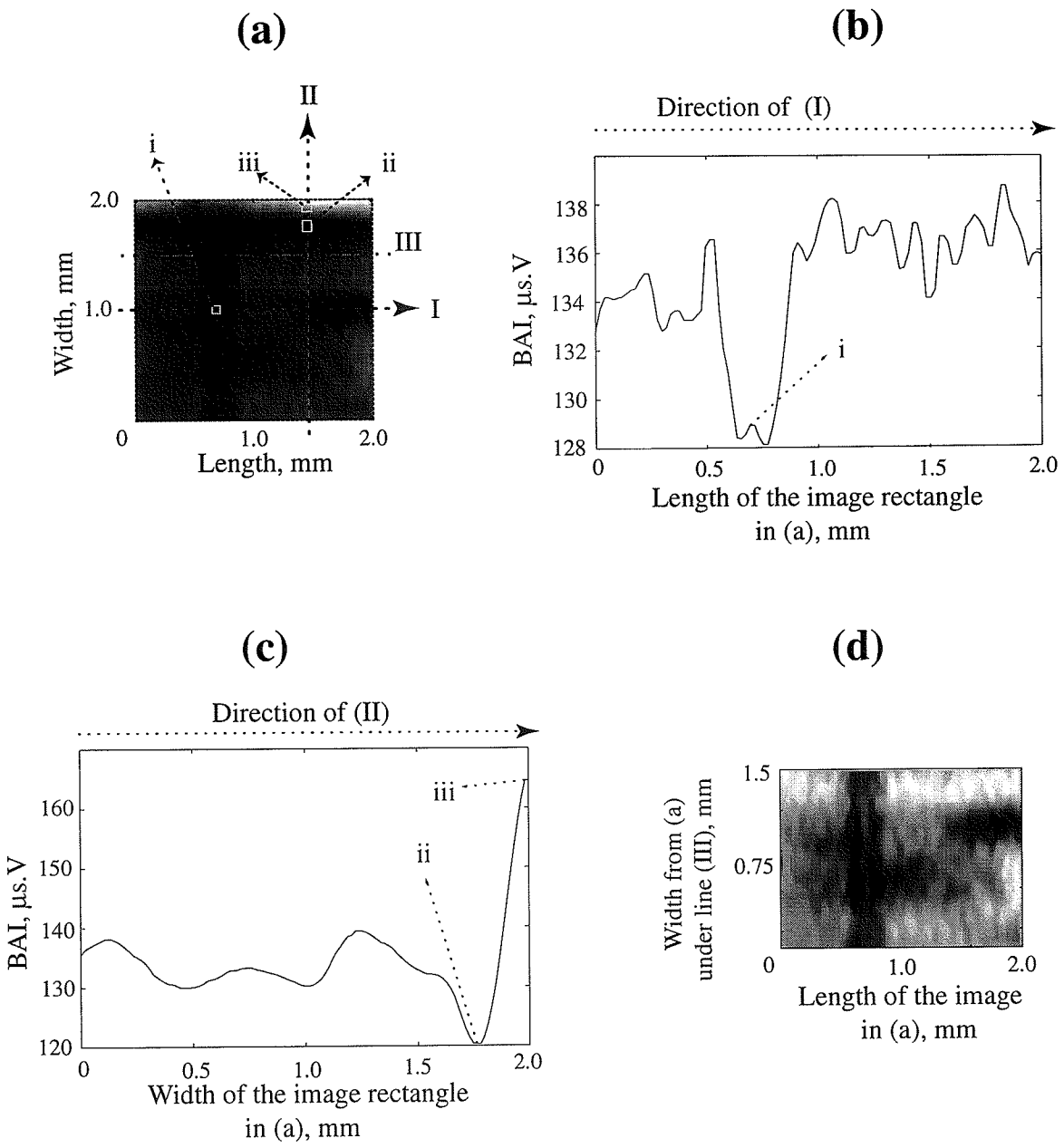

Figure - 3.13. (a) BAI-mode image of 50-µm air-filled channel within the all-plastic seal; (b) variation of BAI values in the direction of (I) demonstrated in (a); (c) variation of BAI values in the direction of (II); (d) BAI-mode image of the section under the line (III) as illustrated in (a).

suggest that the transducer and sample should be positioned such that the scanning area includes only the seal region.

It was indicated in section 2.G.2. in chapter-2 that nondestructive techniques such as X-ray and MRI techniques have low sensitivity to air voids, which might cause microbial penetration through the packaged foods, and that pressure differential testing or gas "sniffer" device does not detect defects which are plugged with the product. The results in this study showed that unlike these nondestructive techniques, the high frequency (17.3 MHz) pulse-echo BAI-mode imaging technique is an effective way to visualize and evaluate both air-filled defects and occluded particles in the seal area of flexible packaging materials, such as all-plastic (transparent) and foil-containing (opaque) retortable pouches.

The engineering trade-off of nondestructive evaluation in diagnostic ultrasound resolution is between resolution and depth of penetration. As the ultrasonic frequency is increased, resolution increases and penetration decreases. At the ultrasonic frequency (17.3 MHz) we used, the seal area of flexible food packages can be reliably inspected. However, if better resolution is desired, that can be achieved by increasing the ultrasonic frequency while keeping reasonable penetration depth (~0.2-0.4 mm) for detection of defects in the seal region of flexible food packages. To improve resolution, research is needed to evaluate the BAI technique at higher ultrasonic frequencies.

3.E. CONCLUSION

The BAI-mode imaging technique has the capability of subwavelength detection of channel and inclusion defects, e .g. detection of defect whose size is smaller than the wavelength of the sound in the propagation medium (λ = 183 μm and

λ =142 μm for all-plastic and foil containing pouches, respectively). Therefore, high-frequency ultrasound imaging can provide the proper sensing method for the construction of a real-time, non-destructive package seal-integrity inspection device. Moreover, the method is already exceeding the reliability of human inspectors by being able to detect defects that are buried in opaque material and are too small for human inspectors to see.

Variation of baseline BAI_{max} in the BAI-mode image might be correlated with the heat seal processing conditions or packaging material; and thus, this variation might be used as a quality and process control parameter if this imaging technique is implemented for the on-line inspection of the heat seal region of flexible packaging materials.

-4-

CONTRAST DESCRIPTOR, ΔBAI

4.A. INTRODUCTION

Raum et al. (1998) described a contrast descriptor for the channel defect on a BAI-mode image, and it was named ΔBAI. It is calculated by subtracting the BAI value in the center location of the channel defect from that of the undisturbed region adjacent to channel defect. A relation was observed between the contrast descriptor ΔBAI and the channel diameter. However, the response of ΔBAI to a wider variety of seal defects is still in question for packaging materials and defect types beyond those in the study.

In this study, channel defects (air-filled and water-filled) ranging from 6 to 100 μm in diameter, and solid inclusion defects ranging from 20 to 150 μm were fabricated in the seal area of all-plastic and foil-containing packaging films. Strands from mouse tail tendon as a food-simulating biomaterial were used to generate solid inclusion defects. The 17.3-MHz ultrasonic pulse-echo Backscattered Amplitude Integral (BAI) method as illustrated in Chapter-3 was used to visualize and evaluate these seal defects

4.B. OBJECTIVES

The purpose of this study is

- to demonstrate the instability of the contrast descriptor, ΔBAI, obtained

by using the procedure defined by Raum et al. (1998).

- to demonstrate a new calculation procedure for the ΔBAI between the defect region and the undisturbed region using the BAI-mode image
- to evaluate the ΔBAI for two packaging materials, three defect types, and sizes.

4.C. MATERIALS & METHODS

4.C.1. Sample Preparation and Validation

The same all-plastic and foil-containing trilaminate films as in Chapter-3 were used for sample production. Three types of defects (air-filled channels, water-filled channels and solid inclusions) in the seal region of both all-plastic and foil-containing packages were created. Smooth, die-drawn tungsten wires (California Fine Wire Company, Grover City, CA) with 6, 10, 15, 37, 50, 75 and 100 μm diameters were used to prepare channel defects. To prepare solid inclusion defects; strands of mouse tail tendon, biomaterial to simulate meat fiber and other food fibers were used. Defect samples were prepared, and they were validated by the light transmission microscope as described in section 3.D.1 and 3.D.2. in Chapter-3.

4.C.2. System Description and Data Acquisition

The same data acquisition system as in Figure-3.4 was used. Refer to section 3.D.3 and 3.D.5 in Chapter-3 for system description and data acquisition. The only difference was that the field-of-view of scanned samples varied from the smallest 1.5 mm (parallel to seal's major axis) × 1.0 mm (transverse to seal's major axis) to the largest 4.0 mm × 2.0 mm area.

4.C.3. BAI-mode Imaging and ΔBAI Contrast Descriptor

BAI-mode image of samples was generated by the same procedure as described in section 3.D.6 in Chapter-3. As a measure of contrast in the BAI-mode image for the channel defect, Raum et al. (1998) suggested the quantity, ΔBAI, which has been defined by:

$$\Delta BAI = BAI_{undisturbed} - BAI_{mid\text{-}channel} \qquad 4.1.$$

where the $BAI_{undisturbed}$ is the unnormalized BAI value from the undisturbed region adjacent to the channel defect, and the $BAI_{mid\text{-}channel}$ is the unnormalized BAI value from the center location of the channel defect. However, this calculation procedure did not produce a stable result for samples produced for this study, i.e., the ΔBAI calculated by Equation-4.1 produced different values at different undisturbed regions. In some instances, the ΔBAI varied by region as much as ± %200. The reason is that the distance between the undisturbed and the defect region has not been stated clearly. In this study, the ΔBAI contrast value for the defect on the image was calculated by

$$\Delta BAI = BAI_{background} - BAI_{defect} \qquad 4.2.$$

where the $BAI_{background}$ is the average unnormalized BAI value of ten spatially separated random locations from regions, which do not include the defect. The BAI_{defect} is the average unnormalized BAI value in the defect location. Figure-4.1 indicates the background and defect locations on the BAI-mode image. For calculation purposes, "Imcrop", built-in image processing function in MATLAB®, was used to select the subimages from the background and defect locations. Individual subimage areas were approximately 0.3 mm × 0.3 mm, and ten different

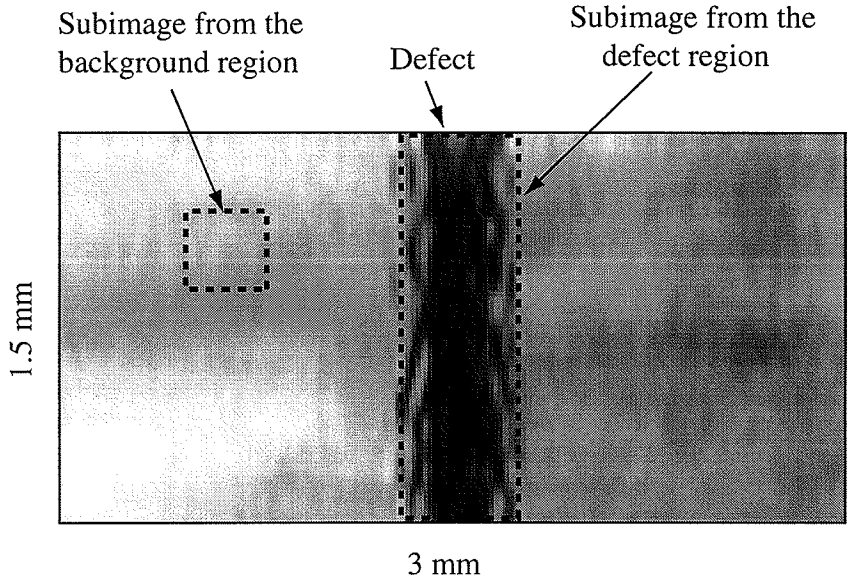

Figure - 4.1. A BAI-mode image of water-filled channel defect (38 μm) in the seal region of all-plastic film. Dashed rectangles are used to calculate the contrast descriptor, ΔBAI, of the defect.

subimages were used to estimate the $BAI_{background}$ value. The same procedure was followed for the calculation of the BAI_{defect}; however, only one subimage was selected which longitudinally covered the defect region. The program coded by MATLAB to calculate the ΔBAI value and the list of data files are shown in Appendixes, A.3 and A.6, respectively.

4.C.4. Statistical Analysis

Regression analysis between the size of defects and ΔBAI contrast values for each defect type was executed. Statistical calculations were performed by the built-in functions in Microsoft Excel® 97.

4.D. RESULTS & DISCUSSION

Channel defects were classified as: air-filled channel defect within all-plastic film (ACP), water-filled channel defect within all-plastic film (WCP), air-filled channel defect within foil-containing film (ACF), and water-filled channel defect within foil-containing film (WCF). Since seven different tungsten wires (6, 10, 15, 38, 50, 75, and 100 μm) were used to create these defects, and since five replications for each wire size were produced, thirty-five channel defects were fabricated for each group. Thus, a total of 140 channel defect samples were evaluated. Also, eighteen inclusion defects within all-plastic (IDP) and fifteen inclusion defects within foil-containing film (IDF) were evaluated.

4.D.1. Lateral Size Measurement

Due to the opaque nature of foil-containing films (ACF, WCF and IDF), the lateral size of the defect in these samples could not be optically measured. Only the lateral size of ACP, WCP, and IDP samples was measured. Figure-4.2a demonstrates the top view of a seal defect in the all-plastic sample, which was used for lateral size measurement. The lateral size fraction ($f_{lateral}$) was calculated for ACP and WCP samples by

$$f_{lateral} = \frac{d_{lateral}}{d_{wire}} \qquad 4.3.$$

where the $d_{lateral}$ is the lateral size of the defect (μm) measured using the light microscope image, and the d_{wire} is the diameter of the tungsten wire used to create the defect. The $f_{lateral}$ was 0.91 ± 0.06 for these tested seventy samples. Consequently, these channels' lateral size was apparently smaller than the size of the tungsten wires used to create the respective defect.

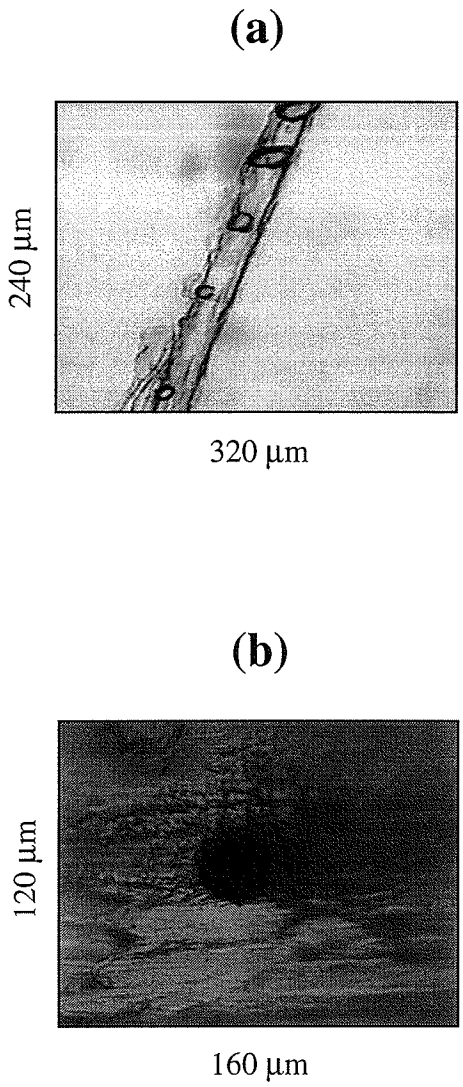

Figure - 4.2. Light microscope images; (a) top view of inclusion defect (minimum lateral size = 29.8 µm); (b) cross-sectional view of air-filled channel defect (36.8 µm) in the seal region of all-plastic films.

The lateral size of eighteen-inclusion defect samples (IDP) was also measured. Since the tendon strands' shape changed throughout their longitudinal axis, the size measured on their lateral axis also varied as shown in Figure-4.2a. Therefore, the smallest lateral size of IDP samples was measured, and it varied between 15 and 130 μm.

4.D.2. Size Measurements from The Cross Section

Although foil-containing films were opaque from the top view for lateral size measurements, defects in this material and all-plastic films could be measured from the cross section under the light transmission microscope. Figure-4.2b illustrates the light microscope image of a seal defect from the side view. 140 channel defect samples (ACP, WCP, ACF, and WCF) were inspected under the microscope; however, thirty-three of them could not be measured under the microscope. Of these unidentified samples, twenty-four of them were the channel defects created by 6- and 10-μm diameter tungsten wires. The smearing of the packaging material on the cut surface did not allow the detection of particularly small defects (≤10μm). The cross-sectional channel shape of the defect was elliptical for all other 107 identified samples. To measure the eccentricity of the elliptical geometry of the defect, the fraction f_{defect} was defined by

$$f_{defect} = \frac{d_{major}}{d_{minor}} \qquad 4.3.$$

where the d_{major} is the size on the major defect axis, and the d_{minor} is the size on the minor defect axis (See Figure-3.3a in Chapter-3). The average and standard deviation of f_{defect} were 1.16 ± 0.14 for these unidentified 107 samples, and its minimum and maximum values were 0.88 and 1.76, respectively.

All inclusion defects- eighteen IDP and fifteen IDF- were measured from their cross-sections, and the shape of these defects was also elliptical. The average and standard deviation of f_{defect} was 2.14 ± 0.81 for these samples, and its minimum and maximum values were 1.02 and 3.72, respectively, which clearly indicated that the d_{major} of tendon strands was much larger than their d_{minor} compared to channel defect samples. Furthermore, the d_{major} of these defects ranged from 20 to 150 μm, and the minimum detected d_{major} for IDP and IDF samples was 20 and 26.4 μm, respectively. The reason of expansion of these defects through the major axis might be the blade of cyrostat (used to cut samples) that squeezed the sample from the top.

For definition purposes, the d_{major} is the value quoted hereafter for the size of both channel defects and inclusion defects. As explained in earlier discussion, some of the channel defects (thirty-three of them) could not be identified from their cross sectional view. For these samples, the wire diameter was quoted for their size.

4.D.3. BAI-mode Images

Figure-4.3, 4.4, and 4.5 demonstrate the BAI-mode images of various types of defects with different d_{major} produced in both all-plastic and foil-containing samples. The BAI-mode imaging technique had the capability of subwavelength detection of channel and inclusion defects, e.g., detection of defects in sizes below 100 μm whereas λ (=c/*f*) is 138 μm for all-plastic films and 142 μm for foil-containing films at the center frequency of 17.3 MHz. All tendon strands and channels (d_{major} > 15 μm) were easily detected on the BAI-mode image. However, some small channel defects ($d_{major} \leq$ 15μm) did not produce the same efficient results. Figure-4.6 shows two example BAI-mode images to indicate

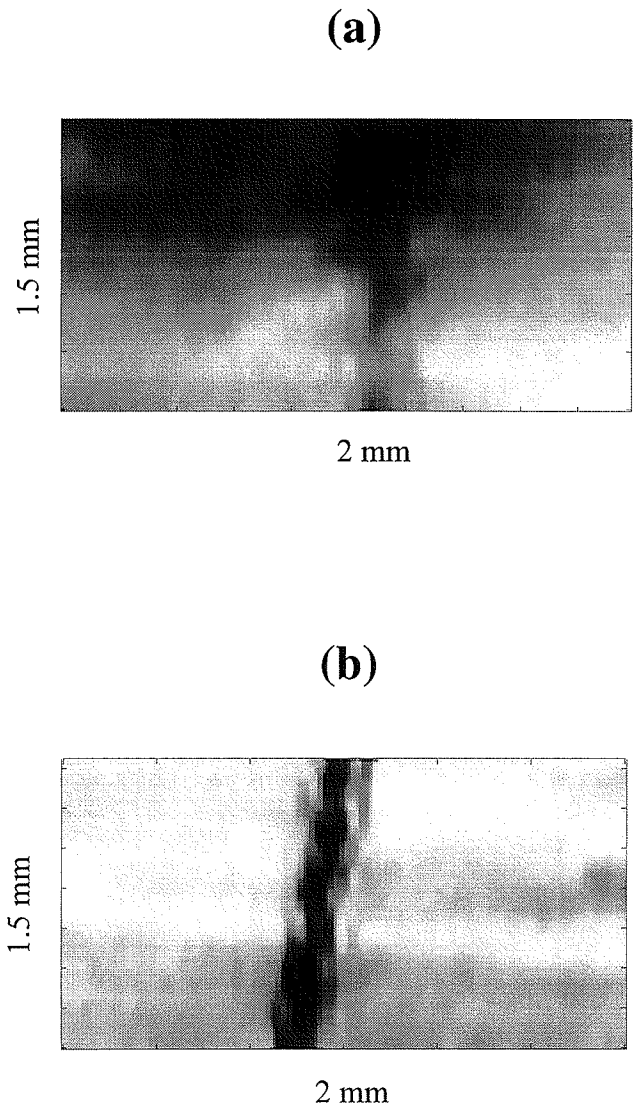

Figure - 4.3. The BAI-mode images of (a) 14.6 μm water filled channel defect and (b) 73.5 μm air-filled channel defect in all-plastic film.

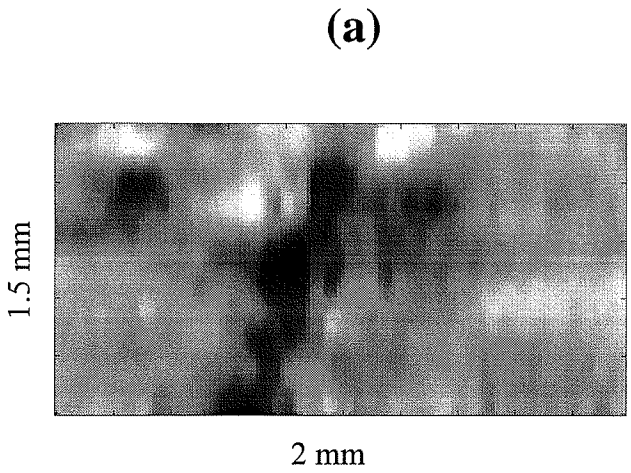

Figure - 4.4. The BAI-mode images of (a) 6 µm air-filled channel defect and (d) 48.7µm water-filled channel defect in foil-containing film.

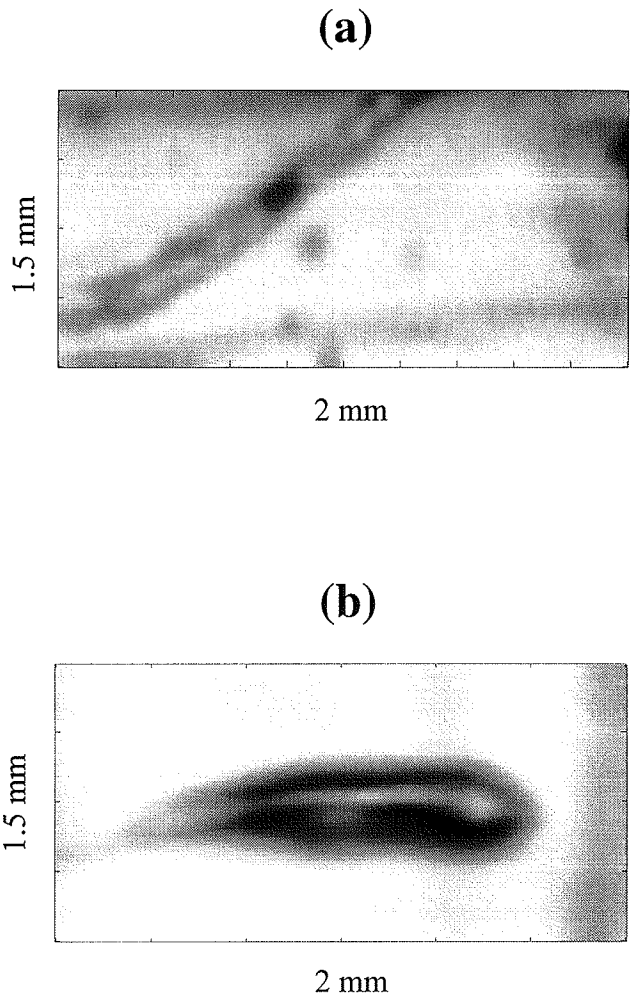

Figure - 4.5. The BAI-mode image of tendon defects in (a) all-plastic film and (b) foil-containing film. The lateral size of tendon defects varied in their lateral axis.

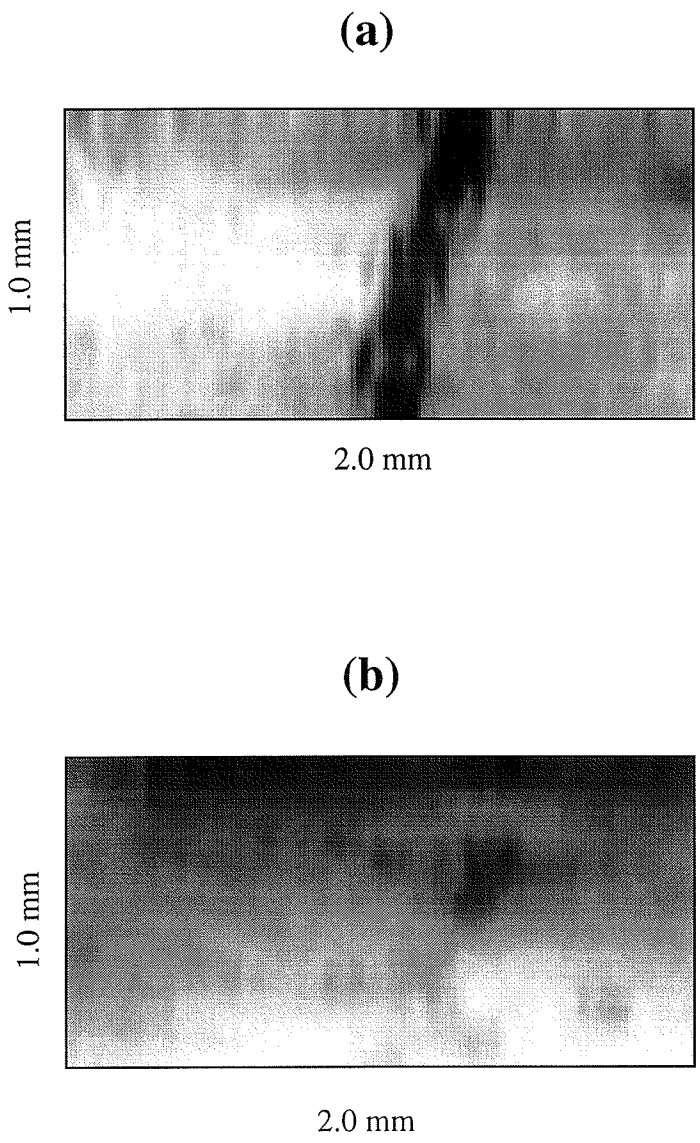

Figure - 4.6. The BAI-mode image of detected air-filled channel defect (d_{major} = 6 μm) in the seal region of foil-containing film and (b) undetected water-filled channel defect (d_{major} = 6 μm) in the seal region of all-plastic film.

Table - 4.1. Unidentified channel defects (≤ 15 μm) on BAI-mode images

Wire used to create the channel defect (μm)	Types of packaging material				Percentage of unidentified channel defects on the BAI-mode image (%)**
	All-plastic pouch		Foil-containing pouch		
	Channel type				
	Air*	Water*	Air*	Water*	
15	0	0	2	2	20
10	3	2	2	3	50
6	5	4	2	3	70

* Column represents a total number of unidentified channel defects out of 5 replications.

** The percentage was calculated by

$$\text{Percentage} = \frac{100 \times \text{total number of unidentified images for the given wire type}}{20}$$

the difference between the detected and undetected defects. Table-4.1 shows the number of defect samples that were not detected on the BAI-mode images. For illustrative purposes, the results were grouped by diameter of the forming wire instead of the real defect size (d_{major}). The failure of defect detection (as a percentage) was calculated for the corresponding wire group, and each wire group generated a total of 20 samples. This failure increased from 20% for defects produced by 15-μm diameter wires to 70% for those produced by 6-μm diameter wires. These results indicate that the BAI-mode resolution decreased dramatically as the size of these defects decreased.

In addition, the size of defects on the BAI-mode image was much larger than its actual size (d_{major}) and varied approximately between 150 and 200 μm.

Similar results have also been obtained by the study in Chapter-3, and that was correlated with the lateral resolution or the -6-dB transmit-receive beam width of the transducer.

4.D.4. Contrast descriptor, ΔBAI

Figure-4.3, 4.4, and 4.5 illustrates that the contrast of the defect region on the image was different from that of the undisturbed region, and this result was consistent for all BAI-mode images that apparently demonstrated the defect. The BAI values in the defect region were smaller than those in the undisturbed region, i.e., the total reflected echo energy from the defect region was lower than that of the undisturbed region.

Figure-4.7 shows the relationship between the ΔBAI value and the defect size. The relationship of ΔBAI values with defect sizes showed a linear correlation for each sample group (ACP, WCP, ACF, WCF, IDP and IDF). Table-4.2 indicates the slope of fitted lines (defect size vs. ΔBAI) and the corresponding correlation

Table - 4.2. Slope of fitted lines (d_{major} vs. ΔBAI) in Figure-4.7 and correlation coefficients obtained by linear regression analysis

Sample Group	Slope (V·s/m)	Correlation Coefficient (R^2)
ACP	0.233	0.91
WCP	0.250	0.89
ACF	0.359	0.88
WCF	0.317	0.91
IDP	0.124	0.79
IDF	0.081	0.75

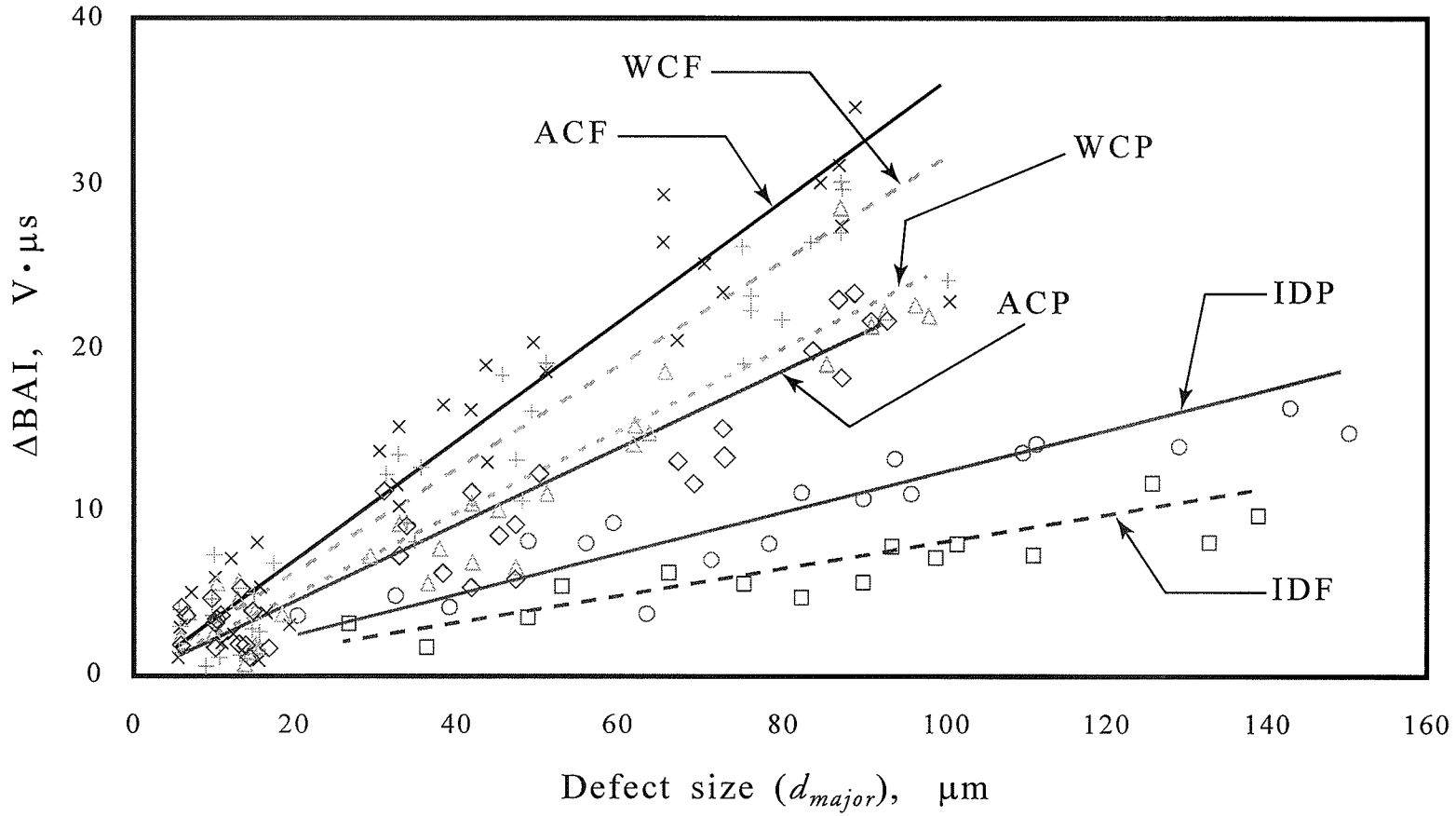

Figure - 4.7. The size of defects vs. ΔBAI. The line-fit of each group was drawn according to its regression constants in Table-4.2.

coefficient (R^2) obtained by the linear regression. The fitted lines in Figure-4.7 were drawn according to results obtained by the regression analysis. High correlation coefficients clearly indicate that the ΔBAI contrast value decreased as the defect size decreased, i.e. BAI values in the defect region (BAI_{defect}) became close to those in the background region ($BAI_{background}$) as the defect size declined.

Figure-4.8 demonstrates the 95% confidence interval of the slope ($\Delta BAI/d_{major}$) of the fitted lines in Figure-4.7. The right arrow (>) and the left arrow (<) in Figure-4.8 indicate the lower and upper limit of confidence intervals, respectively.

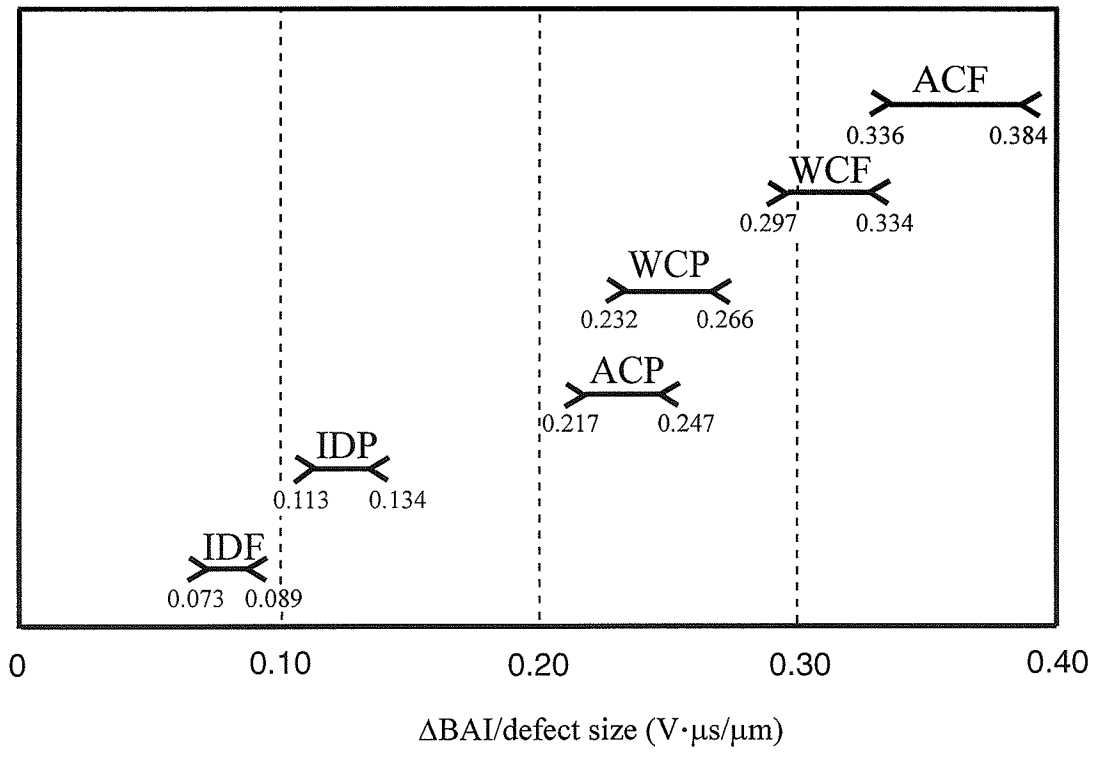

Figure - 4.8. 95% confidence intervals of the slope of fitted lines in Figure-4.5

According to this figure, only the confidence intervals of WCP and ACP samples, i.e. channel defects in the seal region of all-plastic films, overlap to each other. Consequently, at 95% confidence level the ΔBAI values of WCP samples were not significantly different from those of ACP samples for the same d_{major}. On the other hand, ΔBAI values of other samples were significantly different from each other for the same d_{major}. As a result, the contrast descriptor, ΔBAI, varied with defect types (air-filled channels, water-filled channels and inclusion defects), defect sizes (d_{major}), and types of packaging materials (all-plastic and foil-containing films).

4.E. CONCLUSION

It has been shown that there is a linear relationship between the defect size and the contrast value, denoted ΔBAI , and that different defect types and packaging materials have a significant impact on the ΔBAI value. The ΔBAI can be used in two ways. First, the BAI-mode image is limited for characterizing the defect in terms of its size. However, by knowing the packaging material's characteristics and by estimating what kind of defect might be involved to contaminate the seal region of the package, the size of the defect can be approximated using the calibration curve (ΔBAI vs. defect size). Different defects have different impacts on the ΔBAI value for the same packaging material. After recognizing all significant defect types within the seal region of a packaging material, the calibration curves can be prepared in the laboratory for use by on-line equipment.

Second, the ΔBAI contrast descriptor on the BAI-mode image can provide a simple yet quite effective sensing method for on-line package inspection. After the minimum defect size is safely identified by the BAI-mode image (15 μm in this study), the corresponding minimum ΔBAI contrast value can be set. This

minimum value would provide stable and robust criteria for deciding whether the package is rejected from the inspection line or not. Application of results in this study will require further research. The calculation of ΔBAI contrast descriptor is currently limited by manual data collection algorithms. A new technique, which automatically recognizes the defect on the BAI-mode image, and automatically calculates the ΔBAI contrast descriptor, is necessary for on-line inspection of packages.

-5-

INSPECTION OF SEAL DEFECTS BY VARIATION OF BAI VALUES

5.A. INTRODUCTION

So far, the BAI-mode imaging technique has been evaluated for seal regions which included either a channel or an inclusion type defect. In this chapter, the limitation of the BAI mode imaging will be illustrated for other types of defects, and a new technique will be presented to overcome the limitation of the imaging technique.

Figure-5.1a demonstrates the BAI-mode image of the seal region of all-plastic pouch that does not include any defect. Figure-5.1b indicates the BAI-mode image of the seal region of the same pouch that has visible bubbles and wrinkles on its surface. As demonstrated in these two samples, the BAI-imaging technique has no capability to differentiate the solid seal from the defective seal in which wrinkles, bubbles, and blisters are distributed in the region. In addition to that, blisters, bubbles, and wrinkles are NFPA-defined major defects (see 2.F in Chapter-2) which might compromise the package integrity, and thus, they should be inspected.

Any irregularities either on the surface or inside the seal will affect the reflected echo signal, and therefore the coefficient of variation of the BAI-value, which indicates data's magnitude of variation relative to mean magnitude (standard

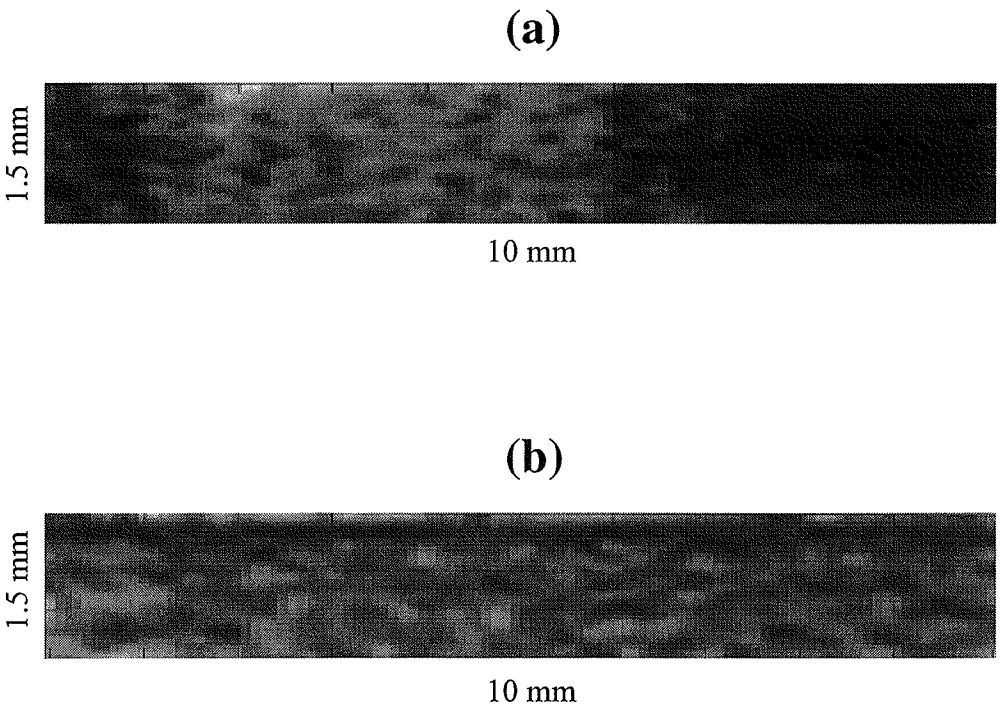

Figure - 5.1. The BAI-mode image of all-plastic films in the seal region. (a) Sample does not contain any visible defect; (b) Sample has visible wrinkles and bubbles in its surface.

deviation/average). This figure will give a simple measure of seal quality.

To prepare samples for this study, the sealing-bar temperature was varied. It is hypothesized that at low sealing-bar temperatures, the package material used would not weld completely, and non-bonding regions might occur within the sample. In addition to that, it is also presumed that high sealing-bar temperatures might cause the wrinkle formation.

5.B. OBJECTIVE

To develop a new technique to detect macroscale defects such as non-bondings, delaminations, wrinkles, and bubbles which the BAI-mode imaging can not identify.

5.C. MATERIALS & METHODS

5.C.1. Sample Preparation

The same all-plastic and foil-containing trilaminate films as in Chapter-3 were used for sample production. Samples were produced by welding the two identical layers of the packaging material at different temperatures using the same automatic band sealer (Doboy HS-C42051, Doboy Co., New Richmond, WI) as in Chapter-3 (See Figure-3.1). The sealing bar temperature was adjusted by thermostat knob of the sealer, and it was 90-200°C for all-plastic films and 140-250°C for foil-containing films, with samples constructed at 10°C intervals.

5.D.2. Sample Validation

A scanning laser acoustic microscope, SLAM (Sonomicroscope 100®, Sonoscan, Inc., Bensenville, IL), operating at an acoustic frequency of 100 MHz, was used to examine samples. Operational details of SLAM have been discussed in 2.I.1, Chapter-2. A small representative region from the seal area was cut out by using razor blade. Next, the specimen was located on the microscope stage along with a thin layer of water, and the semi-reflective cover slip was placed on the sample. The real-time interference image of the specimen was displayed on a standard television monitor. The sample was magnified by approximately 100X. The field-of-view of the image was approximately 3 mm horizontally by 2 mm vertically. A frame grabber was used to digitize the video signal of the interference images.

Eight digitized images per sample were collected and saved as TIFF (tagged-image file format) format. The average of these eight digitized images was obtained to remove the foggy appearance. The averaged image was improved by histogram equalization to enhance the contrast. Finally, the median filter was applied to remove the salt and pepper noise on the image. All image-processing calculations were performed by Image Processing Toolbox in Matlab® (The Math Works, Inc., Natick, Mass.).

5.C.3. Data Acquisition

The same data acquisition system as in Figure-3.4 was used. Refer to section 3.D.3 and 3.D.5 in Chapter-3 for system description and data acquisition. The sample was scanned in a rectangular grid pattern by moving the transducer to the fixed-position sample (Figure-3.4). The horizontal and vertical grid spacings on the rectangular surface of the sample were 200 μm and 100 μm, respectively. The horizontal direction on the rectangle was parallel to the sealing direction. Field-of-view was 1.5 mm (vertical direction) × 10.0 mm (horizontal direction). The number of waveforms (Radio frequency (RF) echo signals) is 50 (10mm/200μm) in the horizontal direction and 15 (1.5 mm/100 μm) in the vertical direction for the total number of 750 (50 × 15) waveforms. Since each waveform included 170 data points, the three dimensional data set contains 750 170-point RF data acquisitions.

5.C.4. Coefficient of Variation of The BAI-value Matrix

The three-dimensional data set was processed as in 3.D.6, Chapter-3 to produce the two-dimensional BAI-value matrix. The average and the standard deviation of the BAI-value matrix were calculated. Using these two values, the coefficient of variation (CV) for each sample was calculated by:

$$CV = \frac{\text{Standard Deviation of BAI values in the BAI-matrix}}{\text{Average of BAI values}} \cdot 100$$

The program coded using the MATLAB to calculate the coefficient of variation of BAI-values and the list of data files are demonstrated in Appendixes, A.4 and A.7, respectively.

5.C.5. The BAI-mode Imaging

To produce the BAI-mode image, the BAI-value matrix was interpolated by a factor of ten in the direction horizontal to the image rectangle (200μm/10) and by a factor of five in the direction vertical to it (100μm/5). The interpolation resulted in pixel sizes of 20 μm × 20 μm with the number of rows and columns in the BAI matrix of 75 (15 by 5) and 500 (50 by 10), respectively. The final normalized image matrix was used to yield the gray scale image. Image processing was performed using Matlab® (The Math Works, Inc., Natick, Mass.).

5.D. RESULTS AND DISCUSSION

The sealing-bar temperature range was 90-200°C and 140-250°C for all-plastic and foil-containing films, respectively. Two samples were produced at 10°C intervals resulting in twenty-four samples for each packaging material.

5.D.1. The BAI-mode Imaging

The BAI-mode image of twenty-four all-plastic and twenty-four foil-containing samples was constructed. Figure-5.1 illustrates the BAI-mode image of all-plastic samples produced at 150°C and 200°C, respectively, and Figure-5.2 demonstrates

the BAI-mode image of foil-containing samples generated at 150°C and 210°C, respectively. The sample surface in Figure-5.1a and Figure-5.2b was smooth, whereas the seal region of the sample in Figure-5.1b had obvious blisters and bubbles, and that in Figure-5.2.a was delaminated after collecting the BAI data. These visual observations were validated by SLAM interference images, which will be discussed in the next section. Examination of other samples indicated

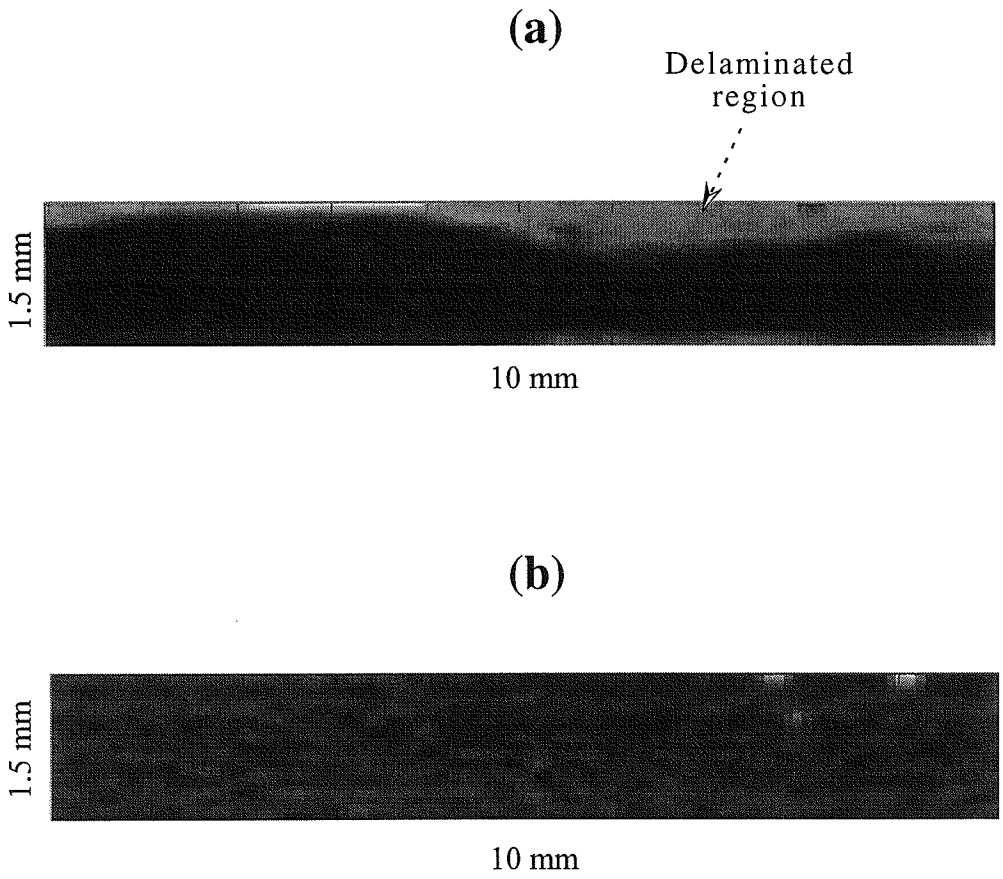

Figure - 5.2. The BAI-mode image of foil-containing films in the seal region. Samples were constructed at (a) 150°C and (b) 210°C.

that even though defects in the seal region of some samples were apparent, the BAI-mode imaging did not distinguish the defect samples from solid ones.

5.D.2. Sample Validation by SLAM

The scanning laser acoustic microscope (SLAM) interference images were generated from all samples. Figure-5.3, -5.4, and -5.5 demonstrate interference images of samples (three all-plastic samples and three foil-containing samples) constructed at different sealing bar temperatures. The interference image field of view contains vertical interference lines. A shift from the SLAM interference image was observed in the sample plastic boundary, which is demonstrated in Figure-5.3a. There was a contrast between the specimen and water region, and the specimen region was always darker than the water region in SLAM interference images. Interference lines in foil-containing samples were barely visible compared to those in all-plastic samples. The reason might be attributed to the thickness of the foil-containing film that was approximately 20 μm larger than that of all-plastic film.

Figure-5.3 illustrates SLAM interference images whose interference lines disappeared in some areas within the sample. This situation was observed from all-plastic samples and foil-containing samples produced in the sealing-bar temperatures ranging from 90 to 120°C and 140 to 170°C, respectively. Some of the more poorly fused samples exhibited complete separation after the completion of the experiment. When there is a delamination or non-bonding in the seal region, air fills the region. SLAM interference lines disappear in these regions since the impedance of air is much lower than that of polymeric materials.

Figures-5.4 demonstrates SLAM interference images whose interference lines were vertically parallel to each other. This type of vertical, uninterrupted

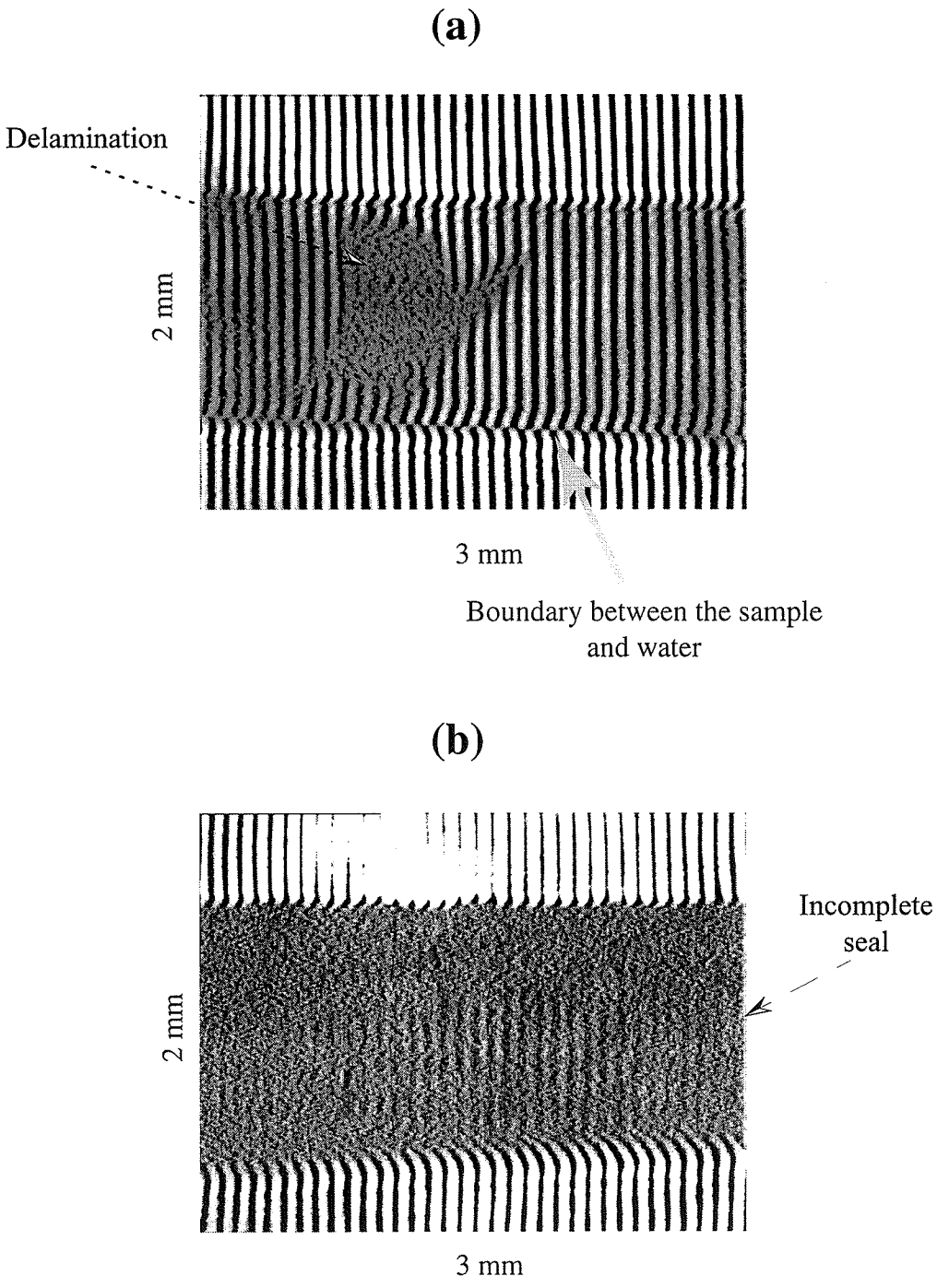

Figure - 5.3. SLAM interference image of (a) all-plastic sample and (b) foil-containing sample constructed at *low* sealing-bar temperatures, which were 90°C and 150°C for (a) and (b), respectively.

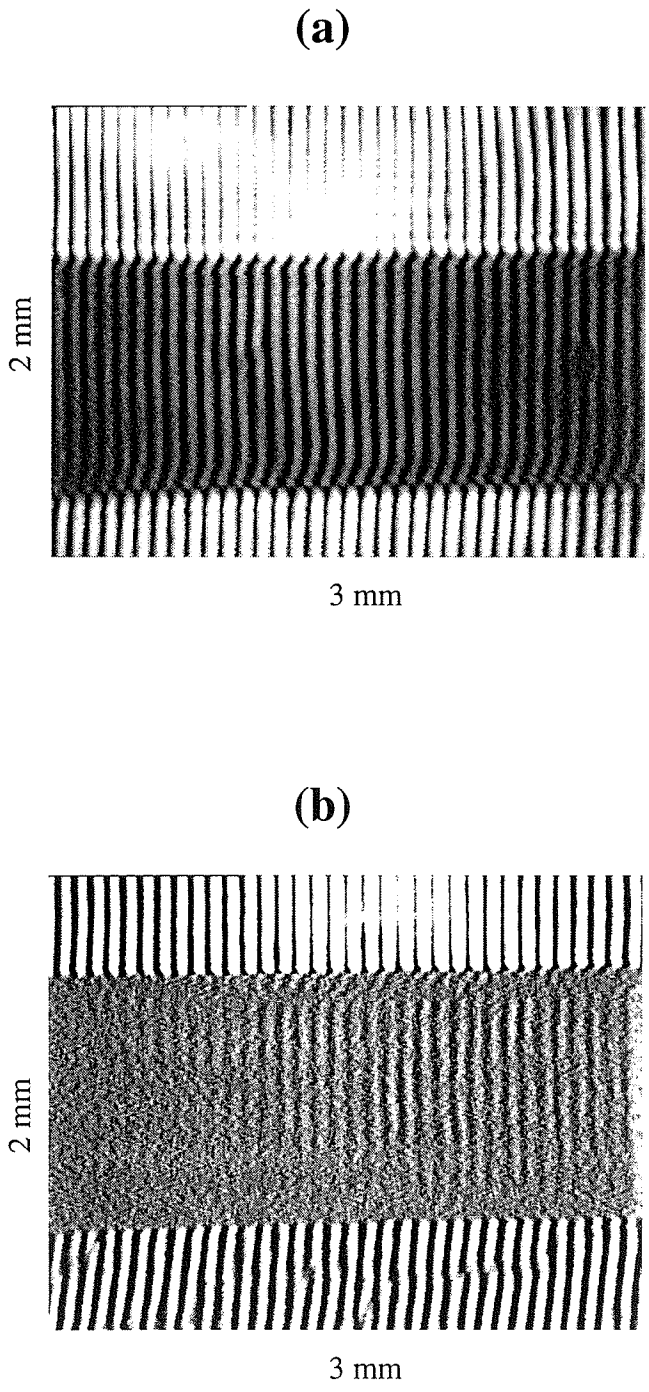

Figure - 5.4. SLAM interference image of (a) all-plastic sample and (b) foil-containing sample constructed at *optimum* sealing-bar temperatures, which were 150 °C and 220°C for (a) and (b), respectively.

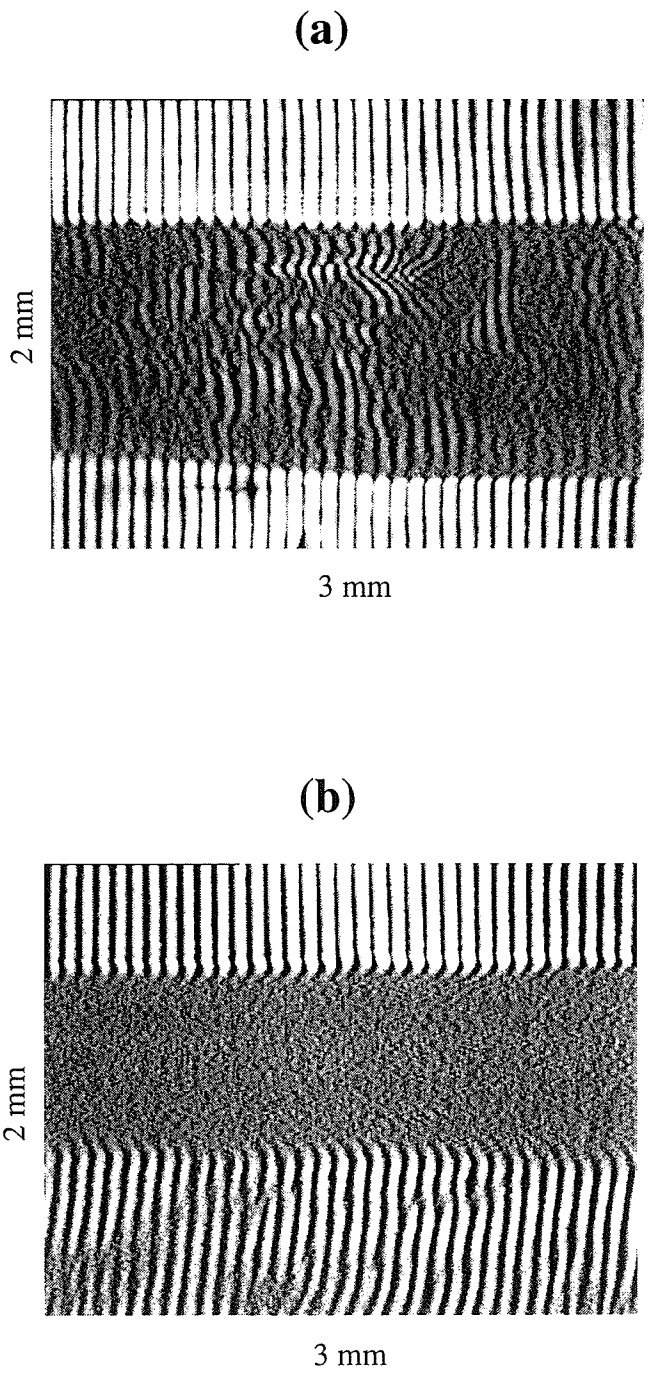

Figure - 5.5. SLAM interference image of (a) all-plastic sample and (b) foil-containing sample constructed at *high* sealing-bar temperatures, which were 200 °C and 240°C for (a) and (b), respectively.

interference lines were noticed from all-plastic samples and foil-containing samples created at the sealing-bar temperatures ranging from 130 to 170°C and from 180 to 220°C, respectively. The surface of these samples was also inspected visually, and very smooth surfaces were observed. In brief, as long as the interior of the seal region does not contain air void, SLAM yields ordered vertical interference lines in the region.

Figure-5.5 shows SLAM interference images whose interference lines are twined inside the specimen region. All-plastic samples and foil-containing samples constructed at the sealing-bar temperatures above 180°C and 230°C, respectively, yielded the same results. Wrinkles, discoloration, bubbles, and blisters were visually observed from these samples.

Until now, three sealing-bar temperature regions have been categorized for all-plastic and foil-containing materials using the SLAM: (I) low sealing-bar temperature range; (II) optimum sealing-bar temperature range; and (III) high sealing-bar temperature range. Table-5.1 illustrates these regions for each sample group and summarizes the SLAM study.

5.D.3. Average BAI-value of The BAI-value Matrix

Figure-5.6 demonstrates average BAI-values of samples produced at different sealing bar temperatures. Average BAI-values were calculated using the BAI-matrix, and the matrix was formed by 750 (50×15) BAI values. Since BAI-values in the matrix contained 170 RF data acquisition, each data point shown in the Figure-5.6 was the result of 127500 (750×170) RF data acquisition. The three sealing-bar temperature regions obtained by SLAM and visual observations were placed in the figure to compare the difference of average BAI-values for these regions. As clearly indicated in the figure, the average BAI values declined with

Table - 5.1. Evaluation of sealing bar-temperature on all-plastic and foil-containing samples using SLAM

Region	Packaging material	Sealing-bar temperature range	Observations
I Low sealing-bar temperature range	all-plastic film	90-120°C	SLAM: Interference lines disappeared in non-bonding region
	foil-containing film	140-170°C	Visual: Some samples were delaminated after the data collection
II Optimum sealing-bar temperature range	all-plastic film	130-170°C	SLAM: Smooth vertical interference lines in the specimen area
	foil-containing film	180-220°C	Visual: No visual defect and smooth sample surface
III High sealing-bar temperature range	all-plastic film	180-200°C	SLAM: Interference lines were tangled
	foil-containing film	230-250°C	Visual: Wrinkles, discoloration, bubbles and blisters were clearly visible

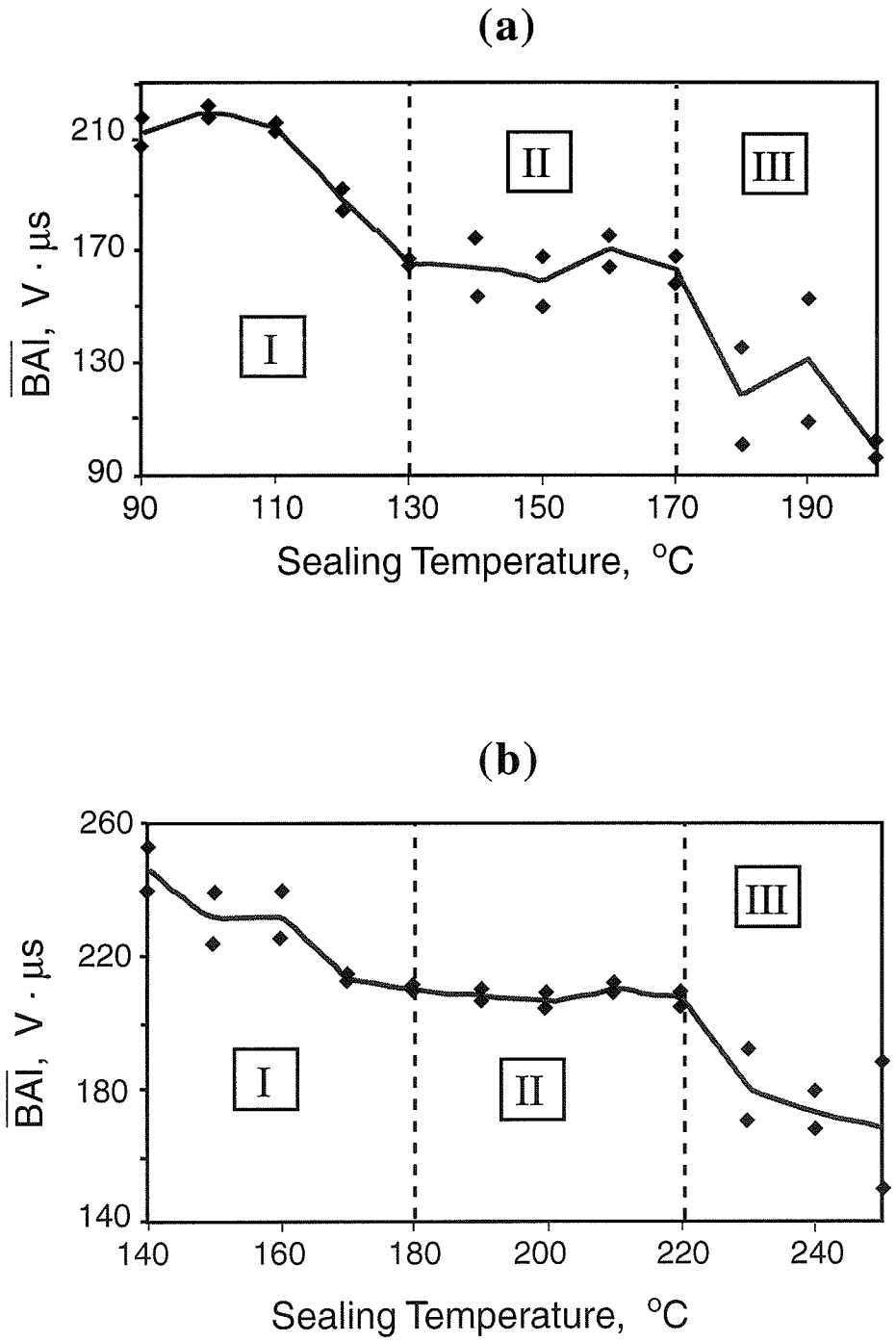

Figure - 5.6. Average BAI values of (a) all-plastic films and (b) foil-containing films constructed at different sealing-bar temperatures. Solid lines indicate the average of two data at the same sealing-bar temperature.

the increase in the sealing bar temperatures in the region-I and region-III, and those became approximately constant in the region-II. In addition to that, average BAI values in region-I were higher than those in region-II and -III, and those in region-II were more elevated than those in region-III.

As explained before, any irregularities either on the surface or inside the seal will affect the reflected echo signal, and therefore the BAI value. In region-I, the low sealing-bar temperature caused delaminations, large air voids, or non-bonding in the seal area of package materials. High average BAI values in region-I suggest that the intensity of reflected echo signal in that region was stronger than that in other regions. Consequently, the delamination or nonbonding of a seal caused more reflected echo signal to return to the transducer because of high acoustic-impedance difference between the air in the defect and the polymeric package material.

In region-III, high sealing-bar temperature application caused the formation of many observable wrinkles, bubbles, and blisters. Low average BAI values in region-III imply that the intensity of reflected echo signals diminished. The reason might be the geometry of defects in these regions. If the defect's front surface is not normal to the ultrasonic beam, the transducer will not be able to catch some of the reflected echo signal, which decreases the signal intensity. Defects such as bubbles, blisters, and wrinkles may have diverted the incident energy, and thus, the intensity of reflected signal decreased.

Average BAI-values were stable in region-II. They ranged from 150 to 175 V·μs and from 205 to 211 V·μs for all-plastic films and foil-containing samples, respectively. Figure-5.5 indicates this region as a slightly varying horizontal line. SLAM and visual observations had previously shown that samples produced

at the optimum sealing-bar temperature range (region-II) had good surfaces and the inside of the sample was solid. Hence, as long as sealing is performed at optimum conditions, the average BAI-value of the package seal will be in certain limits.

5.D.4. Coefficient of Variation of The BAI-value Matrix

The coefficient of variation (CV) is the data's magnitude of variation relative to average size, i.e., the ratio of standard deviation to the average of data. The lower the CV, the smaller the variation in the data, i.e., values in the data get close to the average value.

Figure-5.7 demonstrates the CV of BAI-values for samples produced at different sealing bar temperatures. The CVs were high in regions I and III (defect containing samples) compared to region II (solid samples). In region II, the CVs were lower than 10% and 2.5% for all-plastic and foil-containing films, respectively. In conclusion, if the seal region of the package contains defects, the variation of the BAI-values in the data will be elevated, and this can be measured by calculating the coefficient of variation of the data.

5.D.5. The Coefficient of Variation Versus Average BAI

Calculated average BAI-values and the CVs for samples were gathered in Figure-5.8 that was completed using Figure-5.6 and -5.7. For all-plastic samples, the average BAI-values between 150 and 175 V·μs and the CVs lower than 10% bounded the region-II as indicated in Figure-5.8a. For foil-containing samples, region-II was enclosed by average BAI-values between 205 and 211 V·μs and the CVs lower than 2.5% as shown in Figure-5.8b. Other data points in these figures belonged to region-II and region-III. Figure-5.8 concludes that as long

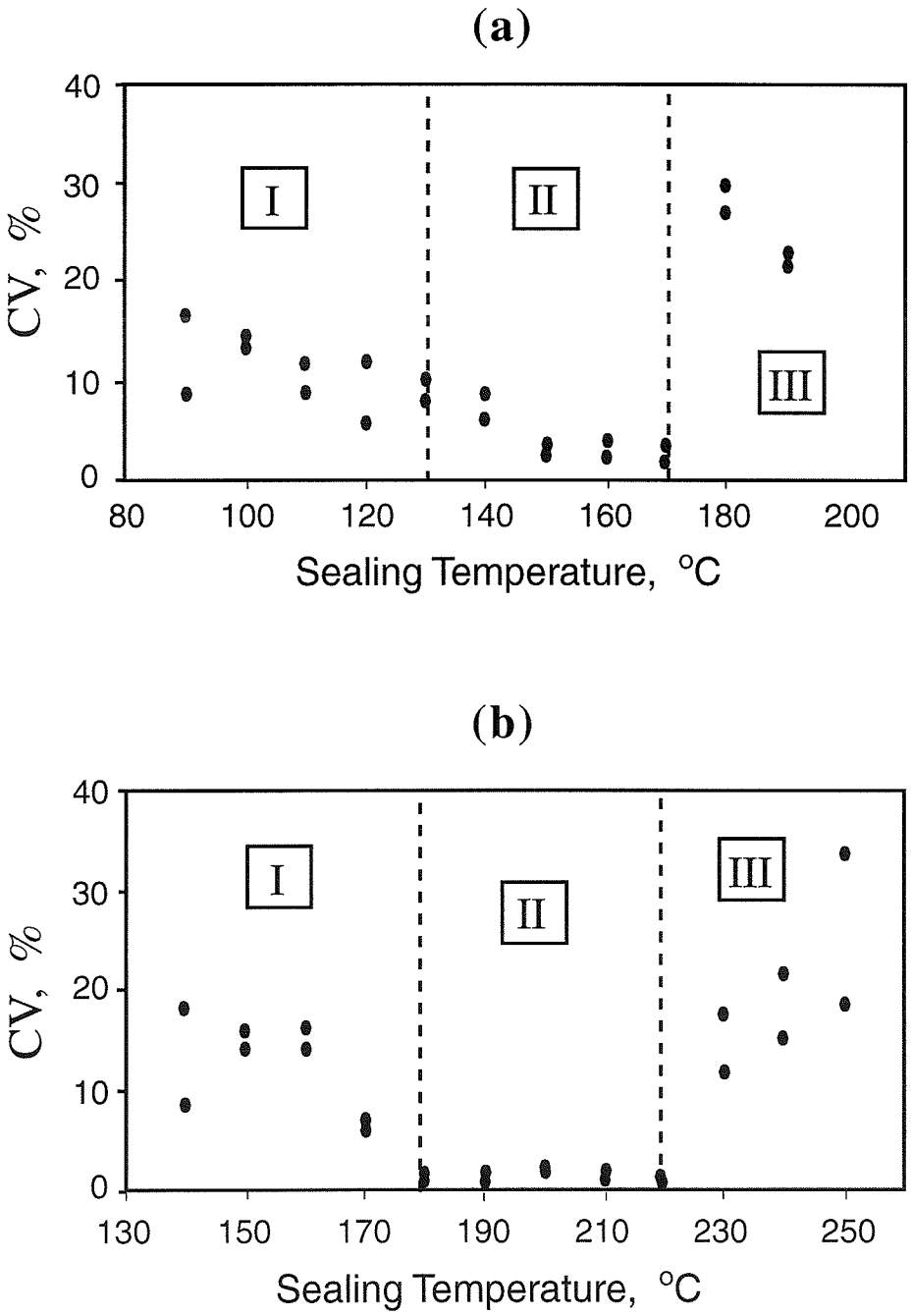

Figure - 5.7. Coefficient of variation of BAI values in the BAI-matrix for (a) all-plastic films and (b) foil-containing films created at different sealing-bar temperatures

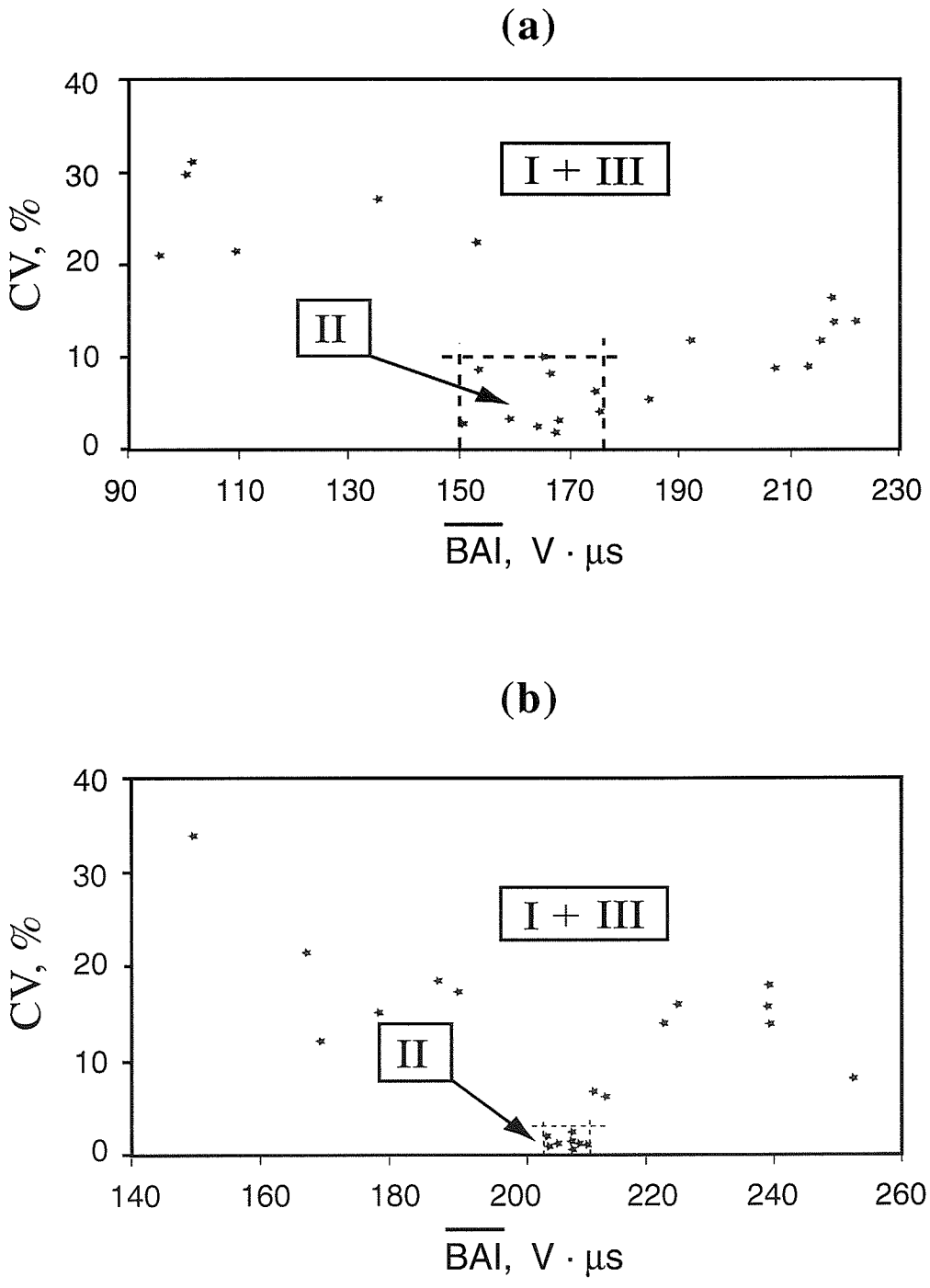

Figure - 5.8. Coefficient of variation (CV) values versus average BAI values for (a) all-plastic films and (b) foil-containing films. Data points were collected from Figure-5.6 and -5.7.

as the package seal contains no defect, its average BAI-value should be in acceptable limits, and its CV should be lower than the maximum acceptable value.

The distribution of data can ideally be demonstrated by the bell-shaped Gaussian curve as indicated in Figure-5.9 if there is sufficient amount of data. It is a symmetric curve with its highest ordinate at its center, tailing off to zero in both directions. The region-I, - II, and -III are demonstrated in Figure-5.10 by Gaussian curves. As determined before, average BAI-values ($\overline{BAI}$) for these regions were $\overline{BAI}_I < \overline{BAI}_{II} < \overline{BAI}_{III}$, where subscripts indicate the region. Thus, the average of the $\overline{BAI}$ ($\overline{\overline{BAI}}$) becomes $\overline{\overline{BAI}}_I < \overline{\overline{BAI}}_{II} < \overline{\overline{BAI}}_{III}$. In addition to that, CVs were higher in region-I and -III than in region-II. In Gaussian curve, that is indicated by the dispersion of the data. As indicated in Figure-5.10, the bell shape of region-I and -III is more dispersed than that of region-III, i.e., fat

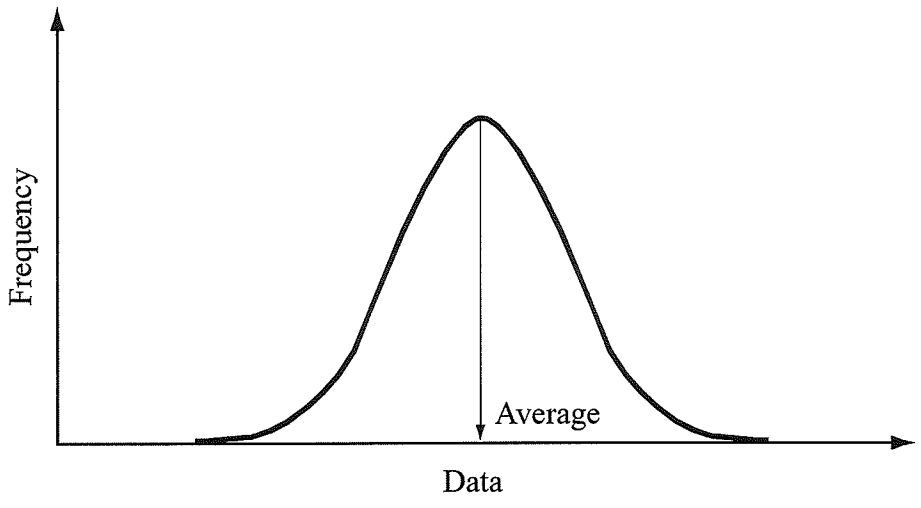

Figure - 5.9. The normal (Gaussian) distribution of the data

tails in region-I and -III due to the high variation of data. On the other hand, the $\overline{BAI}$-values get close to the $\overline{\overline{BAI}}$-value in region-II, and the frequency of the data will increase near the $\overline{\overline{BAI}}$-value resulting in slim tails in the curve. In an ideal package-sealing operation, to minimize possible formation of defects, the highest ordinate of the Gaussian curve should be forced upward, i.e., the $\overline{BAI}$-values should be very close to the $\overline{\overline{BAI}}$, which lessens the coefficient of variation of the BAI-values. This situation is represented by *Ideal Region* in Figure-5.10.

5.E. CONCLUSION

When developing a packaging system where seal integrity is paramount, everything should be done in the design of the system and its equipment to eliminate chances for seal defects. In that regard, testing the sealer's performance will improve the on-line inspection of packages. Average BAI-values and coefficient of variation of seals can test the performance of sealing operation. As long as the sealer operates at optimum conditions, i.e., it does not cause any defect formation, the average BAI-value and the coefficient of variation of the BAI-values in the seal region will be in acceptable levels. When these values start deviating from acceptable levels, the operation can be shut down automatically. Consequently, this method offers the advantage of real-time, on-line control by being able to sense whether seal has achieved a proper state of fusion or not.

This study showed that the BAI-mode imaging itself would not be effective to detect seal defects when they are distributed within the seal area. Although the BAI-mode imaging is not adequate to detect multiple defects, it still contains valuable data which helps the detection of such defects.

The average BAI-value and the variation of the BAI-values in the seal

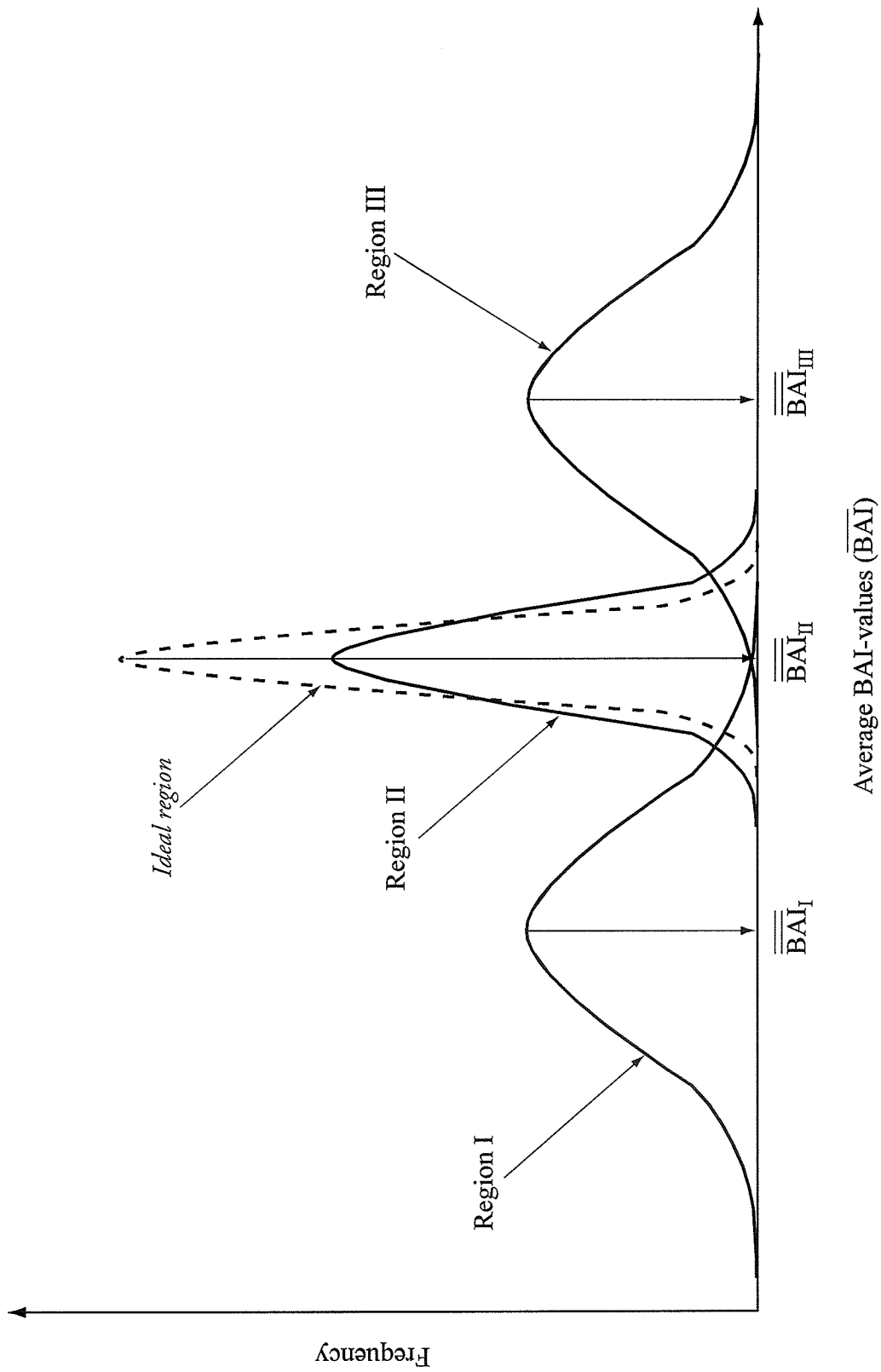

Figure - 3.10. The ideal Gaussian distribution for a conceptual population of average $\overline{BAI}$ (BAI) values. $\overline{\overline{BAI}}$ indicates the average of $\overline{BAI}$ values

region provided an effective way to detect delaminations, non-bondings, wrinkles, blisters, and bubbles which the BAI-mode imaging could not detect when many of them occurred in the seal area. At optimum sealing conditions, the average BAI-value of the solid seal was in certain limits, and the coefficient of variation of the BAI-values was lower than the maximum acceptable levels. It was indicated in this study that the upper and lower limits for average BAI values and the maximum acceptable coefficient of variation would be different for different packaging materials.

Combination of average BAI-value, coefficient of variation of the BAI-values, and the BAI-mode imaging can perform thorough inspection of package seals. The average BAI-value and the coefficient of variation of BAI-values provide detection of macroscale seal defects such as non-bondings, delaminations, wrinkles, bubbles, and blisters, and the BAI-mode imaging suggests the detection of microscale defects. Whenever the macroscale defects are detected by the inspection system, further testing for microscale defects will be unnecessary, and thus, there will be no need for the BAI-mode imaging, which reduces the inspection time.

-6-

SUMMARY

This project was initiated to study the feasibility of the ultrasonic pulse-echo technique to nondestructively inspect the defects in the seal region of flexible food packages, which might compromise the product quality and consumer safety. The preliminary study indicated that the ultrasonic pulse-echo technique could be applied to inspect seal defects in thin plastic packages (~200 μm).

Initially, A-scan and B-scan types of imaging were evaluated to visualize seal defects after processing RF echo signals obtained from the pulse-echo technique. Results indicated that in spite of the fact that these usual techniques worked for large defects (>95μm), they did not detect micro-defects. However, results and observations from B-scan images leaded for developing a different imaging procedure.

The high frequency backscattered amplitude (BAI) -mode imaging was developed and evaluated for seal defects. Like the C-scan, the BAI-mode imaging is a plane projection of the internal details of a specimen. In the C-scan, the echoes are restricted to a particular time, which corresponds to a constant depth in the specimen whereas in the BAI-mode imaging, the echoes are integrated, which corresponds to the energy reflected from the specimen under evaluation. Any defect in the specimen results in the reflected energy to alter and, thus, brings about the BAI-value in the defect location to change.

Results indicated that the high frequency BAI mode imaging had the capability of subwavelength detection of defects, e.g. detection of defects whose size is smaller than the wavelength of the sound in the propagation medium. Although the technique detected channel defects as small as 6 μm in diameter, the technique was more effective for defects larger than 15 μm. The method is already exceeding the reliability of human inspectors by being able to detect defects that are smaller than 50 μm and buried in opaque material.

As a measure of contrast in the BAI-mode image, the ΔBAI-value was described for the defect in the seal area. The ΔBAI-value varied with defect types, sizes, and types of packaging materials and there was a linear relation between the ΔBAI-value and the defect size. The BAI-mode imaging was limited for characterizing the defect size. However, if the ΔBAI-value and the type of the defect are known, this value can be used to approximate the size of the defect. It can also be used as an alarm for on-line package inspection. After it is determined for the largest allowable defect size, any package having defect whose ΔBAI-value is larger than the predetermined value can be rejected from the inspection line.

The study indicated that although the BAI-mode imaging technique was very effective to detect microscale seal defects, it was not successful for macroscale defect such as non-bondings, wrinkles, and bubbles when they were present abundantly in the seal region. To overcome this problem, a new technique was introduced to inspect them automatically. In this technique, the average of the BAI-values and their coefficient of variation in the BAI-matrix were calculated. Results indicated that if the seal area of the package does not contain these defects, the average BAI-value of the seal region would be within a certain limit, which changes

with the different package material, and the coefficient of variation of the BAI-values will be lower than the experimentally determined maximum acceptable level.

The ultrasonic BAI-mode imaging technique, the ΔBAI contrast value, the average BAI-value of the seal region, and the coefficient of variation of the BAI-values would permit 100% inspection of packages for seal integrity and thus provide the safety assurance of the package. These techniques will allow wider implementation of energy- and material-efficient retortable pouches and trays, by reducing inspection costs. That would also diminish the requirement of chill-chain distribution system, which is energy consuming and inefficient with regard to utilization of space, since the freezer space is a scarce piece of real estate at the retail level. Thus, methods developed in this study would make these packages more financially competitive and expand their applicability beyond a niche market.

REFERENCES

Adams, J.P., Peterson, W.R., and Otwell, W.S. 1983. Processing of seafood in institutional-sized retort pouches. Food Technology. 37: 123-127.

Ahvenainen, R. 1988. Quality assurance and quality control of aseptic packaging. Food Rev. 4(1): 45-76.

Allemeier, R.T. 1995. Electronic speckle pattern interferometry for food package integrity verification. Ch. 10 in "Plastic Package Integrity Testing Assuring Seal Quality", B.A Blakistone and C. L. Harper (Ed.). Institute of Packaging Professionals, Herndon, VA, USA. pp.113-118.

Axelson, L., Cavlin, S., and Nordstörm, J. 1990. Aseptic integrity and microhole determination of packages by electrolytic conductance measurement. Packaging Technology and Science. 3: 141-162.

Badenhop, A.F. and Milleville, H.P. 1980. Institutional size retort pouches. Food Processing. 44: 82-86.

Bakker, M. 1986. The Wiley Encyclopedia of Packaging Technology. John Wiley and Sons, New York.

Blakistone, B.A. 1994. Proceedings of the IoPP Packaging Technology Conference, November 11-12, 1994, Chicago, Illinois, Institute of Packaging Professionals, Herndon, VA.

Blakistone, A.B., Keller, S.W., Marcy, J.E., Lacy, G.H., Hackney, C.H., and Carter, W.H., Jr. 1996. Contamination of flexible pouches challenged by immersion biotesting. Journal of Food Protection. 59(7): 764-767.

Blitz, J. The basic principles of ultrasonic testing. 1960. Chp. 5 in "Techniques of Non-Destructive Testing". Adlard and Son Limited, London. pp.1-7.

Blitz, J. and Hogarth, C.A. 1960. Non-destructive testing. 1960. Chp. 1 in "Techniques of Non-Destructive Testing". Adlard and Son Limited, London. pp.83-121.

Bray, D.E. and Stanley, R.K. 1997. Nondestructive Evaluation. CRC Press, Inc., Boca Raton, FL.

Briggs, A. 1985. An Introduction to Scanning Acoustic Microscopy. Oxford University Press, Oxford.

Briggs, A. 1992. Acoustic Microscopy. Clarendon Press, Oxford.

Boving, K.G. 1989. NDE Handbook. Butterworths, London.

Cartz, L. 1996. Nondestructive Testing. ASM International, Materials Park, OH.

Charbonneau, J. and Arndt, G. 1995. In search of microleaks NFPA researchers discover new method to detect microholes in food packages. Food Processing. 114-116.

Chen, C., Harte, B., Lai, C., Pestka, J., and Henyon, D. 1991. Assessment of package integrity using a spray cabinet technique. Journal of Food Protection. 54(8): 643-647.

Delaquis, P.J., Baker, R., and McCurdy, A.R. 1986. Microbiological stability of pasteurized ham subjected to a secondary treatment in retort pouches. Journal of Food Protection. 49(1): 42-46.

Durance, T.D and Collins, L.S. 1991. Quality enhancement of sexually mature chum salmon oncorhynchus keta in retort pouches. Journal of Food Science. 56(5): 1282-1286.

Embree, P.M., Foster, S.G., Bright, G., and O'Brien, W.D., Jr. 1984. Ultrasonic velocity spatial distribution of biological materials with the scanning laser acoustic microscope. Acoustic Imaging. 13: 203-216.

Ensminger, D. 1988. Ultrasonics. Marcel Dekker, Inc., New York, NY.

Flexible Package Integrity Committee of the National Food Processors Association. 1989. Flexible Package Integrity Bulletin, NFPA Bulletin 41-L, NFPA, Washington, D.C.

Floros, J.D. 1994. Packaging technologies and inspection news: Critical leak size and package integrity. Packaging Technologies and Inspection, Vol. IV, Tuckahoe, NY.

Floros, J.D. and Gnanasekharan, V. 1992. Principles, technology and applications of destructive and nondestructive package integrity testing. In "Advances in Aseptic Processing Technologies". R. K Singh, and P. E. Nelson (Ed.). Elsevier Applied Science, New York, NY. pp.157-188.

Frazier, C. H., Ozguler, A., Morris, S.A., and O'Brien, W.D., Jr. 1998. High-contrast images of defects in material seals, 1997 IEEE Ultrasonic Symposium Proceedings, vol. 1, pp. 627-630.

Foxboro. 1966. General Catalog of Industrial Instrumentation. Bul. 565, A54. Foxboro Co., Foxboro, Mass.

Gilchrist, J.E., Shah, D.B., Radle, D.C., and Dickerson, R.W. 1989. Leak detection in flexible retort pouches. J. Food Protection. 52(6): 412-415.

Gilchrist, J.E., Rhea, U.S., Dickerson, R.W., and Campbell, J.E. 1985. Helium leak test for micron-sized holes in canned foods. J. Food Protection. 48(10): 856-860.

Gnanasekharan, V. and Floros, J.D. 1994. Package integrity evaluation: Criteria for selecting a method. Packaging Technology & Engineering. 3(6): 44-48.

Griffin Jr., R.C., Sacharow, S., and Brody, A.L. 1985. Materials and package testing, Ch. 5 in "Principles of Package Development". Van Nostrand Reinhold Company, New York, NY. pp. 130-167.

Goss, S.A. and O'Brien, W.D., Jr. 1979. Direct ultrasonic velocity measurements of mammalian collagen threads. Acoustic Society of America. 65(2): 507-511.

Gros, X.E. 1997. NDT Data Fusion. John Wiley and Sons, Inc., New York.

Halmshaw, R. 1991. Non-destructive Testing. Edward Arnold - A Division of Hodder & Stoughton, London.

Harper, C.L. 1995. A microbial challenge procedure for identification of defective flexible plastic pouch seals. Ch. 10 in "Plastic Package Integrity Testing Assuring Seal Quality". B.A Blakistone and C. L. Harper (Ed.). Institute of Packaging Professionals, Herndon, VA, USA. pp. 79-82.

Harper, C.L., Blakistone, B.S., Litchfield, J.B., and Morris, S.A. 1995. Developments in food package integrity testing. Food Technol. 6(10): 336-340.

Howard, G. and Duberstein, R. 1980. A case of penetration of 0.2 micron rated membrane filters by bacteria. J. Parental Drug. Assoc. 34(2): 95-102

Hu, K.H., Nelson, A.I., Legault, R.R., and Steinberg, M.P. 1955. Feasibility of using plastic film packages for heat processed foods. Food Technol. 19(9): 236-240.

Hull, B. and John, V. 1988. Non-Destructive Testing. Springer-Verlag, Inc., New York, NY.

Jarman, D., Farahbakhsh, B., and Herzig, R. 1994. Ultrasonic inspection of seal integrity of bond lines in sealed containers. U.S. Patent, no. 5,372,042.

Jenkins, W.A. and Harrington, J.P. 1991. Packaging Foods with Plastics. Technomic Publishing Company, Inc., Lancaster, PA.

Jones, T.S. and Berger, H. 1989. Application of nondestructive inspection methods to composites. Mater. Eval. 47(4): 390-400.

Keller, S.W., Marcy, J.E., Blakistone, B.A., and Lacy, G.H. 1995. Bioaerosol exposure method for package integrity testing. J. Food Prot. 59(7): 768-771.

Kinsler, L.E., Frey, A.R., Coppens, A.B., and Sanders, J.V. 1982. Fundamentals of Acoustics. John Wiley and Sons, New York, NY.

Kluter, R.A., Nattress D.T., Dunne, C.P., and Popper, R.D. 1994. Shelf life evaluation of cling peaches in retort pouches. Journal of Food Science. 59(4): 849-865.

Lampi, R.A. 1980. Retort pouch: the development of a basic packaging concept in today's high technology era. J. Food Process Eng. 4: 1-18

Lampi, R.A. 1977. Flexible packaging for thermoprocessed foods. In "Advance Food. Research". C. O. Chichester, E. M. Mrak, and G. F. Stewart (Ed.), vol.23. Academic Press, New York. pp. 305-428.

Lampi, R.A., Schulz, G.L, Ciavarini, T., and Burke, P.T. 1976. Performance and integrity of retort pouch seals. Food Technology. 30: 38-48.

Lampi, R.A., Fiori, F., Hu, K.H., Ordway, G.B., Schulz, G.L., Roberts, N.D., and Costanza, F.A. 1973. Infrared radiometric scanning system for flexible package seal defects. Tech. Report 74-36-GP. U.S. Army Natick Development Center, Natick, Mass.

Leisk G.G. and Saigal, A. 1996. Material Evaluation. 54, 840-843.

Leonard, B.E. and Gardner, C.G. 1973. Ultrasonics. In "Nondestructive Testing". NASA SP-5113, National Aeronautics and Space Administration, Washington, D.C.

Lin, R.C., King, P.H., and Johnston, M.R. 1984. Examination of containers for integrity. Ch 4 in "Bacteriological Analytical Manual". 6th ed., Association of Official Analytical Chemists, Arlington, Virginia.

Long, F.E. 1962. Flexible packages now withstand heat processing temperatures of foods. Package Engineering. 7(3): 63-80.

Matty, J.T., Stevenson, J.A., and Stanton, S.A. 1991. Packaging for the 90's: convenience versus shelf stability or seal peelability versus seal durability. In "Food Packaging Technology". Henyon, D.K. (Ed.). American Society for Testing and Materials, Philadelphia. pp. 74-90.

Maunder, D.T., Folinazzo, J.F., and Killoran, J.J. 1968. Bio-test method for determining integrity of flexible packages of shelf-stable food. Food Technology. 22: 615-618.

McEldowney, S. and Fletcher, M. 1990. The effect of physical and microbiological factors on food container leakage. J. Appl. Bacteriol. 69: 190-205.

McGonnagle, W.J. 1966. Nondestructive Testing. Gordon and Breach Science Publishers, Inc, New York, NY.

McMaster, R.C. 1982. Nondestructive Testing Handbook. 2nd Ed., vol. 2, Amer. Soc. for Nondestructive Testing, Metals Park, OH.

McRae, T.G. 1989. Remote sensing techniques for leak testing of components and systems, Materials Eval. 47(11): 1308-1312.

Mermelstein, N.H. 1976. The retort pouch in the U.S. Food Technology. 30(2): 28-37.

Mix, P.E. 1987. Introduction to non-destructive testing: A training guide. John Wiley and Sons, New York.

Morris, C.E. 1989. Return of the pouch. Food Eng. 2: 44-46.

Morton, D.K. 1987. Container/closure integrity of parenteral vials. J. Parenteral Sci. and Technol. 145-158.

Morton, D.K., Lordi, N.G., Troutman, L.H., and Ambrosio, T.J. 1989. Quantitative and mechanistic measurements of container/closure integrity. Bubble, liquid and microbial leakage tests. J. Parenteral Sci. and Technol. 43(3):104-108

Nelson, A.I. and Steinberg, M.P. 1956. Retorting foods in plastic bags. Food Eng. 28(1): 92-93.

Nelson, A.I., Hu, K.H., and Steinberg, M.P. 1956. Heat processible food films. Mod. Packag. 20(10): 173-179.

Nughes, F. 1974. European developments in retortable pouch packaging. Presented at Ann. Packaging Inst. Forum, Chicago.

O'Brien, W.D., Jr. 1981. Quantitative acoustical assessment of wound maturation with acoustic microscopy. Acoustical Society of America. 69(2): 575-579

Oppenheim, A.V. and Schafer, R.W. 1975. Digital Signal Processing. Prentice Hall, Englewood Cliffs, New Jersey.

Ozguler, A., Morris S.A., and O'Brien, W.D., Jr. 1998. Evaluation of defects in seal region of food packages using the backscattered amplitude integral (BAI) technique. 1997 IEEE Ultrasonic Symposium Proceedings, vol. 1, pp. 689-692.

Pestka, J. and Henyon, D. 1991. Assessment of package integrity using a spray cabinet technique. J. of Food Prot. 54(8):643-647.

Paine, F.A. and Paine, H.Y. 1992. A Handbook of Food Packaging, Blackie Academic & Professional, London, UK.

Pohlhammer, J.D., Edwards, C.A., and O'Brien, W.D., Jr. 1981. Phase insensitive ultrasonic attenuation coefficient determination of fresh bovine liver over an extended frequency range. Med. Phys. 8(5): 692-694.

Put, H.M.C., Van Doren, H., Warner, W.R., and Kruiswjik, J.T. 1972. The mechanism of microbiological leak spoilage of canned foods: A Review. J. Appl. Bacteriol. 35: 7-27.

Put, H.M.C., Witvoet, W.R., and Warner, W.R. 1980. The mechanism of leaker spoilage of canned foods: Biophyscal aspects. J. Food Protection. 43: 488-497.

Raum, K., Ozguler, A., Morris, S.A, and O'Brien, W.D., Jr. 1998. Channel defect detection in food packages using integrated backscatter ultrasound echo imaging. IEEE Transactions on Ultrasonics, Ferroelectrics, and Frequency Control. 45(1): 30-40.

Raum, K. and O'Brien, W.D., Jr. 1997. Pulse-echo field distribution measurement technique for high-frequency ultrasound sources. IEEE Transactions on Ultrasonics, Ferroelectrics and Frequency Control. 44(4): 810-815.

Rose, D. 1994. Risk factors associated with post-processing contamination of heat sealed semi-rigid packaging. Campden & Chorleywood Food Research Memorandum No. 708, Campden & Chorleywood Food and Drink Association, Gloucestershire, GL55 6LD, UK.

Safvi, A.A., Meerbaum, H.J., Morris, S.A., Harper, C.L., and O'Brien, W.D., Jr. 1997. Acoustic imaging of defects in flexible food packages. Journal of Food Protection. 60(3): 309-314.

Scott, I.G. and Scala, C.M. 1982. A review of non destructive testing of composite materials. Nondestructive Testing International. 15(2): 75-86.

Selfridge, A.R. 1985. Approximate material properties in isotropic materials. IEEE Transactions on Sonics and Ultrasonics, SU-32(3): 381-395.

Sloan, A.E. 1985. Accepting Technology. Food Engineering. 57: 48-49.

Smith, G.C. 1986. The scanning acoustic microscope - a new tool for the materials scientist. Materials Science and Technology. 2: 881-887.

Stauffer, T. 1988. Nondestructive in-line detection of leaks in food and beverage packages - An analysis of methods. Journal of Packaging Technology. 30(2): 38-48.

Steffe, J.F., Williams, J.R., Chinnan, M.S., and Black, J.R. 1980. Energy requirements and costs of retort pouch vs. can packaging system. Food Technology. 34(9): 39-43.

Szilard, J. 1982. Ultrasonic Testing. John Wiley & Sons, N.Y.

Szilard, J. 1987. Ultrasonics. In "Encyclopedia of Physical Science and Technology". R. A. Meyers (Ed.), vol. 14. Academic Press, Inc., Orlando, FL. pp. 191-209.

Tervola, K. M. U., Steven, G. F., and O'Brien, W.D., Jr. 1985. Attenuation coefficient measurement technique at 100 MHz with the scanning laser acoustic microscope. IEEE Transactions on Sonics and Ultrasonics. SU-32(2): 259-265.

Tsutsumi, Y. 1974. The growth of food packed in retortable pouches in Japan. Presented at Ann. Packaging Institute Forum, Chicago.

United Stated Code of Federal Regulations. 9CFR§381.301(d). Published by the Office of the Federal Register. Superintendent of Documents, U.S. Government Printing Office, Washington, DC.

Warrick, D. 1990. Aseptics: the problems revealed. Food Manufac. 65(10): 63-66.

Williams, J.R., Steffe, J.F., and Black, J.R. 1983. Sensitivity of selected factors on costs of retort pouch packaging systems. Food Technology. 37: 92-100.

Wilson, W.D. 1959. Speed of sound in distilled water as a function of temperature ans pressure. J. Acoustic. Soc. Amer. 31: 1067-1072.

Yam, K.L. 1995. Pressure differential techniques for package integrity inspection. Ch. 17 in "Plastic Package Integrity Testing Assuring Seal Quality". B.A. Blakistone and C.L Harper (Ed.). Institute of Packaging Professionals, Herndon, VA. pp.137-145.

Yamaguchi, K. 1990. Retortable packaging. In "Food Packaging". Kadoya, T. (Ed.). Academic Press, Inc., San Diego, CA. pp. 185-211.

APPENDIXES

A.1. The Scanning And Data Collection Program Coded By Using The C-Programming language

```
/*                    Program name: BAI_Scan.c

   ______________________________________________________________
   | Purpose: This program provides a two-dimensional scanning of the      |
   |          specimen and creates a set of A-scan lines along two axises. |
  |______________________________________________________________          |
   | The distance between two A-scan lines (stepsize) and the total length |
   |  of a scan row are selectable as well as the axis of the DAEDAL  system.|
   | The direction of the scan is always in the positive  axis direction.
   |                                                                       |
   | The scope shoul run in enhanced mode, otherwise scan information      |
   | will not be stored correctly.                                         |
   |                                                                       |
   | Two files will be created. A binary file with an extension .bin  contains |
   | the unscaled integer signal points. The second file with extension .dat |
   |  is an ASCII file, wich contains waveform and scan  information.      |
   |^^^^^^^^^^^^^^^^^^^^^^^^^^^^^^^^^^^^^^^^^^^^^^^^^^^^^^^^^^^^^^^^^^^^^^^|
*/

#include <conio.h>
#include <stdio.h>
#include <string.h>
#include <stdlib.h>
#include "c:\qc2\include\msgraph.h"
#include <time.h>
#include "c:\at-gpib\c\decl.h"
#define ERR      (1<<15)       /* Error detected */
#define TIMO      (1<<14)       /* Timeout */
#define RQS      (1 <<11)       /* Device needs service*/

void introduction(void);
void init_parameter(void);
void init_files(void);
void init_device(void);
void measure(void);
 FILE
  *fopen(),
  *ptr_dat,
  *ptr_bin;

char filebin[25],
   filedat[25],
   fileout[5],
   filenam[50],
   go1[40],
```

```
  go2[40],
  gostep[30],
  comeback1[40],
  comeback2[40],
  wait1[20],
  wait2[20],
  wfm[2250],
  op,
  asr1[4],
  asr2[4];

char ax_number1,
     ax_number2;

unsigned long int inter1, inter2;
int   gpib0,
 dev0,
 dev1,
 dev2,
 delaytime;

struct data
  {
  unsigned long int number_point,numscan1,numscan2;
  float xincr,xmult,xzero,ymult,yzero;
  };

struct data info;

main( int argc, char *argv[])
  {
  int z;
  char zc[2];
  introduction();
  init_parameter();
  init_device();
  for(z=1; z<=argc;++z)
   {
    itoa(z,zc,10);
    strcpy(filenam,"c:\\ayhan\\scan\\");
    strcat(filenam,fileout);
    strcpy(filebin,filenam);
    strcpy(filedat,filenam);
    strcat(filebin,zc);
    strcat(filebin,".bin");
    strcat(filedat,zc);
    strcat(filedat,".dat");
    init_files();
    measure();
    ibwrt(dev1," E ",3);
    strcpy(gostep, "MN A10 2V10 D");
    strcat(gostep, *(argv+z));
    strcat(gostep, " G ");
    ibwrt(dev1, gostep, strlen(gostep));
    while (asr1[1] != 'R')
    {
     ibwrt(dev1,wait1,strlen(wait1));
     ibrd(dev1,asr1,3);
```

```
    }
    asr1[1] = 'B';
    ibwrt(dev1," F ",3);
   }
}

void introduction()
  {
  _clearscreen(_GCLEARSCREEN);
  printf("                    .... BAI_SCAN.C .... ");
  }

 void init_parameter()
  {
  static char intervall1[5],
     intervall2[5],
     distance1[20],
     distance2[20];
     unsigned long int1, int2, dist1, dist2;

  printf("\n Enter a 6 char output filename          : ");
  scanf("%s",fileout);
  printf(" Enter the first scanaxis (1-5)     : ");
  ax_number1=getche();
  op=getche();
  printf("\n Axis [%c] (stepsize in um or 1/100degr.)     : ",ax_number1);
  scanf("%s",intervall1);
  printf(" Axis [%c] (total length in um !!!! or 1/100degr.)  : ",ax_number1);
  scanf("%s",distance1);
  inter1=atoi(intervall1);
  dist1=atoi(distance1);
  info.numscan1=(dist1/inter1+1);
  ltoa(info.numscan1*inter1,distance1,10);
  printf("\n Enter the second scanaxis (1-3)     : ");
  ax_number2=getche();
  op=getche();
  printf("\n Axis [%c] (stepsize in um)      : ",ax_number2);
  scanf("%s",intervall2);
  printf(" Axis [%c] (total length in um!!!)  : ",ax_number2);
  scanf("%s",distance2);
  inter2=atoi(intervall2);
  dist2=atoi(distance2);
  info.numscan2=(dist2/inter2+1);
  ltoa(info.numscan2*inter2,distance2,10);

  switch(ax_number1)
{
    case'1':
     dev1=ibfind("axis1");
     strcpy(go1, "MN A1 1V.05 D");
     strcat(go1, intervall1);
     strcat(go1, " G ");
     strcpy(comeback1, "H- MN A1 1V10 D-");
     strcat(comeback1, distance1);
     strcat(comeback1, " G ");
     strcpy(wait1," 1R ");
     break;
    case'2':
```

```
      dev1=ibfind("axis2");
      strcpy(go1, "MN A20 2V35 D");
      strcat(go1, intervall1);
      strcat(go1, " G ");
      strcpy(comeback1, "H- MN A20 2V35 D-");
      strcat(comeback1, distance1);
      strcat(comeback1, " G ");
      strcpy(wait1," 2R ");
      break;
    case '3':
      dev1=ibfind("axis3");
      strcpy(go1, "MN A10 3V25 D");
      strcat(go1, intervall1);
      strcat(go1, " G ");
      strcpy(comeback1, "H- MN A10 3V25 D-");
      strcat(comeback1, distance1);
      strcat(comeback1, " G ");
      strcpy(wait1," 3R ");
      break;
    case '4':
      dev1=ibfind("axis4");
      strcpy(go1, "MN A10 4V35 D");
      strcat(go1, intervall1);
      strcat(go1, " G ");
      strcpy(comeback1, "H- MN A10 4V35 D-");
      strcat(comeback1, distance1);
      strcat(comeback1, " G ");
      strcpy(wait1," 4R ");
break;
  case '5':
      dev1=ibfind("axis5");
      strcpy(go1, "MN A1 5V.05 D");
      strcat(go1, intervall1);
      strcat(go1, " G ");
      strcpy(comeback1, "H- MN A1 5V10 D-");
      strcat(comeback1, distance1);
      strcat(comeback1, " G ");
      strcpy(wait1," 5R ");
      break;
    default:
      printf("\n unknown axis1");
      op=getche();
      _clearscreen(_GCLEARSCREEN);
      exit(0);
  }

 switch(ax_number2)
  {
   case'1':
      dev2=ibfind("axis1");
      strcpy(go2, "MN A1 1V.05 D");
      strcat(go2, intervall2);
      strcat(go2, " G ");
      strcpy(comeback2, "H- MN A1 1V10 D-");
      strcat(comeback2, distance2);
      strcat(comeback2, " G ");
      strcpy(wait2," 1R ");
      break;
```

```
 case'2':
      dev2=ibfind("axis2");
      strcpy(go2, "MN A1 2V.05 D");
      strcat(go2, intervall2);
      strcat(go2, " G ");
      strcpy(comeback2, "H- MN A1 2V10 D-");
      strcat(comeback2, distance2);
      strcat(comeback2, " G ");
      strcpy(wait2," 2R ");
      break;
 case '3':
      dev2=ibfind("axis3");
      strcpy(go2, "MN A10 3V0.05 D");
      strcat(go2, intervall2);
      strcat(go2, " G ");
      strcpy(comeback2, "H- MN A10 3V0.05 D-");
      strcat(comeback2, distance2);
      strcat(comeback2, " G ");
      strcpy(wait2," 3R ");
      break;
 case '4':
      dev2=ibfind("axis4");
      strcpy(go2, "MN A20 4V20 D");
      strcat(go2, intervall2);
      strcat(go2, " G ");
      strcpy(comeback2, "H- MN A20 4V20 D-");
      trcat(comeback2, distance2);
      strcat(comeback2, " G ");
      strcpy(wait2," 4R ");
      break;
 case '5':
      dev2=ibfind("axis5");
      strcpy(go2, "MN A1 5V.05 D");
      strcat(go2, intervall2);
      strcat(go2, " G ");
      strcpy(comeback2, "H- MN A1 5V10 D-");
      strcat(comeback2, distance2);
      strcat(comeback2, " G ");
      strcpy(wait2," 5R ");
      break;
     default:
      printf("\n unknown axis2");
      op=getche();
      _clearscreen(_GCLEARSCREEN);
      exit(0);
   }
 }

void init_device(void)
  {
static char quest1[50],
     quest2[50],
     quest3[50],
     trace[4],
     output[12],
     select[12],
     deltime[4],
     dummy[2000];
```

```
    printf("\n\n Enter Trace (e.g. C2)          : ");
    scanf("%s",trace);
    printf("\n Delay? (0-2000)");
    scanf("%s",deltime);
    delaytime=atoi(deltime);
    printf("\n Delay: [%d]",delaytime);
    gpib0=ibfind("gpib0");
    dev0=ibfind("LECROY");
    ibwrt(dev0,"WAVEFORM_SETUP SP, 3, NP, 170, FP, 0",36);
          /* SParse=0 => no Int. betw. pts. NumPts=0 => send all pts. */
    ibwrt(dev0,"Comm_Format OFF,WORD,BIN ",25);
    ibwrt(dev0,"Comm_ForMat?",12);
    ibrd(dev0,quest1,45);
    ibwrt(dev0,"Comm_Order LO ",14);
    ibwrt(dev0,"Comm_Order?",11);
    ibrd(dev0,quest2,45);
    ibwrt(dev0,"Comm_Header OFF ",16);
    ibwrt(dev0,"Comm_Header?",12);
    ibrd(dev0,quest3,45);
    ibwrt(dev0,"C2:INSP? 'WAVE_ARRAY_COUNT'",27);
                                                    /* C2= Channel#:2 */
    ibrd(dev0,wfm,1);
    ibrd(dev0,wfm,100);
    printf("\n %s",wfm);
    sscanf(wfm,"WAVE_ARRAY_COUNT    : %lu ",&info.number_point);
    ibwrt(dev0,"C2:INSP? 'HORIZ_INTERVAL'",25);
    ibrd(dev0,wfm,1);
    ibrd(dev0,wfm,100);
    sscanf(wfm,"HORIZ_INTERVAL      : %g ",&info.xincr);
    ibwrt(dev0,"C2:INSP? 'HORIZ_OFFSET'",23);
    ibrd(dev0,wfm,1);
   ibrd(dev0,wfm,100);
    sscanf(wfm,"HORIZ_OFFSET        : %g ",&info.xzero);
    ibwrt(dev0,"C2:INSP? 'VERTICAL_GAIN'",24);
    ibrd(dev0,wfm,1);
    ibrd(dev0,wfm,100);
    sscanf(wfm,"VERTICAL_GAIN       : %g ",&info.ymult);
    ibwrt(dev0,"C2:INSP? 'VERTICAL_OFFSET'",26);
    ibrd(dev0,wfm,1);
    ibrd(dev0,wfm,100);
    sscanf(wfm,"VERTICAL_OFFSET     : %g ",&info.yzero);
    printf("\n\n Sample points per A-scan : %lu",info.number_point);
    printf("\n Xincr : %g",info.xincr);
    printf("  Xzero : %g",info.xzero);
    printf("\n Ymult : %g",info.ymult);
    printf("  Yzero : %g",info.yzero);
    printf("\n Axis[%c] scan points :%lu",ax_number1,info.numscan1);
    printf("\n Axis[%c] scan points :%lu",ax_number2,info.numscan2);
    printf("\n\n");
    ibwrt(dev1," F ",3);
    ibwrt(dev2," F ",3);
    }

void init_files()
   {
   if ((ptr_dat = fopen(filedat,"w")) == NULL)
  {
  printf(" error opening data file \n");
```

```
exit(0);
}
 if ((ptr_bin = fopen(filebin,"wb")) == NULL)
{
printf(" error opening binary file \n");
exit(0);
}
 fprintf(ptr_dat,"%g %g %g %lu %lu %lu  %g %lu %lu",
 info.ymult,   info.yzero,   info.xincr,     info.number_point,
 info.numscan1, info.numscan2, info.xzero,  inter1, inter2);
 fprintf(ptr_dat,"\nymult yzero xincr number_point numscan1 numscan2");
 fprintf(ptr_dat," xzero stepsize1 stepsize2\n");
 fclose(ptr_bin);
 fclose(ptr_dat);
 }

void measure()
 {
 unsigned long int i,j,k,delay,count;
 float win;
 static char curv[1020],
    winmove[20],
    winch[20];

 if ((ptr_bin = fopen(filebin,"ab")) == NULL)
{
 printf(" error appending to binary file \n");
 exit(0);
}
 count=1;
 for(k=0;k<=(info.numscan2-1);k++)
 {
 ibwrt(dev1," E ",3);
 for(i=0;i<=(info.numscan1-1);i++)
    {
    for(delay=0;delay<=delaytime;delay++)
  {
  printf("\r .....Delay.....");
  }
    printf(" [%lu of %lu]",count,(info.numscan1)*(info.numscan2));
    count=count+1;
    ibwrt(dev0,"C2:WF? DAT1",11);
    ibrd(dev0,curv,(info.number_point*2));
    ibwrt(dev1, go1, strlen(go1));
    for (j=1;j<=(info.number_point*2);j++)
 {
 fputc(curv[j],ptr_bin);
 }
    while (asr1[1] != 'R')
 {
 ibwrt(dev1,wait1,strlen(wait1));
 ibrd(dev1,asr1,3);
 }
 asr1[1] = 'B';
   printf("\r           ");
    }

 ibwrt(dev1, comeback1, strlen(comeback1));
```

```
 while (asr1[1] != 'R')
   {
   ibwrt(dev1,wait1,strlen(wait1));
   ibrd(dev1,asr1,3);
   }
 asr1[1] = 'B';
 ibwrt(dev1," F ",3);
 ibwrt(dev2," E ",3);
 ibwrt(dev2, go2, strlen(go2));
 while (asr2[1] != 'R')
  {
  ibwrt(dev2,wait2,strlen(wait2));
  ibrd(dev2,asr2,3);
  }
 asr2[1] = 'B';
 ibwrt(dev2," F ",3);
 }
 ibwrt(dev2," E ",3);
 ibwrt(dev2, comeback2, strlen(comeback2));
 while (asr2[1] != 'R')
{
ibwrt(dev2,wait2,strlen(wait2));
ibrd(dev2,asr2,3);
}
 asr2[1] = 'B';
 ibwrt(dev2," F ",3);
 fclose(ptr_bin);
 }
```

A.2. The BAI-Mode Image Generating Program Coded By Using The MATLAB® (The Math Works, Inc., Natick, Mass.) Programming Language

```
%                    Program name: BAI_Image.m

% BAI_Image.m creates an BAI-image from  a 3D-data set and stores the
% result as a TIFF-file

% file name input and reading of .dat file information
%_____________________________________________________________
n=input('Enter a filename : ','s');

bin=[n '.bin'];
dat=[n '.dat'];
tif=[n '.tif'];

fid=fopen(dat,'r');
A=fscanf(fid,'%f',[9,1]);
ymult=A(1,1);
yzero=A(2,1);
xincr=A(3,1);
number_point=A(4,1);
numscan1=A(5,1);
numscan2=A(6,1);
xzero=A(7,1);
stepsize1=A(8,1);

stepsize2=A(9,1);
status=fclose(fid);

clear A status fid dat

% opens .bin file reads row by row, scales it, makes Hilbert-transformation
% and integration (summation)
%_____________________________________________________________

fid=fopen(bin,'rb','b');
Int=zeros(numscan2,numscan1);
  for(i=1:numscan2)
    B=fread(fid,[number_point,numscan1],'short');
    B=B.*ymult;
    B=B-yzero;
    H=abs(hilbert(B));
    Int(i,:)=sum(H);
  end

clear B H;

% reorientation, interpolation, median filter, intensity to RGB conversion
%_____________________________________________________________

Int=fliplr(Int);
```

```
Int1=zeros(numscan2,numscan1*2);
 for (i=1:numscan2)
     Int1(i,:)=interp(Int(i,:),2);
 end

Int2=zeros(numscan2*7,numscan1*2);
 for(i=1:numscan1*2)
     Int2(:,i)=interp(Int1(:,i),7);
 end
clear Int1 i

BAI=zeros(numscan2*7,numscan1*2);
BAI=medfilt2(Int2,[3 3]);

[r,c]= size(BAI);

BAI(1,1)=BAI(2,1);
BAI(1,c)=BAI(2,c);
BAI(r,1)=BAI(r,2);
BAI(r,c)=BAI(r,c-1);

NBAI=BAI./max(max(BAI));
NBAI=flipud(NBAI);

[X,map]=gray2ind(NBAI);
[R,G,B]=ind2rgb(X,bone);

x=[0 (numscan1-1)*stepsize1/1000];
y=[0 (numscan2-1)*stepsize2/1000];

imagesc(x,y,NBAI);colormap(bone);axis('image');axis('xy');title(n);
xlabel('Horizontal distance');
ylabel('Vertical distance');

clear Int2 X map

% makes a TIFF-file now
%_____________________________________________________________

tiffwrite(R,G,B,tif);
```

A.3. The Program Code To Calculate The Contrast Descriptor ΔBAI In The BAI-Mode Image (Coded By Using The MATLAB® (The Math Works, Inc., Natick, Mass.) Programming Language)

```
%                    Program Name: Delta_BAI.m

% This program prompts you to collect data from disturbed and undisturbed
% regions in the BAI-mode image.
% Cropping of 10 undisturbed regions and one disturbed region will be prompted
% After the data is collected, it calculates delta_BAI

% Note: The "Maximum BAI-value" on the image matrix must be provided
%       before calculations
% Crop the complete area from the defect region of the BAI-mode image
uci=1
uc=imcrop
uc=mean(mean(uc))
% Crop five regions from the left hand side of the defect
% Cropped area should be around 0.3mm * 0.3 mm
n=1
a1=imcrop
n=2
a2=imcrop
n=3
a3=imcrop
n=4
a4=imcrop
n=5
a5=imcrop
% Crop five regions from the right hand side of the defect
% Cropped area should be around 0.3mm * 0.3 mm
n=6
a6=imcrop
n=7
a7=imcrop
n=8
a8=imcrop
n=9
a9=imcrop
n=10
a10=imcrop
ub=zeros(10,1)
ub(1)= mean(mean(a1));
ub(2)= mean(mean(a2));
ub(3)= mean(mean(a3));
ub(4)= mean(mean(a4));
ub(5)= mean(mean(a5));
ub(6)= mean(mean(a6));
ub(7)= mean(mean(a7));
ub(8)= mean(mean(a8));
ub(9)= mean(mean(a9));
ub(10)= mean(mean(a10));
maxBAI =input('Enter the maximum BAI-value in the matrix  :  ');
dbai =abs(maxBAI*(ub-uc));
% Average Delta-BAI value
AveDBAI=mean(dbai)
```

A.4. The Program Code To Calculate The Coefficient Of Variation Of BAI-Values Image (Coded By Using The MATLAB® (The Math Works, Inc., Natick, Mass.) Programming Language)

```
%                Program name: CV_BAI.m

% This program calculates the average, standard deviation, and
% coefficient of variation of BAI-values using the data collected
% from the seal area of samples

n=input('Enter a filename : ','s');
bin=[n '.bin'];
dat=[n '.dat'];

fid=fopen(dat,'r');
A=fscanf(fid,'%f',[9,1]);
ymult=A(1,1);
yzero=A(2,1);
xincr=A(3,1);
number_point=A(4,1);
numscan1=A(5,1);
numscan2=A(6,1);
xzero=A(7,1);
stepsize1=A(8,1);
stepsize2=A(9,1);
status=fclose(fid);
clear A status fid dat
% opens .bin file reads row by row, scales it, makes H-transformation
% and integration (summation)
%_____________________________________________________________

fid=fopen(bin,'rb','b');
Int=zeros(numscan2,numscan1);
for(i=1:numscan2)
   B=fread(fid,[number_point,numscan1],'short');
   B=B.*ymult;
   B=B-yzero;
   H=abs(hilbert(B));
   I(i,:)=sum(H);
end
clear B H
i=1;
 for(l=1:numscan2)
       for(m=1:numscan1)
          BAI(i,1) = I(l,m);
          i=i+1;
       end
 end

% Calculation of average, standard deviation, and coefficient of
% variation values.
Average = mean(BAI)
Standart_deviation = std(BAI)
Correlation = Standart_deviation/Average
hist(BAI,30)
```

A.5. Data Files Collected For The Study In Chapter-3

Symbols used for naming the data file:

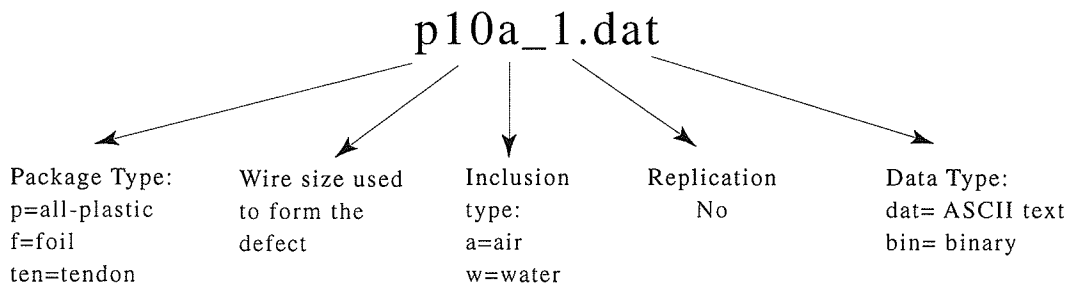

p15a_1.dat	p15a_1.bin	f15a_1.dat	f15a_1.bin
p15a_2.dat	p15a_2.bin	f15a_2.dat	f15a_2.bin
p15w_1.dat	p15w_1.bin	f15w_1.dat	f15w_1.bin
p15w_2.dat	p15w_2.bin	f15w_2.dat	f15w_2.bin
p10a_1.dat	p10a_1.bin	f10a_1.dat	f10a_1.bin
p10a_2.dat	p10a_2.bin	f10a_2.dat	f10a_2.bin
p10w_1.dat	p10w_1.bin	f10w_1.dat	f10w_1.bin
p10w_2.dat	p10w_2.bin	f10w_2.dat	f10w_2.bin
p6a_1.dat	p6a_1.bin	f6a_1.dat	f6a_1.bin
p6a_2.dat	p6a_2.bin	f6a_2.dat	f6a_2.bin
p6w_1.dat	p6w_1.bin	f6w_1.dat	f6w_1.bin
p6w_2.dat	p6w_2.bin	f6w_2.dat	f6w_2.bin
p_ten_1.dat	p_ten_1.bin	f_ten_1.dat	f_ten_1.bin
p_ten_2.dat	p_ten_2.bin	f_ten_2.dat	f_ten_2.bin
p_ten_3.dat	p_ten_3.bin	f_ten_3.dat	f_ten_3.bin

A.6. Data Files Collected For The Study In Chapter-4

Note: Symbols in the file naming are illustrated in Appendixes, A.5.

p100a_1.dat	p100a_1.bin	f100a_1.dat	f100w_1.bin
p100a_2.dat	p100a_2.bin	f100a_2.dat	f100w_2.bin
p100a_3.dat	p100a_3.bin	f100a_3.dat	f100w_3.bin
p100a_4.dat	p100a_4.bin	f100a_4.dat	f100w_4.bin
p100a_5.dat	p100a_5.bin	f100a_5.dat	f100w_5.bin
p75a_1.dat	p75a_1.bin	f75a_1.dat	f75w_1.bin
p75a_2.dat	p75a_2.bin	f75a_2.dat	f75w_2.bin
p75a_3.dat	p75a_3.bin	f75a_3.dat	f75w_3.bin
p75a_4.dat	p75a_4.bin	f75a_4.dat	f75w_4.bin
p75a_5.dat	p75a_5.bin	f75a_5.dat	f75w_5.bin
p50a_1.dat	p50a_1.bin	f50a_1.dat	f50w_1.bin
p50a_2.dat	p50a_2.bin	f50a_2.dat	f50w_2.bin
p50a_3.dat	p50a_3.bin	f50a_3.dat	f50w_3.bin
p50a_4.dat	p50a_4.bin	f50a_4.dat	f50w_4.bin
p50a_5.dat	p50a_5.bin	f50a_5.dat	f50w_5.bin
p38a_1.dat	p38a_1.bin	f38a_1.dat	f38w_1.bin
p38a_2.dat	p38a_2.bin	f38a_2.dat	f38w_2.bin
p38a_3.dat	p38a_3.bin	f38a_3.dat	f38w_3.bin
p38a_4.dat	p38a_4.bin	f38a_4.dat	f38w_4.bin
p38a_5.dat	p38a_5.bin	f38a_5.dat	f38w_5.bin
p15a_1.dat	p15a_1.bin	f15a_1.dat	f15w_1.bin
p15a_2.dat	p15a_2.bin	f15a_2.dat	f15w_2.bin
p15a_3.dat	p15a_3.bin	f15a_3.dat	f15w_3.bin
p15a_4.dat	p15a_4.bin	f15a_4.dat	f15w_4.bin
p15a_5.dat	p15a_5.bin	f15a_5.dat	f15w_5.bin
p10a_1.dat	p10a_1.bin	f10a_1.dat	f10w_1.bin
p10a_2.dat	p10a_2.bin	f10a_2.dat	f10w_2.bin
p10a_3.dat	p10a_3.bin	f10a_3.dat	f10w_3.bin
p10a_4.dat	p10a_4.bin	f10a_4.dat	f10w_4.bin
p10a_5.dat	p10a_5.bin	f10a_5.dat	f10w_5.bin

p6a_1.dat	p6a_1.bin	f6a_1.dat	f6w_1.bin
p6a_2.dat	p6a_2.bin	f6a_2.dat	f6w_2.bin
p6a_3.dat	p6a_3.bin	f6a_3.dat	f6w_3.bin
p6a_4.dat	p6a_4.bin	f6a_4.dat	f6w_4.bin
p6a_5.dat	p6a_5.bin	f6a_5.dat	f6w_5.bin

p_ten_1.dat	p_ten_1.bin	f_ten_1.dat	f_ten_1.bin
p_ten_2.dat	p_ten_2.bin	f_ten_2.dat	f_ten_2.bin
p_ten_3.dat	p_ten_3.bin	f_ten_3.dat	f_ten_3.bin
p_ten_4.dat	p_ten_4.bin	f_ten_4.dat	f_ten_4.bin
p_ten_5.dat	p_ten_5.bin	f_ten_5.dat	f_ten_5.bin
p_ten_6.dat	p_ten_6.bin	f_ten_6.dat	f_ten_6.bin
p_ten_7.dat	p_ten_7.bin	f_ten_7.dat	f_ten_7.bin
p_ten_8 .dat	p_ten_8.bin	f_ten_8.dat	f_ten_8.bin
p_ten_9.dat	p_ten_9.bin	f_ten_9.dat	f_ten_9.bin
p_ten_10.dat	p_ten_10.bin	f_ten_10.dat	f_ten_10.bin
p_ten_11.dat	p_ten_11.bin	f_ten_11.dat	f_ten_11.bin
p_ten_12.dat	p_ten_12.bin	f_ten_12.dat	f_ten_12.bin
p_ten_13.dat	p_ten_13.bin	f_ten_13.dat	f_ten_13.bin
p_ten_14.dat	p_ten_14.bin	f_ten_14.dat	f_ten_14.bin
p_ten_15.dat	p_ten_15.bin	f_ten_15.dat	f_ten_15.bin
p_ten_16.dat	p_ten_16.bin		
p_ten_17.dat	p_ten_17.bin		
p_ten_18.dat	p_ten_18.bin		

A.7. Data Files Collected For The Study In Chapter-5

Symbols used for naming the data file:

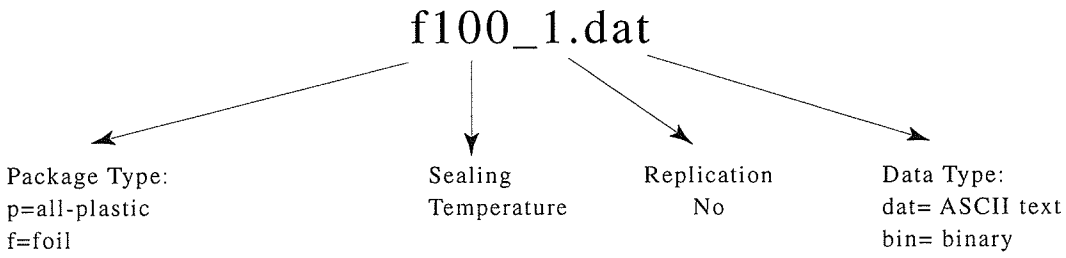

p90_1.dat	p90_1.bin	f140_1.dat	f140_1.bin
p90_2.dat	p90_2.bin	f140_2.dat	f140_2.bin
p100_1.dat	p100_1.bin	f150_1.dat	f150_1.bin
p100_2.dat	p100_2.bin	f150_2.dat	f150_2.bin
p110_1.dat	p110_1.bin	f160_1.dat	f160_1.bin
p110_2.dat	p110_2.bin	f160_2.dat	f160_2.bin
p120_1.dat	p120_1.bin	f170_1.dat	f170_1.bin
p120_2.dat	p120_2.bin	f170_2.dat	f170_2.bin
p130_1.dat	p130_1.bin	f180_1.dat	f180_1.bin
p130_2.dat	p130_2.bin	f180_2.dat	f180_2.bin
p140_1.dat	p140_1.bin	f190_1.dat	f190_1.bin
p140_2.dat	p140_2.bin	f190_2.dat	f190_2.bin
p150_1.dat	p150_1.bin	f200_1.dat	f200_1.bin
p150_2.dat	p150_2.bin	f200_2.dat	f200_2.bin
p160_1.dat	p160_1.bin	f210_1.dat	f210_1.bin
p160_2.dat	p160_2.bin	f210_2.dat	f210_2.bin
p170_1.dat	p170_1.bin	f220_1.dat	f220_1.bin
p170_2.dat	p170_2.bin	f220_2.dat	f220_2.bin
p180_1.dat	p180_1.bin	f230_1.dat	f230_1.bin
p180_2.dat	p180_2.bin	f230_2.dat	f230_2.bin
p190_1.dat	p190_1.bin	f240_1.dat	f240_1.bin
p190_2.dat	p190_2.bin	f240_2.dat	f240_2.bin
p200_1.dat	p200_1.bin	f250_1.dat	f250_1.bin
p200_2.dat	p200_2.bin	f250_2.dat	f250_2.bin

VITA

Ayhan Ozguler was born in Ankara, Turkey, on July 13, 1968. He attended Yildirim Beyazit Technical High School and received the Technical Drawing degree in 1986. He received the B.Sc. degree in Food Engineering from the Middle East Technical University in 1991. In 1993, he was awarded the scholarship by Turkish Ministry of National Education to pursue the master degree in the area of food packaging in the U.S. He received the M.S. degree in 1995 from the University of Illinois, Urbana Champaign. He has been a research assistant by the Food Science and Human Nutrition department under the direction of Dr. Scott A. Morris since 1994.

He is the member of Institute of Food Technologists (IFT), IFT Food Packaging Division, and Gamma Sigma Delta - The Honor Society of Agricultural Sciences. In 1998, he was awarded by The Packaging Education Forum.

PRESENTATIONS

Ozguler, A., Morris, S.A., and O'Brien, W.D, Jr. "Inspection of critical, major, and minor defects in flexible food packages by the ultrasonic "BAI" technique", presented in 1998 IFT Annual Meeting, Atlanta, GA, June 24th, 1998.

Morris, S.A., Ozguler, A., Raum, K., and O'Brien, W.D., Jr. "Pulse-echo/BAI high-frequency ultrasound imaging of defects in food package heatseals", invited presentation to Research and Development Associates/CORANET (Combat Rations Network), Fall International Meeting, Philadelphia, PA, October 29th, 1997.

Morris, S.A., Ozguler, A., Raum, K., and O'Brien, W.D., Jr. "Guidelines for automatic package inspection", invited presentation to FDA National Center for Food Safety and Technology, Chicago, Illinois, October 23rd, 1997.

Ozguler, A., Morris, S.A., and O'Brien, W.D., Jr. "High-frequency ultrasound imaging of defects in food package heatseals", invited presentation to the Packaging Machinery Manufacturers Institute Annual Meeting and Symposium, Las Vegas, NV, October 15th, 1997.

Ozguler, A., Morris, S.A., and O'Brien, W.D., Jr. "Detecting microleaks in shelf-stable food packages using high frequency ultrasound", poster presented at Midwest Food Processing Conference, October 7th, 1997.

Ozguler, A., Morris, S.A., and O'Brien, W.D., Jr. "Evaluation of defects in seal region of food packages using the backscattered amplitude integral (BAI) technique", presented in 1997 IEEE International Ultrasonic Symposium, Toronto, Canada, October 6th, 1997.

Frazier, C. H., Ozguler, A., Morris, S.A., and O'Brien, W.D., Jr. "High-contrast images of defects in material seals", presented in 1997 IEEE International Ultrasonic Symposium,Toronto, Canada, October 6th, 1997.

Ozguler, A., Kortmann, J., Morris, S.A., and O'Brien, W.D., Jr. "Ultrasonic imaging of micro-leaks and defects in shelf-stable food packages by pulse-echo technique", presented in 1997 IFT Annual Meeting, Orlando, FL, June 1997.

Ozguler, A. and Morris, S.A. "Oxygen permeability of corn zein coated papers", presented in 1995 IFT Annual Meeting, Anaheim, CA, June 1995.

PUBLICATIONS

Ozguler, A., Morris, S.A., and O'Brien, W.D., Jr. 1998. "Ultrasonic imaging of micro-leaks and product contamination in flexible food packages by pulse-echo technique", Journal of Food Science, 63(4): 673-678.

Morris S.A., Ozguler, A., and O'Brien, W.D., Jr. 1998. "New sensors for on-line detection of microleaks in heat-sealed food packages: Part 1: Development and evaluation of ultrasonic sensing methods", Packaging Technology & Engineering, 7(7): 42-49.

Morris S.A., Ozguler, A., and O'Brien, W.D., Jr. 1998. "New sensors for on-line detection of microleaks in heat-sealed food packages: Part 2: Development of the BAI pulse-echo sensing method", Packaging Technology & Engineering, 7(8): 52-68.

Raum, K., Ozguler, A., Morris, S.A, and O'Brien, W.D., Jr. 1998. "Channel defect detection in food packages using integrated backscatter ultrasound echo imaging", IEEE Transactions on Ultrasonics, Ferroelectrics, and Frequency Control, 45(1): 30-40.

Ozguler, A., Morris S.A., and O'Brien, W.D., Jr. 1998. "Evaluation of defects in seal region of food packages using the backscattered amplitude integral (BAI) technique", 1997 IEEE Ultrasonic Symposium Proceedings, vol. 1, pp. 689-692.

Frazier, C. H., Ozguler, A., Morris, S.A., and O'Brien, W.D., Jr. 1998. "High-contrast images of defects in material seals", 1997 IEEE Ultrasonic Symposium Proceedings, vol. 1, pp. 627-630.

Ozguler, A., Morris S.A., and O'Brien, W.D., Jr. "Evaluation of defects in seal region of food packages using the ultrasonic contrast descriptor, ΔBAI", Packaging Technology & Science -An International Journal, Feb. 1998: In Press.